The actin-associated protein synaptopodin –
its distribution in hippocampal neurons and its role in spine plasticity

Dissertation

submitted to the Faculty of Biological Sciences

of the Johann Wolfgang Goethe-University of Frankfurt/Main, Germany

for the degree of

Doctor of Natural Sciences

(*doctor philosophiae naturalis, Dr. phil. nat.*)

presented by

Carlos Bas Orth

(Ludwigshafen/Rhein)

Frankfurt/Main, 2007

Accepted by the Faculty of Biological Sciences

of the Johann Wolfgang Goethe-University

Frankfurt/Main, Germany

Dean: Professor Dr. Rüdiger Wittig

Referees: Professor Dr. Thomas Deller

                         Professor Dr. Herbert Zimmermann

Date of disputation: 10.05.2007

'What is there in life except one's ideas.
Good air, good friend, what is there in life?'

Wallace Stevens, The Man with the Blue Guitar

1. Abstract

Synaptopodin is the founding member of a family of actin-associated proline-rich proteins. It is present in a subset of telencephalic dendritic spines, where it is tightly associated with the dendritic spine apparatus, a putative calcium store. Synaptopodin-deficient mice lack the spine apparatus and show deficits in long-term potentiation and spatial memory. Thus, synaptopodin appears to play a role in synaptic plasticity.

In the present thesis, three major questions were addressed: (1) What is the distribution of synaptopodin and the spine apparatus in identified hippocampal neurons? (2) Is the distribution of synaptopodin affected by denervation? (3) Is synaptopodin involved in the regulation of denervation-induced spine loss?

The major findings of this thesis are: (1) Immunohistochemistry in the hippocampus of wildtype and EGFP-transgenic mice revealed significant layer-specific differences in the prevalence of synaptopodin at the level of individual neurons. (2) Light and electron microscopic analysis also revealed the presence of synaptopodin in axon initial segments of cortical and hippocampal principal neurons. There, it was found to be an essential component of the cisternal organelle, a putative axonal homologue of the dendritic spine apparatus. (3) Immunohistochemistry in the rat fascia dentata before and following entorhinal deafferentation revealed changes in synaptopodin expression in denervated and non-denervated layers of the hippocampus, suggesting that the distribution of synaptopodin in hippocampal neurons is regulated by presynaptic signals. (4) The dynamics of denervation-induced spine plasticity were studied in vitro using confocal live imaging of organotypic entorhino-hippocampal slice cultures. Whereas spines were remarkably stable under control conditions, spine loss and spine formation were seen following denervation. No significant differences were observed between cultures from wildtype and synaptopodin-deficient mice, suggesting that synaptopodin is not involved in lesion-induced spine plasticity. (5) Finally, a set of transgenic mice expressing fluorescently tagged synaptopodin were generated to facilitate future experiments on the dynamics and function of synaptopodin.

In summary, this thesis presents novel findings on (1) the subcellular distribution of synaptopodin in spines and the axon initial segment, (2) the molecular composition of the cisternal organelle, and (3) the dynamics of spines and the spine apparatus organelle following deafferentation in vivo and in vitro.

2. Introduction

"Men ought to know that from nothing else but the brain come joys, delights, laughter and sports, and sorrows, griefs, despondency, and lamentations. And by this, in an especial manner, we acquire wisdom and knowledge, and see and hear and know what are foul and what are fair, what are bad and what are good, what are sweet, and what are unsavory... And by the same organ we become mad and delirious, and fears and terrors assail us...when it is not healthy... In these ways I am of the opinion that the brain exercises the greatest power in the man."

(Hippocrates, On the Sacred Disease)

Since the time of Hippocrates, people have believed that the brain is the center of mental functions. Like all other organs, it is made of individual cells, in this case a huge number of nerve cells, or neurons (estimated 10^{11} in humans) and a variety of supporting cells like astroglia and microglia. For its function, the brain depends on the coordinated action of its neurons, which are highly interconnected to form large networks.

One approach to learn more about the brain is, therefore, to study the cell biology of its major functional unit, the neuron.

2.1. Neuronal morphology

Neurons are highly polarized cells that extend numerous long processes, called neurites. During the development of a neuron usually one of these neurites differentiates into an axon, which serves to relay information to other neurons via specialized cell-cell connections, termed synapses. The remaining neurites differentiate into dendrites, which receive information from connected neurons. Axons and dendrites are morphologically and molecularly distinct. For example, axons have a cylindrical shape with a constant diameter and typically send off collateral branches at right angles while dendrites often show a decreasing diameter towards their distal ends and branch at sharp angles. On a molecular level, for example, axons contain the microtubule associated protein (MAP) tau whereas MAP2 is restricted to the somatodendritic compartment.

The dendrites of many neurons contain small (~0.5-2 μm) membranous protrusions, called dendritic spines (Fig. 1). These were first described by Ramon y Cajal, who conclusively

demonstrated that they are a specific feature of a large population of neurons rather than a staining artefact as believed by many of his contemporaries (Ramon y Cajal, 1888; Ramon y Cajal, 1896). Spines typically consist of a bulbous head connected to the dendritic shaft by a thin neck. However, spines can have various shapes and - although spine shapes represent a continuum rather than distinct classes (Trommald and Hulleberg, 1997) - they are often assigned to one of three groups: (1) mushroom spines, having a large head and a narrow neck; (2) thin spines, having a smaller head and a long neck; and (3) stubby spines, having no obvious neck (Peters and Kaiserman-Abramof, 1970; see Harris and Kater, 1994, for review). Dendritic spines are the predominant termination site of excitatory afferents in the central nervous system (Gray, 1959a; Gray, 1959b; see Fig. 1 E) and it is thought that the spine neck acts as a diffusion barrier for small signaling molecules, thereby biochemically isolating the spine synapse from the parent dendrite (Muller and Connor, 1991; Guthrie et al., 1991; Svoboda et al., 1996; Finch and Augustine, 1998; Volfovsky et al., 1999; Sabatini et al., 2002; Korkotian et al., 2004; Bloodgood and Sabatini, 2005). Thus, the main function of dendritic spines might be to allow for localized, synapse specific modifications, e.g. of synaptic strength.
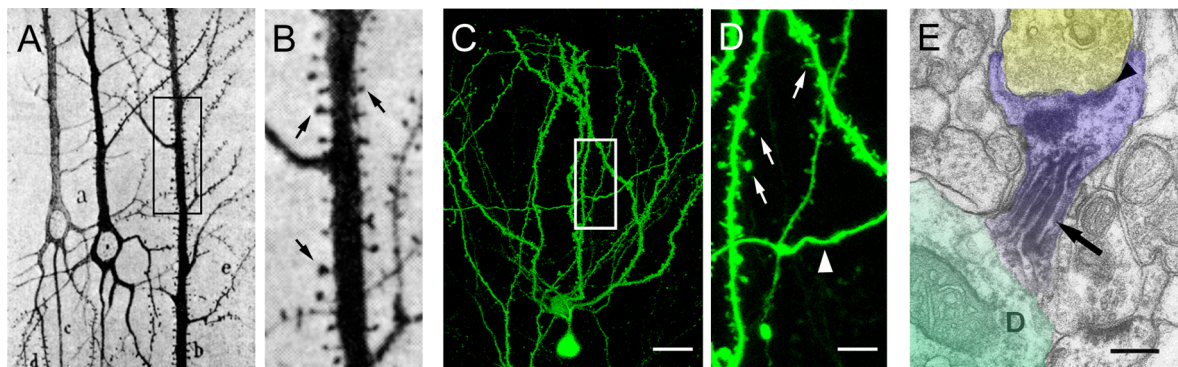
Figure 1. Dendritic spines in the mammalian central nervous system.
A: Drawing of pyramidal neurons in the cerebral cortex of a rabbit, stained with the Golgi technique. **B:** Higher magnification of the boxed area in A, highlighting the numerous spines (arrows) along the dendritic surface. **C:** Confocal image of a living granule cell in a mouse organotypic hippocampal slice culture. **D:** Higher magnification of the boxed area in C. Dendrites are studded with numerous spines (arrows). The arrowhead points to an axon, which is devoid of spines. **E:** Electron micrograph of a dendritic spine (pseudo-colored in blue) in the rat fascia dentata, emerging from a dendritic shaft (D, pseudo-colored in green) and forming a synapse (arrowhead) with an axonal bouton (pseudo-colored in yellow). Note spine apparatus in the spine neck labeled for synaptopodin by pre-embedding DAB histochemistry (arrow). (A, B modified from Ramon y Cajal, 1896. E modified from Deller et al., 2000 with permission of Wiley-Liss, Inc. a subsidary of John Wiley & Sons, Inc.)
Scale bars: C = 20 µm; D = 5 µm; E = 0.2 µm.

A subpopulation of dendritic spines in the forebrain contains a spine apparatus, a cytoplasmic organelle consisting of 2-8 cisterns of endoplasmic reticulum interdigitated by plates of electron dense material (Gray, 1959a; Westrum and Blackstadt, 1962; Hamlyn, 1962; Spacek, 1985; Spacek and Harris, 1997; see Fig. 1 E). The electron dense material contains actin and α-actinin (Wyszynski et al., 1998; Capani et al., 2001) and often extends, in form of thin filaments, towards the postsynaptic density (Spacek, 1985; Capani et al., 2001). Spine apparatuses are predominantly found in large, mushroom shaped spines (Spacek, 1985), or in mature spines that are at least several days old (Knott et al., 2006). Functionally, the spine apparatus is supposed to act as an internal calcium store (Fifkova et al., 1983) although it might also be involved in local protein synthesis (Pierce et al., 2000; Pierce et al., 2001) and receptor cycling (Fabian-Fine et al., 2001).

Axons are not homogenous throughout their entire length but often contain a specialized microcompartment, the axon initial segment, extending from the axon hillock to the beginning of the myelin sheath. In the electron microscope, axon initial segments are characterized by (1) an electron dense undercoating of the plasma membrane, (2) fascicles of microtubules, and (3) clusters of ribosomes (Palay et al., 1968; see Fig. 2). The axon initial segment is regarded as the site of action potential generation (Eccles, 1964; Stuart et al., 1997) and it has been implicated in the sorting of axonal vs. somatodendritic proteins (Winckler et al., 1999; Nakada et al., 2003).
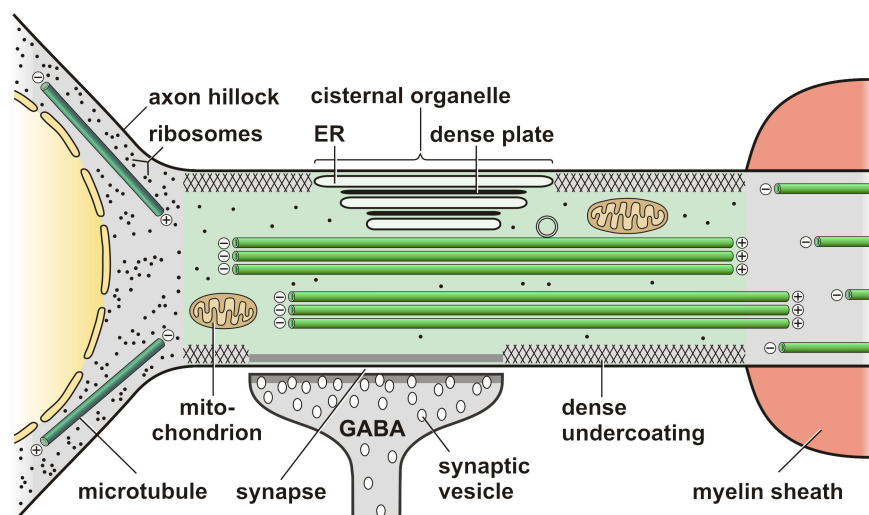
Figure 2. Schematic illustration of the axon initial segment.
Characteristic features of the AIS like the dense undercoating of the plasma membrane and fascicles of microtubules are illustrated. Note the absence of the dense undercoating at sites of synaptic contact and next to cisternal organelles. Artwork courtesy of Inge Szasz.

Frequently, the axon initial segment of cortical principal neurons contains a cisternal organelle, consisting of stacked cisterns of smooth endoplasmic reticulum separated by an electron dense material (Palay et al., 1968; Peters et al., 1968; Kosaka, 1980; Somogyi et al., 1983). This organelle is located directly beneath the plasma membrane and often shows close proximity to GABAergic terminals (Kosaka, 1980; Benedeczky et al., 1994). Based on its structure, some authors have compared it to the dendritic spine apparatus (Peters et al., 1968; Kosaka, 1980; Benedeczky et al., 1994) and similar to its dendritic counterpart, it is supposed to be a local calcium store (Benedeczky et al., 1994).

2.2. Dendritic spine plasticity

Synapses are not static, but rather are subject to modification during development, experience and learning, as well as disease. These changes in synaptic morphology and efficacy are generally subsumed under the term synaptic plasticity. Soon after their initial description and until today, dendritic spines have been considered as major sites of synaptic plasticity in the central nervous system (Ramon y Cajal, 1891; see Yuste and Bonhoeffer, 2001; Nimchinsky et al., 2002; Segal, 2005, for review). During development, spine numbers rapidly increase during a period of exuberant synapse formation. Later on spine numbers are reduced and reach a stable level in adults (reviewed in Harris, 1999). During this stabilization, overall spine morphology changes from filopodia-like to more mushroom-like spines, although shape may not be a reliable indicator of maturity at the single spine level (Knott et al., 2006). Spines have also been shown to change morphologically and moleculary after induction of long-term potentiation (LTP), an experimental paradigm for experience dependent synaptic plasticity (see Malenka and Bear, 2004, for a review on long-term potentiation). Morphological changes include an increase in spine size (Van Harreveld and Fifkova, 1975; Matsuzaki et al., 2004) as well as the generation of new spines (Engert and Bonhoeffer, 1999; Maletic-Savatic et al., 1999; Toni et al., 1999), whereas molecular changes include an increase in postsynaptic density area and glutamate receptor numbers (Desmond and Levy, 1986; Rao and Craig, 1997; O'Brien et al., 1998; Shi et al., 2001). Interestingly, morphological and molecular changes appear to be highly correlated and, accordingly, spine size is proportional to the area of the postsynaptic density (Harris and Stevens, 1989), the number of glutamate receptors (Takumi et al., 1999; Racca et al., 2000), and the size of the presynaptic active zone

(Schikorski and Stevens, 1997), indicating that larger spines form stronger synapses. Finally, dendritic spines are affected in a number of neurological diseases (see Blanpied and Ehlers, 2004, for review). For example, in patients with fragile X mental retardation syndrome, dendritic spines have an increased density and exhibit a more immature, filopodia-like morphology (Rudelli et al., 1985; Irwin et al., 2001). In contrast, spine density is decreased in neocortex and hippocampus of patients with Down syndrome (Suetsugu and Mehraein, 1980; Takashima et al., 1989).

2.3. Denervation-induced plasticity

Denervation-induced plasticity is a form of neuronal plasticity that is of particular interest in the context of neurological disease. Since neurons are highly interconnected cells, the degeneration of a given neuronal population will often affect additional, remote neurons. If, for example, a population of neurons degenerates after a traumatic injury, the target cells of these neurons will lose some of their input, i.e. they will be partially denervated. Although not directly affected by the lesion, the postsynaptic neurons are subject to transneuronal changes including the loss of dendritic spines, dendritic atrophy and even cell death (Matthews et al., 1960; Globus and Scheibel, 1966; Parnavelas et al., 1974; Caceres and Steward, 1983; Frotscher, 1983; Diekmann et al., 1996; see also Steward, 1994; Deller and Frotscher, 1997, for review). The severity of transneuronal changes depends on several factors, including the extent of denervation, the amount of remaining alternative afferents, and the age of the animal. If a denervated neuron degenerates, its target cells will also be denervated, potentially leading to a cascade of neurodegeneration. In any case, denervation-induced transneuronal changes will significantly potentiate the effects of an initial lesion of the nervous system. Although denervation-induced plasticity in the central nervous system has been studied in much detail, little is still known about the molecular mechanisms and signaling pathways governing the processes described above. Metaphorically spoken, the question of how the postsynaptic neuron "knows" that it has lost its afferent input remains unresolved. One hypothesis (see Deller and Frotscher, 1997, for review) states that denervation leads to a massive release of glutamate from degenerating axonal terminals. This would in turn lead to a pathological rise of postsynaptic calcium, activating calcium-dependent proteases (e.g. calpain) and phosphatases (e.g. calcineurin), that have been shown to be involved in cytoskeletal remodeling (Halpain et al., 1998; Ginsberg et al., 1999; Chan and Mattson, 1999; Wu et

al., 2004). Assuming that a rise in intracellular calcium is crucially involved in denervation-induced transneuronal changes, it is of interest to see whether this rise is predominantly mediated by the influx of calcium from the extracellular space or by a release of calcium from intracellular stores.

2.4. Entorhinal cortex lesion as a model for denervation-induced plasticity

Entorhinal cortex lesion (ECL) is an established and well-studied model of denervation-induced plasticity in vivo (Lynch et al., 1972; Cotman and Nadler, 1978; Del Turco et al., 2003; Dehn et al., 2006) and in vitro (Frotscher and Heimrich, 1993; Li et al., 1993; Li et al., 1995; Prang et al., 2001; Prang et al., 2003). This model takes advantage of the laminar cytoarchitecture of the fascia dentata with its highly organized pattern of afferent inputs (Frotscher, 1988; Frotscher, 1991; see Fig. 3).The dentate granule cells are situated in a compact cellular layer and extend their dendrites into the molecular layer. The molecular layer can be divided into (1) the inner molecular layer, receiving input from commissural and associational fibers and (2) the outer molecular layer, receiving input from the entorhinal cortex, the medial septum and commissural and associational fibers. The entorhinal input to the outer molecular layer originates predominantly from layer II stellate neurons of the entorhinal cortex and accounts for 80-90 % of all excitatory synapses in this layer (Matthews et al., 1976a). Following transection of the entorhino-dentate projection, axon terminals in the outer molecular layer begin to degenerate within the first 24-48h postlesion and are almost completely lost during the first week (see Steward, 1991, for review). As a result of this denervation, up to 50% of dendritic spines on distal granule cell dendrites are lost during the first days post lesion in vivo (Parnavelas et al., 1974; Caceres and Steward, 1983). In addition, a loss of granule cell dendrites occurs and dendrites develop varicosities (Caceres and Steward, 1983; Diekmann et al., 1996). In vivo, reorganization processes including sprouting of remaining axons that terminate in the denervated area take place after ECL, reaching a peak 1-2 weeks post lesion (Steward and Vinsant, 1983). This leads to a partial reinnervation of the outer molecular layer and a concomitant regeneration of dendrites and spines. Although dendritic regeneration has been reported by several authors, the extent of regeneration differs markedly between studies (e.g. almost complete regeneration in Caceres and Steward, 1983; but long-lasting dendritic atrophy in Diekmann et al., 1996). In vitro, mossy cell axons that normally are confined to the inner molecular layer have been shown to sprout into the outer molecular

layer after ECL, starting between 5 and 10 days post lesion (Prang et al., 2003). The effect of this reinnervation on dendritic morphology has not been determined, however. Also, the dynamics and the extent of spine and dendrite atrophy have not been studied in detail.
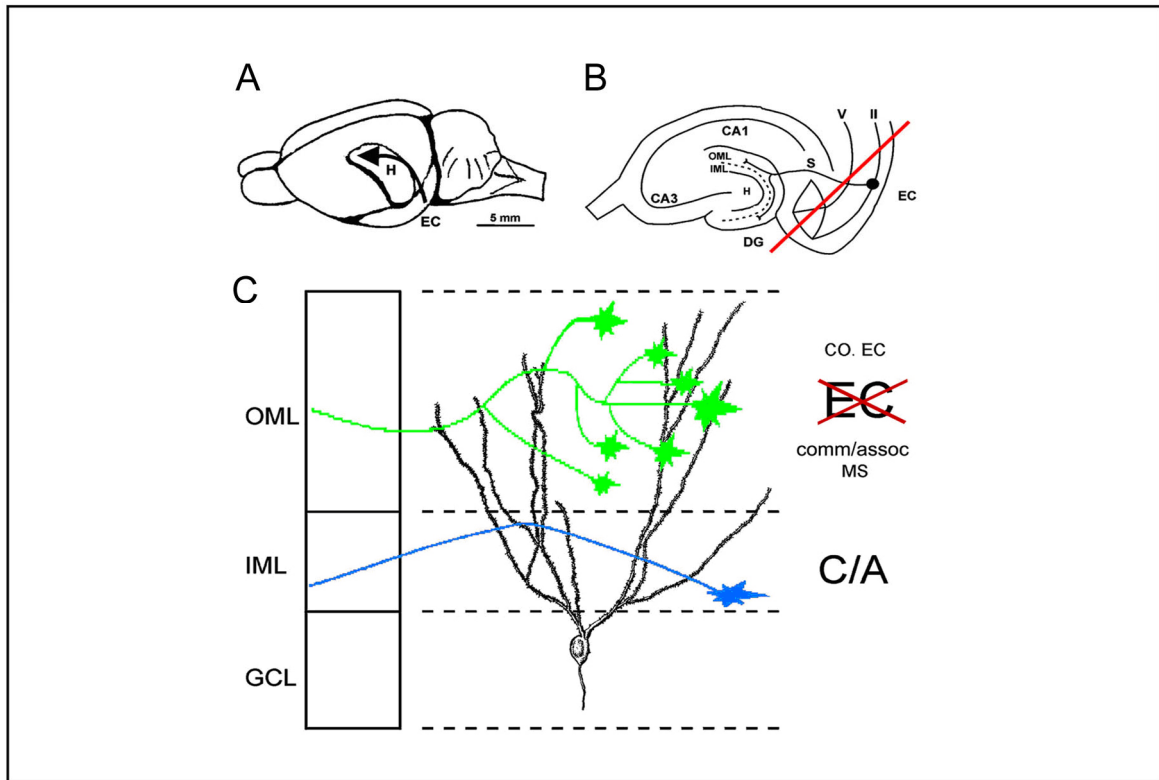
Figure 3. Schematic illustration of the entorhinal cortex lesion model (Deller, 1998).
A: Topography of the entorhino-hippocampal projection. Fibers of the EC project to the hippocampus (H) in a topographically ordered, lamina-specific manner.
B: Horizontal section of the hippocampal formation. Neurons located in layer II of the EC form the perforant pathway projecting to the OML of the DG. Additionally, fibers from the EC project to stratum lacunosum-moleculare of CA1-CA3. The red line indicates the site where the perforant pathway is transected.
C: Lamina-specific termination and sprouting of afferent fibers in the DG. A typical granule cell is illustrated. On the right hand side the major afferent fiber systems are indicated. The size of the lettering indicates the relative contribution of these fibers to the innervation of the DG. Following ECL, the entorhinal input is lost. The remaining fiber systems sprout and reinnervate the DG in a layer-specific fashion. The green fiber indicates sprouting afferents that reinnervate the OML following denervation. Fibers that terminate in the non-denervated adjacent IML (blue fiber) do not invade the denervated zone in vivo.
CA1, CA3: hippocampal subfields, DG: dentate gyrus, EC: entorhinal cortex, ECL: entorhinal cortex lesion, GCL: granule cell layer; H: hippocampus, IML: inner molecular layer, OML: outer molecular layer

2.5. The actin-associated protein synaptopodin

Synaptopodin was cloned in 1997 (Mundel et al., 1997) as the founding member of a novel family of actin-associated proline-rich proteins that now also includes myopodin (Lin et al., 2001) and fesselin (Beall and Chalovich, 2001). Two splice variants of synaptopodin have been described, namely (1) a 100 kDa isoform that is exclusively expressed in brain and (2) a 110 kDa isoform that contains additional amino acid residues at the carboxy-terminus and is specific for differentiated kidney podocytes (Mundel et al., 1997; Asanuma et al., 2005). Both isoforms contain actin- and α-actinin-binding sites as well as two PPXY motifs which are important for protein-protein interactions with proteins containing WW domains.

In kidney podocytes synaptopodin is found in foot processes, where it is a part of the actin-based contractile apparatus (Mundel et al., 1997). It regulates foot process motility by modulating the bundling of actin (Asanuma et al., 2005) and by interacting with the small GTPase RhoA (Asanuma et al., 2006).

In the brain expression of synaptopodin protein starts around postnatal day (P) 5 and reaches the adult expression pattern at P12 (Czarnecki et al., 2005). The expression of the brain specific isoform is restricted to the telencephalon, i.e. the olfactory bulb, cerebral cortex, striatum and hippocampus (Mundel et al., 1997; Deller et al., 2000a). Within these regions, synaptopodin protein is only found in spine-bearing neurons (Czarnecki et al., 2005). Whereas synaptopodin mRNA is only observed in the perikarya of these cells, the protein is targeted to dendritic spines, where it is closely associated with the spine apparatus (Deller et al., 2000a; Deller et al., 2002). Accordingly, synaptopodin immunoreactivity is strong in dendritic layers and weak or almost absent in cellular layers in laminated areas of the telencephalon like the hippocampus. Interestingly, dendritic layers in the hippocampus are not evenly labeled for synaptopodin but exhibit region- and lamina-specific differences in staining intensity (Deller et al., 2000a; Deller et al., 2002).

To analyze the function of synaptopodin, mice with a targeted deletion of the synaptopodin gene were generated (Deller et al., 2003). These mice do not have obvious alterations in the gross morphology of their brains and dendritic spine numbers and shapes are unchanged, at least in the CA1 region of the hippocampus. However, synaptopodin-deficient mice completely lack the spine apparatus organelle. Functionally, these mice show impaired LTP and have deficits in spatial memory as assessed by a radial arm maze

test (Deller et al., 2003). This phenotype indicates a role for synaptopodin and the spine apparatus in synaptic plasticity and learning.

2.6. Aims of the thesis

The objective of the present thesis was to learn more about the role of synaptopodin in neuronal plasticity. In a first step, the distribution of synaptopodin and its regulation were studied. Then, a potential role of synaptopodin in denervation-induced plasticity was investigated. Finally, synaptopodin-transgenic mice were generated to provide an additional tool for the study of synaptopodin. Specifically, the aims of the thesis were:

(1) To analyze the distribution of synaptopodin in the rodent hippocampus.

(2) To investigate the influence of a partial denervation on the distribution of synaptopodin.

(3) To establish an imaging setup for the analysis of the dynamics and extent of denervation-induced dendritic spine changes in vitro.

(4) To investigate a potential role of synaptopodin in denevervation-induced plasticity.

(5) To generate synaptopodin-transgenic mice.

3. Material and Methods

3.1. Animals and tissue preparation

For immunostaining, adult male C57BL/6JOlaHsd mice (3-6 months; Harlan-Winkelmann, Borchen, Germany; n=20), adult male Thy1GFP transgenic mice (Thy1GFP-M line; Feng et al., 2000; 4 months; n=7), adult synaptopodin-deficient mice (Deller et al., 2003; n=7) and adult male Sprague-Dawley rats (250-350 g; Charles River, Sulzfeld, Germany; n=25) housed under standard laboratory conditions were used. Animals were deeply anesthetized with an overdose of pentobarbital (300 mg/kg body weight Narcoren, Merial GmbH, Hallbergmoos, Germany) and transcardially perfused with 0.9% NaCl followed by fixative containing 4% paraformaldehyde (for immunofluorescence) or 4% paraformaldehyde and 0.5% glutaraldehyde (for electron microscopy) in 0.1 M phosphate buffered saline (PBS, pH 7.4, paraformaldehyde was from Merck, Darmstadt, Germany; glutaraldehyde was from Agar Scientific, Stansted, UK). Brains were removed and postfixed for 24 hours in 4% paraformaldehyde at 4°C. Serial frontal sections (50 μm) were cut with a vibratome (VT 1000S, Leica, Bensheim, Germany). All animal experiments were performed in agreement with the German law on the use of laboratory animals.

3.2. Entorhinal cortex lesion

All surgical procedures were performed under deep pentobarbital anaesthesia (50 mg/kg body weight). Lesions were performed as previously described (Deller et al., 1996; Deller et al., 2006). In brief, the head of the animal was horizontally aligned in a stereotaxic frame (Kopf Instruments, Tunjunga, USA) and a hole was drilled above the lesion site using a handheld dental drill (Proxxon Micromot 50, Hickory NC, USA; drill head: Dremel 107, Leinenfelden-Echterdingen, Germany). A standard electrocoagulator (Erbe, Tübingen, Germany) was used to perform a complete unilateral electrolytic lesion of the entorhinal cortex. The following coordinates measured from the interaural line were used for the two cuts: frontal cut: AP +1, L +3 to +7, V down to the base of the skull; sagittal cut: AP +1 to +4, L +6.7, V down to the base of the skull (Paxinos and Watson, 1982). Finally, the head wound was closed and the animal was carefully returned to the cage. For postoperative

analgesia metamizol-sodium was added to the drinking water (0.1% Novaminsulfon, Ratiopharm Merckle GmbH, Blaubeuren, Germany).

Because lesion quality is essential, completeness of ECL was verified prior to analysis. On serial horizontal sections through the EC, the correct location and size of the lesion were verified. All animals with even the slightest injury to the temporal hippocampus were excluded. On serial septal sections, every fifth section was used for histochemical staining for acetylcholinesterase (AChE; see Deller et al., 2006). In the case of complete lesions, a dense AChE-positive fiber band appears in the denervated outer two thirds of the molecular layer between 5 and 10 days post lesion (Nadler et al., 1977; Zimmer et al., 1986). Animals (5 days post lesion and later) without the dense AChE-positive fiber band were excluded. To control lesion quality in animals with shorter survival times post lesion, immunostaining with an antibody against calpain-cleaved spectrin was employed. This antibody labels degenerating axons and terminals and reliably demonstrates the zone of degeneration (Kiss et al., 1996; Deller et al., 2006).

3.3. Immunostaining

The immunostaining procedures employed in this thesis involved the following steps:

(1) Blocking of unspecific staining and permeabilization of the tissue. Sections were incubated in serum from the donor species of the secondary antibody to reduce unspecific binding of the secondary antibody. A detergent (Triton X-100, Merck, Darmstadt, Germany) was added to increase antibody penetration and availability of antigen. (2) Binding of the primary antibody to its specific antigen. (3) Binding of the secondary antibody to species-specific regions of the primary antibody. The secondary antibody was either labeled with a fluorophore or with biotin. In the latter case, a standard avidin-biotin-peroxidase system with diaminobenzidine (DAB) as a chromogen was used for detection of the secondary antibody (Hsu et al., 1981). Staining conditions (permeabilization, dilution of antibody, incubation time) were optimized for each antibody.

Staining protocol for immunofluorescence

Free-floating vibratome sections were incubated in 5% normal serum, 0.5% Triton X-100 in 0.1 M phosphate buffered saline (PBS, pH 7.4) for 1 hour at room-temperature (RT) and

subsequently incubated for 24-48 hours at 4°C with the primary antibody in 1% bovine serum albumin, 0.1% Triton X-100 in PBS. After three washing steps in PBS, sections were incubated with an Alexa dye-labeled secondary antibody (Molecular Probes, Eugene, OR, USA) in 1% bovine serum albumin, 0.1% Triton X-100 at RT for 2 hours. Sections were washed again, transferred onto glass slides and mounted under glass coverslips with anti-fading mounting medium (DAKO© Fluorescent Mounting Medium; Dako, Hamburg, Germany). For double-immunolabeling, sections were incubated in a mixture of primary antibodies. After washing, sections were incubated with the first secondary antibody, washed again and then incubated with the second secondary antibody.

Staining protocol for DAB- and immunogold-labeling

DAB- and immunogold-labeled sections were used for electron microscopy and, thus, detergent was omitted to optimally preserve the ultrastructure of the tissue.

Free-floating sections were washed in PBS and incubated in PBS containing 10% methanol and 3% hydrogen peroxide (H_2O_2) for 0.5h to reduce endogenous peroxidase activity (for DAB-labeling only). Then, sections were washed (3 x 4 min) and incubated in 5% bovine serum albumin (BSA, BIOMOL GmbH, Hamburg, Germany; 1h). Subsequently, sections were incubated over night at 4°C with anti-phosphorylated-IκBα antiserum (Ser32, Cell Signaling Technology, Frankfurt, Germany; 1:1,000) or with anti-synaptopodin antiserum (NT, Mundel et al., 1997, 1:2,000) in 0.1 M PBS containing 1% BSA. For the detection of the anti-phosphorylated-IκBα antibody, a secondary biotinylated antibody was used (RT, 2 hours). Then, sections were washed (3 x 4min) and transferred to ABC solution (ABC-Elite, Vector Laboratories, Burlingame, USA) for 2h. After washing the sections in PBS, they were stained with a solution containing 0.0025% DAB, 0.005% ammonium-nickel-sulphate, and 0.006% cobalt-chloride activated with 0.001% H_2O_2. For the detection of the anti-synaptopodin antibody, a gold-coupled secondary antibody (10 nm; Amersham, Buckinghamshire, UK) was used. Finally, sections were mounted onto slides, dehydrated through an ascending ethanol series, and embedded between liquid release-coated slides and coverslips. Selected sections were reembedded in blocks, and serial ultrathin sections were collected on single-slot Formvar-coated copper grids. Ultrathin sections were examined in a Zeiss EM109 electron microscope.

Primary antibodies used:

name	antigen	type	host	standard dilution	source
NT	synaptopodin (mouse)	polyclonal	rabbit	1:1000	Dr. Peter Mundel, Mount Sinai School of Medicine, NY, USA
SE-19	synaptopodin (mouse)	polyclonal	rabbit	1:1000	Sigma-Aldrich
26-1E	synaptopodin (rat)	polyclonal	rabbit	1:400	Dr. Peter Mundel, Mount Sinai School of Medicine, NY, USA
MAB 5258	synaptophysin (bovine)	monoclonal	mouse	1:1000	Chemicon, CA, USA
α-βIV-spectrin	βIV-spectrin	polyclonal	chicken	1:1000	M. Komada, Tokyo Institute of Technology, Japan
Ser32	phosphorylated IκBα	polyclonal	rabbit	1:1000	Cell Signaling Technology, Frankfurt, Germany

Secondary antibodies used:

donor species	specificity	label	standard dilution	source
goat	α-rabbit IgG	Alexa 488	1:1000	Molecular Probes, Eugene, OR, USA
goat	α-rabbit IgG	Alexa 568	1:1000	Molecular Probes, Eugene, OR, USA
goat	α-rabbit IgG	Alexa 633	1:1000	Molecular Probes, Eugene, OR, USA
goat	α-mouse IgG	Alexa 488	1:1000	Molecular Probes, Eugene, OR, USA
goat	α-chicken IgG	Alexa 568	1:1000	Molecular Probes, Eugene, OR, USA
goat	α-rabbit IgG	biotin	1:250	Vector Laboratories, Burlingame, USA
goat	α-rabbit IgG	10 nm gold	1:100	Amersham, Buckinghamshire, UK

3.4. Confocal imaging and quantitative analysis of synaptopodin-puncta

Confocal imaging and quantitative analysis of synaptopodin puncta-densities in C57BL/6J mice

Synaptopodin puncta-densities were analyzed in three sections per animal (500 μm, 1000 μm, and 1500 μm from the septal pole of the hippocampal formation) using a Zeiss LSM 510 laser scanning microscope, a Zeiss 63x oil immersion lens (NA 1.4), and 2x scan zoom. Detector gain and amplifier offset were initially set to obtain pixel-densities within a linear range. All images were recorded using exactly the same settings. Per section, a total of 19 frames (frame size: 30 μm x 30μm x 1 μm) was sampled in the dentate gyrus (hilus, granule cell layer, inner-, middle-, and outer molecular layer of the infra- as well as the suprapyramidal blade of the dentate gyrus), area CA3 (strata oriens, pyramidale, lucidum, radiatum, and lacunosum-moleculare), and area CA1 (strata oriens, pyramidale, radiatum, and lacunosum-molecular). Frames were placed as follows: After visual identification of a layer in the confocal microscope the frame was visually positioned in the middle of this layer. Minor variations in the placement of the frames did not affect our quantitative analysis. Images were recorded at tissue levels (3-5 μm below the surface of the section) where immunostaining for synaptopodin was optimal, as confirmed in z-stacks throughout the entire section. Quantitative analysis of confocal images was performed using the ImageJ software package (program available from http://rsb.info.nih.gov/ij). After standardization of the image analysis method (see Results), the following parameters were chosen for analysis: threshold level 50; minimum size 5 pixels. All objects defined by these parameters were counted automatically by the software. Values for threshold as well as minimum object size were kept constant for all measurements. The number of positive puncta and the standard error of the mean (SEM) were calculated and expressed as mean number of puncta per 1000 μm^3 ± 2 x SEM. Layer-specific densities of synaptopodin-positive puncta were compared within each hippocampal subfield. Layers were tested against each other for statistical significance using analysis of variance (ANOVA) followed by Bonferroni's multiple comparisons post hoc test (significance level $p \leq 0.05$).

Confocal imaging and quantitative analysis of synaptopodin-puncta in EGFP-labeled hippocampal principle cells

Hippocampal sections from Thy1GFP transgenic mice stained for synaptopodin were used to study the distribution of synaptopodin-positive puncta in identified principal cells. In these sections, EGFP-labeled granule cells, CA3 pyramidal cells, and CA1 pyramidal cells were randomly selected. To ensure optimal immunolabeling, only those dendritic segments were used for analysis, which were located in the zone of optimal synaptopodin-immunostaining (antibody penetration into the tissue was verified in each section using z-stack analysis). In all cases, secondary or tertiary dendritic segments were used. Confocal image stacks were recorded in the dentate gyrus (inner- and outer-molecular layer), area CA3 (strata oriens, radiatum, and lacunosum-moleculare), and area CA1 (strata oriens, radiatum, and lacunosum-moleculare) using a Zeiss 63x oil immersion lens (NA 1.4) and 4x scan zoom. Up to 70 images with a z-interval of 0.15 μm were recorded per stack. Following data acquisition, dendritic segments were coded and three-dimensionally analyzed blind to their location. To optimally demonstrate the subcellular localization of synaptopodin-immunoreactive structures, selected images were further processed by three-dimensional deconvolution (AutoDeblur software, AutoQuant, USA) and three-dimensional surface rendering (Imaris software, Bitplane, Switzerland).

First, these data were used to determine the percentage of synaptopodin-positive puncta associated with dendritic spines or dendritic shafts. Synaptopodin-positive puncta were considered to be located in spines, if the three-dimensional analysis revealed part of the synaptopodin-positive structure within the spine head or neck. They were considered to be located within dendritic shafts, if three-dimensional analysis revealed no spine-association.

Next, the percentage of synaptopodin-positive spines was determined. For this, the total number of spines and the total number of synaptopodin-positive spines were counted in each dendritic segment. The percentage of synaptopodin-containing spines and the standard error of the mean (SEM) were calculated and expressed as mean percentage of positive spines $\pm$ 2 x SEM. Layers within each hippocampal subfield were tested against each other for statistical significance using analysis of variance (ANOVA) followed by Bonferroni's multiple comparisons post hoc test (significance level $p \leq 0.05$).

Confocal imaging of synaptopodin-labeled mossy cells

Synaptopodin-labeled sections of Thy1GFP-M mice were analyzed using a Zeiss LSM 510 laser scanning microscope, a Zeiss 63x oil immersion lens (NA 1.4), and 2.5x scan zoom. Detector gain and amplifier offset were set to obtain pixel-densities within a linear range. Confocal image stacks of EGFP-positive mossy cells and mossy cell dendrites were recorded in the hilus. Dendritic image stacks consisted of up to 25 images with a z-intervall of 0.25 µm.

Confocal imaging and quantitative analysis of synaptopodin puncta-densities in control rats and rats with entorhinal cortex lesion

Confocal microscopy was performed using a Zeiss LSM 510 laser scanning microscope, a Zeiss 63x oil immersion lens (N.A 1.4), and 2x scan zoom. Detector gain and amplifier offset were set to obtain pixel-densities within a linear range. All images were recorded using exactly the same settings.

The septal portion of the hippocampus was used for the quantitative analysis of synaptopodin puncta-densities. Control rats (n=4), and entorhinal cortex-lesioned rats surviving for 4 days (d) (n=3), 7d (n=3), 10d (n=3), 14d (n=5), 30d (n=4), and 180d (n=3) were used. On average, five septal sections (distance between each section: approximately 100 µm) were analyzed per animal. Per section, 3 frames (IML, MML, and OML; frame size: 30 µm x 30 µm x 1 µm) were sampled. To obtain a representative average throughout the entire denervated zone, data from the MML and OML were pooled and compared to the non-denervated IML. Confocal images were analyzed using the ImageJ software from the National Institute of Health (NIH). First, a threshold was set manually (threshold level: 70) and all objects with lower intensity values than this threshold were set equal to background. Minimum size was set at 5 pixels. Finally, all objects defined by these criteria were counted automatically by the software. Values for threshold as well as minimum object size were kept constant for all measurements. The number of positive puncta and the standard error of the mean (SEM) were calculated and expressed as mean number of puncta per 1000 µm^3 ± SEM.

On synaptopodin-labeled sections, the non-denervated IML and the denervated zone (MML and OML) could readily be distinguished. For each time point, the width of these zones was measured at the middle of the granule cell layer on 15 septal sections from 3-4

animals (20x magnification images) using the Zeiss LSM image browser. The average widths of the non-denervated IML, the denervated zone (MML+OML), and the total molecular layer (ML) were calculated for each time point and expressed as mean width ± SEM. The widths of these layers in control animals were set to 1.0 and the values for each time point were expressed relative to control values. For the correction of lesion-induced shrinkage affecting the synaptopodin-density data, raw values were multiplied by this factor for each time point.

Statistical analysis was performed as follows: Layer-specific control data were tested against layer-specific data obtained at 4 days and 180 d post lesion. Homogeneity of the variance was proven using Levene test. Since the variance of synaptopodin puncta-densities and spine apparatus scores were not equal between case and control groups, the non-parametric Mann-Whitney-U Test was employed to determine the significance of difference. Tests were two-tailed and significance set at $p \leq 0.05$. Computations were performed with the aid of SPSS for MS Windows, release 13 (SPSS Inc., 2003, Chicago, IL, USA).

3.5. Cultivation, lesioning and imaging of organotypic slice cultures

Organotypic slice cultures

For the preparation and cultivation of organotypic cultures, the so-called interface-technique developed by Stoppini et al. (1991) was used.

Entorhino-hippocampal slice cultures were prepared from 4-6 day old Thy1GFP transgenic mice (Feng et al., 2000) and Thy1GFP x synaptopodin-/- mice. After decapitation of the animals, brains were removed and cut horizontally (300 μm) with a vibratome (VT 1000S, Leica, Bensheim, Germany). During cutting, brains were immersed in cold (4°C) preparation medium. Entorhinal cortex and hippocampus were excised from the brain sections and the resulting slices were placed onto porous membranes (Millicell-CM, Millipore, Eschborn, Germany). Membranes were put into 6-well plates (Greiner bio-one, Frickenhausen, Germany) containing cultivation medium and cultures were incubated (35°C) in a humidified atmosphere with 5% CO_2. Cultivation medium was exchanged every second day.

Entorhinal cortex-lesion in vitro

After 18-20 days in vitro, slice cultures were completely transected from the rhinal fissure to the hippocampal fissure using a sterile scalpel blade as described previously (Prang et al., 2003).

Live imaging of organotypic slice cultures

For live imaging of slice cultures, Milicell membranes were transferred to a 30 mm petri dish containg warm (37°C) imaging buffer and immobilised using a custom made titanium ring. Cultures were viewed with an upright Zeiss LSM Pascal confocal microscope. 10x magnification images were recorded to identify individual granule cells. Due to the mosaic-like distribution of EGFP-positive cells in the cultures, identified granule cells could readily be found again at each imaging session. Images were then recorded using a 63x objective to identify individual dendritic segments. Finally, an image stack (0.5 μm intervall) of a given dendritic segment was recorded using a 63x objective and 4x scan zoom. After imaging, cultures were transferred back to the incubator. Usually, a set of cultures was screened for suitable EGFP-positive granule cells two days before lesion, using the 10x objective and 4x scan zoom. Images of dendritic segments were then recorded one day before lesion and 2 days (d), 4d, 7d, 10d, 14d, 21d, 30d and 42d after lesion.

Quantification of dendritic spine density

Dendritic spines were counted manually on 3D-image stacks of dendritic segments using the Zeiss LSM image browser to navigate through the stacks. Images were coded and analyzed blind to experimental condition and time point. For each segment, a defined distance (usually 30 μm) from an identified branchpoint was analyzed at each time point. The number of spines per μm was calculated and expressed relative to control value as mean ± standard deviation (SD).

3.6. Protein extraction and Western Blot

Protein extraction

For the biochemical analysis of mouse brain synaptopodin, brain tissue lysates were prepared according to Mundel et al. (1997). Mice were deeply anesthetized with an overdose of isofluran (Abbott, Wiesbaden, Germany) and killed by cervical dislocation. Brains were removed and the cerebral cortex was dissected. One cerebral hemisphere (ca. 70 mg) was homogenated in 500 µl homogenization buffer using a tissue grinder (Pellet Pestle®, Kontes, Vineland, NJ, USA). The homogenate was centrifuged at 25,000 x g at 4°C for 30 min to pellet insoluble material. The resulting supernatant was further processed to obtain a heat-stable protein fraction. The concentration of NaCl was adjusted to a final concentration of 800 mM and 5% β-mercaptoethanol was added. Then, the sample was boiled for 5 min and insoluble material was pelleted by centrifugation at 25,000 x g at 4°C for 30 min. The resulting heat-stable supernatant was stored at -20°C.

Sodium dodecyl sulfate- polyacrylamide gel electrophoresis (SDS-PAGE)

SDS-PAGE (Laemmli, 1970) is a method for high-resolution size separation of proteins. As a matrix, a polyacrylamide gel formed by the polymerization of acrylamide and N,N'-methylenebisacrylamide is used. The anionic detergent SDS binds to proteins resulting in a negative charge of the proteins. In an electrical field, the proteins thus migrate through the gel matrix towards the anode. Smaller proteins are hindered less by the gel matrix than larger proteins and thus migrate faster.

Gels were prepared according to the following protocol:

	stacking gel 4%	separating gel 10%
30% acrylamide/bis-solution (Bio Rad)	1.3 ml	3.3 ml
stacking gel buffer	2.5 ml	-
separating gel buffer	-	2.5 ml
dd H_2O	6.2 ml	4.2 ml
ammonium persulfate (Gibco, Paisley,UK)	100 µl	50 µl
TEMED (Appli Chem, Darmstadt, Germany)	50 µl	25 µl

Samples were mixed 1:1 with sample buffer and boiled at 95°C for 5 min. Then, samples were briefly cooled on ice, spinned in a table top centrifuge and loaded onto the gel. Electrophoresis was performed at 120 V (stacking gel) and 160 V (separating gel) in an electrophoresis tank (Mini-PROTEAN 3 cell, Bio Rad, Munich, Germany).

Western Blot

This method was used to transfer proteins from the polyacrylamide gel to a polyvinyliden-difluoride (PVDF) membrane. Upon binding to the membrane, the separated protein bands get immobilized and can then be further analyzed by immunodetection (see below).

Protocol: Western Blot was always performed directly after SDS-PAGE. The PVDF membrane (Immobilon-P Transfer Membrane, Millipore, Billerica, MA, USA) was briefly activated in methanol and then equilibrated in transfer buffer for 10 min. Pieces of filter paper (3MM, Whatman GmbH, Dassel, Germany) were soaked in transfer buffer. For blotting, a Trans-Blot Semi-Dry system (Bio Rad) was used. Two pieces of filter paper were put on the anode followed by the PVDF membrane, the polyacrylamide gel, two pieces of filter paper and the cathode. Protein transfer was performed at 15 V for 75 min.

Immunodetection

To specifically label synaptopodin on the membrane, a standard immunodetection assay was performed. This involved (1) incubation of the membrane with a blocking solution containing dry milk to saturate all free protein binding sites, (2) incubation with a primary antibody specific for synaptopodin, (3) incubation with a secondary antibody coupled to horseradish peroxidase (HRP) and (4) detection of the antibody-protein complex using enhanced chemiluminescence. HRP catalyzes the oxidation of luminol by hydrogen peroxide, leading to the emission of light (maximum of emission spectrum at 428 nm). Using phenol, the reaction is enhanced by a factor of 1000. The emitted light is detected using an autoradiography film.

Protocol: After protein transfer, PVDF membranes were rinsed in TBS-T buffer and incubated on a shaker for 1h at room-temperature (RT) in TBS-T containing 5% non fat dry milk. After three washing steps in TBS-T, membranes were incubated with the primary antibody (SE-19 rabbit anti-synaptopodin, Sigma-Aldrich, St.Louis, MO, USA; 1:3000) in TBS-T containing 5% dry milk at 4°C over night. Membranes were then washed three times with TBS-T, incubated with the secondary antibody (goat anti rabbit, HRP

conjugated, DAKO, 1:2000) in TBS-T containing 5% dry milk for 2h at RT and washed three times in TBS-T. Finally, membranes were incubated for 5 min at RT with chemiluminescence solution (Super Signal West Pico Kit, Pierce Perbio, Bonn, Germany). Autoradiography films (Biomax MR 1, Kodak, Rochester, NY, USA) were then laid onto the membrane for different exposure times in a darkroom and developed manually (developer: Rodinal, Agfa, Köln, Germany).

3.7. Genotyping of mouse mutants

Preparation of tail tip DNA for genotyping

Mice were anesthetized with Isofluran (Abbott, Wiesbaden, Germany) and marked. Then, 3-4 mm of the tail tip were cut with a sterile scalpel blade and transferred to an autoclaved Eppendorf tube. Scalpel and puncher were disinfected after each mouse. Tail tips were processed immediately or stored at -20°C for several days.

To generate lysates, tail tips were incubated in 180 µl TNES buffer and 20 µl Proteinase K (10 mg/ml, Invitrogen, Karlsruhe, Germany) for 6 hours or over night at 55°C in a thermomixer (Eppendorf, Hamburg, Germany).

Next, samples were incubated at 95°C for 3 min to inactivate Proteinase K and centrifuged for 5 min at 12,000 rpm at 4°C to pellet insoluble material. The supernatant was diluted 1:100 with ddH$_2$O and stored at -20°C.

Polymerase chain reaction

Animals were genotyped using the polymerase chain reaction (PCR). PCR is an in vitro method for the amplification of specific sequences of a given DNA molecule. During each cycle, two oligonucleotide primers (sense and reverse primer) bind to the heat-dissociated complementary DNA strands in opposite direction. Heat stable Taq-DNA polymerase then elongates the primers by attaching nucleotides that are complementary to the parent DNA strand (Mullis et al., 1986).

For details on protocols, programs and primers see tables below. The following controls were used for genotyping of the different mouse lines:

Synaptopodin-deficient mice: As a positive control, DNA from a heterozygous animal was used. As a negative control, no DNA was used. Wildtype alleles gave rise to a 500 bp product whereas mutant alleles gave rise to a 400 bp product.

Thy1GFP-M mice: As a positive control, DNA from a Thy1GFP-transgenic animal was used. DNA from a wildtype animal served as a negative control. Thy1GFP-positive alleles gave rise to a 380 bp product. No PCR product was obtained from wildtype alleles.

Thy1-ECFP/EGFP-Synaptopodin-transgenic mice: As a postive control, a mixture of Thy1-EGFP-Synaptopodin cDNA (2-3 ng) and tail tip DNA from a wildtype mouse was used. As a negative control, DNA from a wildtype animal was used. Transgenic alleles gave rise to a 901 bp (primer pair A) or 713 bp (primer pair B) product. No PCR product was obtained from wildtype alleles.

reaction mix	synaptopodin-deficient	Thy1GFP-M	Thy1-EGFP/ECFP-Synaptopodin
PCR mastermix (Qiagen)	12.5 µl	12.5 µl	12.5 µl
H_2O	7.5 µl	8.5 µl	8.5 µl
forward primer 1	1 µl	0.5 µl	1 µl
forward primer 2	1 µl	-	-
reverse primer	1 µl	0.5 µl	1 µl
DNA	2 µl	3 µl	2 µl

program	synaptopodin-deficient	Thy1GFP-M	Thy1-EGFP/ECFP-Synaptopodin, A	Thy1-EGFP/ECFP-Synaptopodin, B
denaturation	5 min, 94°C	3 min, 94°C	5 min, 94°C	5 min, 94°C
denaturation	1 min, 95°C	20 sec, 94°C	1 min, 95°C	1 min, 95°C
annealing	1 min, 65°C	20 sec, 60°C	1 min, 65°C	1 min, 62°C
elongation	1.5 min 72°C	25 sec, 72°C	1.5 min 72°C	1.5 min 72°C
cycles	40	35	35	35
elongation	10 min, 72°C	5 min, 72°C	10 min, 72°C	10 min, 72°C

primers	synaptopodin-deficient	Thy1GFP-M	Thy1-EGFP/ECFP-Synaptopodin, A	Thy1-EGFP/ECFP-Synaptopodin, B
forward primer 1	mSYNPWT: GCGGTGGGCTGA CTGTGGTGACT	GFP for: CGCACCATCTTC TTCAAGGACGAC	Thy-EGFP-for: TTTTGCCCTCTGC CCTCTGTTCTC	Synpo-PolyA-for: GCGGCCTTCCCT CTATGCTCTGTC
forward primer 2	mSYNPMU: CCAGCTGGCGAA AGGGGGATGTG	-	-	-
reverse primer	mSYNPWM: CAGGCGCAGGCA GAGGGTGAACG	GFP rev: AACTCCAGCAGG ACCATGTGATCG	Thy-EGFP-rev: TTGATGCCGTT CTTCTGCTTGTCG	Synpo-PolyA-rev: TCCTGCCTCCCCT ACCCACCATAC

Agarose gel electrophoresis

This method was used to separate DNA fragments according to their size. During gel electrophoresis, DNA molecules migrate along an electrical field through an agarose matrix. The distance traveled by a DNA molecule is inversely proportional to the logarithm of its size in basepairs. By comparison with a reference DNA of known size, the size of the DNA fragments can be determined. DNA is visualized by the addition of ethidium bromide, which intercalates between bases of nucleic acids. After excitation with UV light the DNA is visible as fluorescent bands due to the formation of fluorescent DNA/ethidium bromide complexes.

Protocol: Agarose (SeaKem® LE Agarose, Cambrex Bio Science, Rockland, ME, USA; final concentration of 0.8% - 1.5% according to separation range) were boiled in TBE buffer. The gel was then poured into an electrophoresis chamber and 1 µl of ethidium bromide (10 µg/ml, Appli Chem) was added. Samples were mixed with 1/5 volume of 6x sample buffer, loaded into the sample wells and separated for 1 h at 120 V (electrophoresis buffer TBE). Detection and documentation of the DNA band pattern was performd with an UV transilluminator (MWG Biotech, Ebersberg, Germany) and an electrophoresis documentation and analysis system (Kodak, Rochester, NY, USA).

3.8. Cloning

Transformation

Transformation is a method for introducing plasmid DNA into a bacterial host. The plasmid DNA is amplified by the synthesis machinery of the host and propagated to the daughter cells at each cell division. Transformed bacteria are selected based on resistance to selective antibiotics which is confered to them by the plasmid DNA.

plasmid used	antibiotic resistance
pEGFP-C1_SPfull	Kanamycin
pDsRed2-C1	Kanamycin
pECFP-C1	Kanamycin
pThy1.2	Ampicillin

Protocol: 50 µl of competent bacteria (XL-1 blue subcloning grade or SCS110 competent cells, Stratagene, La Jolla, CA, USA) were thawed on ice. Cells were then mixed with 10 ng plasmid or with 1/10 volume of a ligation reaction and incubated on ice for 20 min. After a heat-shock for 45 sec at 42°C, cells were cooled on ice for 2 min, mixed with 0.9 ml SOC and incubated on a shaker at 37°C for 1 h. Using sterile glass beads (Soda lime glass balls, 3 mm diameter, Sigma-Aldrich, St.Louis, MO, USA), 50 µl of the transformation mixture were then spread on an agar plate containing the selective antibiotic and incubated over night at 37°C to obtain single colonies.

Analytical plasmid preparation

This method was used to isolate plasmid DNA from bacteria for analytical restriction digests. The preparation was done using the QIAprep Spin Miniprep Kit (Qiagen, Hilden, Germany) according to the manufacturer's protocol.

Protocol: 5 ml LB-media containing a selective antibiotic were inoculated with a single bacterial colony and incubated over night at 37°C on a shaker. 2x 1.5 ml of the obtained

culture were transferred to an Eppendorf-tube and pelleted at 4°C for 1 min at 10,000 x g. The bacterial pellet was resuspended in 250 µl buffer P1. After addition of 250 µl lysis buffer (P2), tubes were inverted 5 times and incubated for 5 min at RT. By adding 350 µl of buffer P3, the pH of the solution was then neutralized and proteins as well as genomic DNA were precipitated. After centrifugation at 4°C for 10 min at 10,000 x g, the supernatant was applied to a spin column. After a centrifugation for 1 min at 4°C and 10,000 x g, the eluate was discarded and the column was washed with 750 µl wash buffer (PE). Wash buffer was removed completely by two centrifugation steps for 1 min at 4°C and 10,000 x g. Finally, columns were placed onto clean Eppendorf-tubes, 50 µl elution buffer (EB) were added to the center of the column and after incubation for 1 min, DNA was eluted by centrifugation for 1 min at 4°C and 10,000 x g. The eluted DNA was stored at -20°C.

Preparative plasmid preparation

This method was used to isolate larger amounts of plasmid DNA from bacteria for cloning. The preparation was done using the Plasmid Midi Kit (Qiagen) according to the manufacturer's protocol.

Protocol: A single colony was picked from a selective agar plate and a starter culture of 5 ml LB medium containing the appropriate selective antibiotic was inoculated. After an incubation for 8 h at 37°C, the starter culture was diluted 1/500 into a final volume of 25 ml selective LB medium and incubated over night at 37°C with vigorous shaking. On the next day, the bacterial cells were harvested by centrifugation at 6,000 x g for 15 min at 4°C. The pellet was resuspended in 4 ml buffer P1, mixed with 4 ml lysis buffer (P2), inverted 5 times and incubated for 5 min at RT. Lysis was stopped by addition of 4 ml chilled buffer P3. Samples were immediately mixed by inverting 5 times and were incubated on ice for 15 min to allow for precipitation of cell debris, proteins, genomic DNA and SDS. Samples were then centrifuged at 20,000 x g for 30 min at 4°C to pellet precipitated material. The supernatant was centrifuged again to remove any residual precipitate and then applied to an equilibrated QIAGEN-tip 100. The column was washed 2 times with 10 ml wash buffer (QC) and DNA was eluted with 5 ml elution buffer (QF). Next, DNA was precipitated by adding 3.5 ml isopropanol (RT) and centrifugation at 15,000 x g for 30 min at 4°C. The DNA pellet was the washed with 2 ml of 70% ethanol

(RT) to remove salts. After centrifugation at 15,000 x g for 10 min at 4°C, the pellet was air-dried for 5-10 min and resuspended in 50-100 µl TE buffer. DNA was stored at -20°C.

Endotoxin free plasmid preparation

For the transfection of eukaryotic cells, high quality plasmid DNA is needed. Because bacterial endotoxins significantly reduce transfection efficiency, the EndoFree Plasmid Maxi Kit (Qiagen) was used in this case. This procedure involves an incubation of the bacterial lysate with a special endotoxin removal buffer which inhibits the binding of endotoxins to the silica matrix of the purification column. The plasmid preparation was performed according to the manufacturer's instructions. The general procedure is identical to the Plasmid Midi Kit. Minor variations are: (1) The bacterial lysate is cleared with a QIAfilter cartridge, instead of centrifugation. (2) The filtered lysate is incubated with endotoxin removal buffer on ice for 30 min. (3) From the elution-step onwards, endotoxin-free plasticware has to be used.

Preparative restriction digest

Preparative restriction digest was used to cut vector- and insert-DNA for subsequent ligation. Restriction endonucleases bind to specific DNA-sequences and cut the double strand at specific positions. Depending on the enzymes used, the resulting DNA fragments can have 5'- or 3'-overhangs (sticky ends) or no overhangs (blunt ends). Whenever possible, enzymes producing compatible sticky ends were selected for the digestion of vector- and insert-DNA.

Protocol: Restriciton endonucleases were purchased from New England Biolabs (Frankfurt, Germany). For each enzyme, the supplied reaction buffer was used. For a restriction digest with two enzymes, the buffer yielding the highest possible activity for both enzymes was chosen. 3-10 µg of DNA were incubated with 5-10 units of enzyme / µg DNA in a total volume of 10-50 µl for 1-2 h at 37°C. Completeness of the restriction digest was checked by gel electrophoresis.

Blunting of DNA-ends

If no suitable restriction sites for the generation of compatible ends are present in the parent plasmids, a blunt end ligation has to be performed. Since the only available cloning site in the pThy1.2 vector is a XhoI site producing sticky ends, these ends had to be blunted after restriction. To this end, cut vector DNA was incubated, in the presence of deoxynucleotides, with the Klenow Fragment of DNA Polymerase I (New England Biolabs), which retains the polymerase activity but lacks the 3' → 5' and 5' → 3' exonuclease activity.

Protocol: 10 μg of cut vector DNA were incubated with 25 units of Klenow Fragment in NEB2 buffer (New England Biolabs) containing 33 μM deoxynucleotides in a total volume of 40 μl for 30 min at 25°C. The enzyme was then heat-inactivated for 20 min at 75°C.

Dephosphorylation of vector DNA

To avoid the religation of the compatible ends of digested vector DNA, the 5'-phosphate groups of the vector DNA were removed by incubation with shrimp alkaline phosphatase. Since the insert DNA still contains 5'-phosphate groups, vectors that have incorporated a copy of the insert can be closed during the ligation reaction.

Protocol: 500 ng of digested vector were incubated with 4 units of shrimp alkaline phosphatase (USB, Cleveland, OH, USA) in a total volume of 10μl for 20 min at 37°C. The enzyme was then heat-inactivated for 15 min at 65°C.

Isolation of DNA fragments from agarose gels

After a preparative restriction digest, the vector- and insert-DNA fragments required for ligation have to be separated from the unrequired fragments. Therefore, fragments were separated according to their size by gel electrophoresis. Subsequently, the desired fragments were isolated from the gel using the QIAquick Gel Extraction Kit from Qiagen. To purify DNA fragments for pronucleus injection, the GeneCleanII Kit from QBiogene (Carlsbad, CA, USA) was used.

Protocol for QIAquick Kit: The required DNA-band was excised from the gel using a clean scalpel blade and transferred to an eppendorf tube. The piece of gel was weighed and 3 volumes of buffer QG (100 mg gel ≈ 100 μl buffer) were added. The mixture was

incubated for 10 min at 50°C with thorough mixing every two minutes. After the piece of gel had dissolved completely, one volume of isopropanol was added and the sample was applied to a QIAquick column. Next, the column was centrifuged for 1 min at 10,000 x g and the eluate was discarded. Then, the bound DNA was washed by adding 750 µl buffer PE. The column was centrifuged for 1 min at 10,000 x g, the wash buffer was discarded and the column was centrifuged again. Finally, the column was placed onto a clean eppendorf tube and the DNA was eluted with 30 µl buffer EB by centrifugation for 1 min at 10,000 x g.

Protocol for GeneCleanII Kit: The required DNA-band was excised from the gel using a clean scalpel blade and transferred to an eppendorf tube. The gel slice was weighed and 0.5 volumes of TBE modifier plus 4.5 volumes of NaI solution were added (100 mg gel ≈ 100 µl buffer). The mixture was incubated for 5-10 min at 50°C with thorough mixing every two minutes to dissolve the agarose. 100 µl of freshly resuspended GLASSMILK® (suspension of proprietary silica matrix) were added and the sample was incubated at room temperature for 15 min while frequently mixing by hand. The GLASSMILK® with bound DNA was then pelleted by centrifugation for 2 min at 14,000 x g. Next, the pellet was washed with 500 µl NEW Wash. After centrifugation at 14,000 x g for 5 seconds, the supernatant was discarded and the wash step was repeated. The pellet was air dried for 5 min to remove residual ethanol. Finally, the DNA was eluted with 50 µl microinjection buffer. The sample was centrifuged for 30 seconds at 14,000 x g to pellet the GLASSMILK® and the supernatant was transferred to a clean eppendorf tube. DNA concentration was adjusted to 2-3 ng / µl by sequential dilution with microinjection buffer and ckecked by gel electrophoresis using standard markers to estimate the amount of DNA per lane.

Ligation

During the ligation reaction, T4-DNA ligase joins the 5'-phosphate- and the 3'-hydroxyl-groups of double stranded DNA fragments resulting in a phosphodiester bond. Prior to ligation, DNA fragmenst were purified by isolation from agarose gels. Vector- and insert-DNA were used in a molar ratio of 1:3 to 1:5. For each ligation, a negative control reaction without ligase was performed to determine the amount of clones containing undigested

vector-DNA. Ligations were performed using the Quick LigationTM Kit (New England Biolabs).

Protocol: 50 ng of vector were combined with a 3 to 5-fold molar excess of insert and the volume was adjusted to 10µl with ddH$_2$O. Then, 10 µl of 2x Quick Ligation Buffer were added and the sample was mixed. Finally, 1 µl of Quick T4 DNA Ligase was added and the sample was mixed again. After incubation for 5 min at 25°C, the mixture was chilled on ice and 2 µl were used for a single transformation

Analytical restriction digest

After ligation, clones containing the desired plasmid DNA were identified by an analytical restriction digest. Restriction endonucleases that produced a characteristic band pattern for plasmids containing the insert-DNA in the correct orientation were chosen for the reaction.

Protocol: Usually, 12-24 single colonies obtained from a transformation with the ligation reaction were picked and grown overnight in 5 ml LB medium containing a selective antibiotic. On the next day an analytical plasmid preparation was performed. 1 µl of the eluted DNA was incubated with 3 units of enzyme in the appropriate buffer in a total volume of 10 µl for 1 h at 37°C. The restriction digest was then analyzed by gel electrophoresis.

3.9. Transfection of primary hippocampal neurons

Transfection stands for the introduction of heterologous DNA into eukaryotic cells. Different transfection methods, using different transfection reagents like cationic polymers, cationic lipids or calcium phosphate, exist. In this thesis, a modified calcium phosphate co-precipitation method (Goetze et al., 2003) was used. Transfections were performed in the laboratory of Dr. Michael Kiebler in Vienna, during a short-term stay. 15 day old cultures of rat hippocampal neurons (prepared at embryonic day 17; Goetze et al., 2003) were supplied by the laboratory.

Protocol for transfection of neurons in a 3 cm petri dish: Cells were transferred to transfection medium (pH 7.5) and kept at 36.5°C without CO$_2$-supply. Then, 6 µl of 2.5 M CaCl$_2$ were mixed with 51 µl H$_2$O. The DNA was diluted to 1 µg/µl in H$_2$O and 3 µl of DNA were added to the CaCl$_2$ solution and mixed well. Next, 60 µl of transfection buffer

(pH 7.2) were added to the DNA/CaCl$_2$ solution drop wise. The reaction tube was gently shaken each time after addition of three drops of BES. The solution was further mixed 10 times by blowing air bubbles into the solution with a pipette. Then, the solution was immediately added drop wise to the cells. Thereafter, cells were incubated at 36.5°C in a humidified incubator without CO2-supply and checked for formation of DNA/calcium phosphate co-precipitate under a light microscope every 20-30 min. Neurons were washed with prewarmed transfection buffer for 5-10 min at 36.5°C and cells were transferred to culture medium and incubated for the desired time (usually over night).

3.10. Digital illustrations

Confocal images were exported from the Zeiss LSM image browser and stored as TIFF files. Conventional fluorescence images were acquired using an attached Spot2 digital camera (Diagnostic Instruments, Sterling Heights, MI, USA) and stored as TIFF files. Figures were prepared using Photoshop 6.0 graphics software (Adobe, San Jose, CA, USA). Image brightness, contrast and sharpness were adjusted.

3.11. Buffers, media, solutions

Cultivation medium for primary neurons (NMEM-B27)	MEM (Invitrogen) supplemented with 1 mM sodium pyruvate (Sigma), 15 mM HEPES (Invitrogen), 2 mM stable L-glutamine (PromoCell), 1x B27 supplement (Invitrogen), 0.22% NaHCO$_3$ (Invitrogen), and 10 mM D-glucose (Sigma-Aldrich)
Cultivation medium for slice cultures	50% MEM, 25% basal medium eagle (BME, Gibco, cat.no. 41010-026), 25% heat-inactivated normal horse serum, 25 mM HEPES buffer (Invitrogen), 0.15% sodium bicarbonate (Sigma-Aldrich), 0.65% glucose (Sigma-Aldrich), 0.1 mg/ml streptomycin (Sigma-Aldrich), 100 U/ml penicillin (Sigma-Aldrich), and 2 mM glutamax (Invitrogen). Adjust pH to 7.3 with 1 M NaOH.
Electrophoresis buffer for SDS-PAGE	dilute 10x stock solution (Bio Rad) with ddH$_2$O to get 1x working solution (25 mM Tris, 192 mM glycine, 0.1% w/v SDS, pH 8.3)
Homogenization buffer for protein extraction	20 mM Tris, 500 mM NaCl, pH 7.5 supplemented with 0.5% Chaps (Sigma-Aldrich), 5 mM EDTA and the following protease inhibitors (Serva, Heidelberg, Germany): 2 µM Pepstatin, 2 µM Leupeptin, 200 µM Pefabloc.
Imaging buffer	129 mM NaCl, 4 mM KCl, 1 mM MgCl$_2$, 2 mM CaCl$_2$, 4.2 mM glucose, 10 mM HEPES, 0.1 mM Trolox (Sigma-Aldrich, cat.no. 56510), 0.1 mg/ml streptomycin, 100 U/ml penicillin. Adjust pH to 7.4 with 1 M NaOH. Adjust osmolarity to 365 mOsm/kg with sucrose.

LB-Agar	LB medium containing 14% agar was prepared by boiling LB-Agar Tablets (Sigma-Aldrich) in an appropriate amount of water (50 ml per tablet).
LB medium	1% Bacto®-tryptone (Sigma-Aldrich), 0.5% Bacto®-yeast extract (Sigma-Aldrich), 1% NaCl, pH 7.5, autoclaved
Microinjection buffer	5 mM Tris, 0.15 mM EDTA, pH 7.4
Phosphate buffered saline (PBS)	solution 1: 0.1 M Na_2HPO_4 (17,79 g/l) solution 2: 0.1 M NaH_2PO_4 (13,78 g/l) mix solutions to get pH 7.4 (ca. 900 ml solution 1 + 100 ml solution 2), add 0.9% NaCl
Preparation medium for slice cultures	Minimal essential medium (MEM, Gibco, cat.no. 21575-022) containing 2 mM glutamax, 0.45% glucose, 0.1 mg/ml streptomycin, 100 U/ml penicillin and 25 mM HEPES buffer. Adjust pH to 7.4 with 1 M NaOH.
Sample buffer for agarose gel electrophoresis	30% (v/v) glycerol, 0.25% (w/v) bromophenol blue
Sample buffer for SDS-PAGE	950 µl Laemmli sample buffer (62.5 mM Tris-HCl pH 6.8, 25% glycerol, 2% SDS, 0.01% bromphenol blue, Bio Rad), 50 µl β-mercaptoethanol (Appli Chem)
Separating gel buffer (Bio Rad)	1.5 M Tris-HCl, pH 8.8

SOC medium	2% Bacto®-tryptone (Sigma-Aldrich), 0.5% Bacto®-yeast extract (Sigma-Aldrich), 10 mM NaCl, 2.5 mM KCl, 10 mM MgCl$_2$, 10 mM MgSO$_4$, 20 mM glucose, pH 7.0, autoclaved
Stacking gel buffer (Bio Rad)	0.5 M Tris-HCl, pH 6.8
TBE buffer (Appli Chem)	Dilute 5x stock solution to get 1x working solution (90 mM Tris, 90 mM boric acid, 20 mM EDTA).
TBS-Tween	Tris buffered saline (TBS) containing 0.1% Tween-20
TE buffer	10 mM Tris, pH 8.0, 1 mM EDTA
TNES buffer	50 mM Tris, 50 mM EDTA, 100 mM NaCl, 1% (w/v) SDS
Transfection buffer	50 mM BES (N,N-Bis(2-hydroxyethyl)-2-aminoethanesulfonic acid, Merck) in H$_2$O
Transfection medium	Same as cultivation medium for primary neurons but without NaHCO$_3$
Transfer buffer for Western Blot	25 mM Tris, 192 mM glycine, 20% methanol
Tris buffered saline (TBS)	0.05 M Tris (Appli Chem), 0.9% NaCl in H$_2$O, pH 7.4

4. Results

4.1. Distribution of synaptopodin in hippocampal neurons

Previous studies have reported an uneven distribution pattern of synaptopodin in the adult rodent hippocampus (Deller et al., 2000a; Deller et al., 2002). This differential distribution was not analyzed quantitatively, however. Furthermore, synaptopodin was shown to be present in a subset of dendritic spines in the rodent telencephalon (Deller et al., 2000a). It remained unclear, however, which percentage of dendritic spines contains synaptopodin and whether this number is constant throughout the hippocampus.

Thus, to obtain a detailed understanding of the distribution of synaptopodin in the mouse hippocampus, a set of immunohistochemical experiments was performed.

4.1.1. Synaptopodin-immunostaining in the mouse hippocampus

Synaptopodin immunofluorescence-labeling of mouse hippocampus revealed regional and laminar differences in the distribution of synaptopodin protein (Fig. 4 A-D), as previously described (Deller et al., 2002). Using high magnification confocal laser scanning microscopy, synaptopodin-immunostaining was resolved into single immunofluorescent puncta, which could readily be distinguished (Fig. 4 E). Similarly, laminar differences in synaptopodin-immunostaining were revealed as differences in synaptopodin puncta-densities (Fig. 5 A-D).

4.1.2. Synaptopodin and synaptophysin double-immunofluorescence staining

To exclude a presynaptic localization of synaptopodin, double-immunofluorescence for synaptopodin and the presynaptic marker molecule synaptophysin was performed. Synaptophysin-positive terminals and synaptopodin-positive puncta were frequently opposed, suggesting that these two structures are part of the same axo-spinous synapse (Fig. 5 E, F). This relationship was especially impressive in stratum lucidum of area CA3, where specialized axon terminals are formed by the granule cell axons, the mossy fibers. These terminals form very large boutons, which engulf specialized spines of CA3 pyramidal cells, the so called thorny excrescences (Amaral and Witter, 1995). These spines
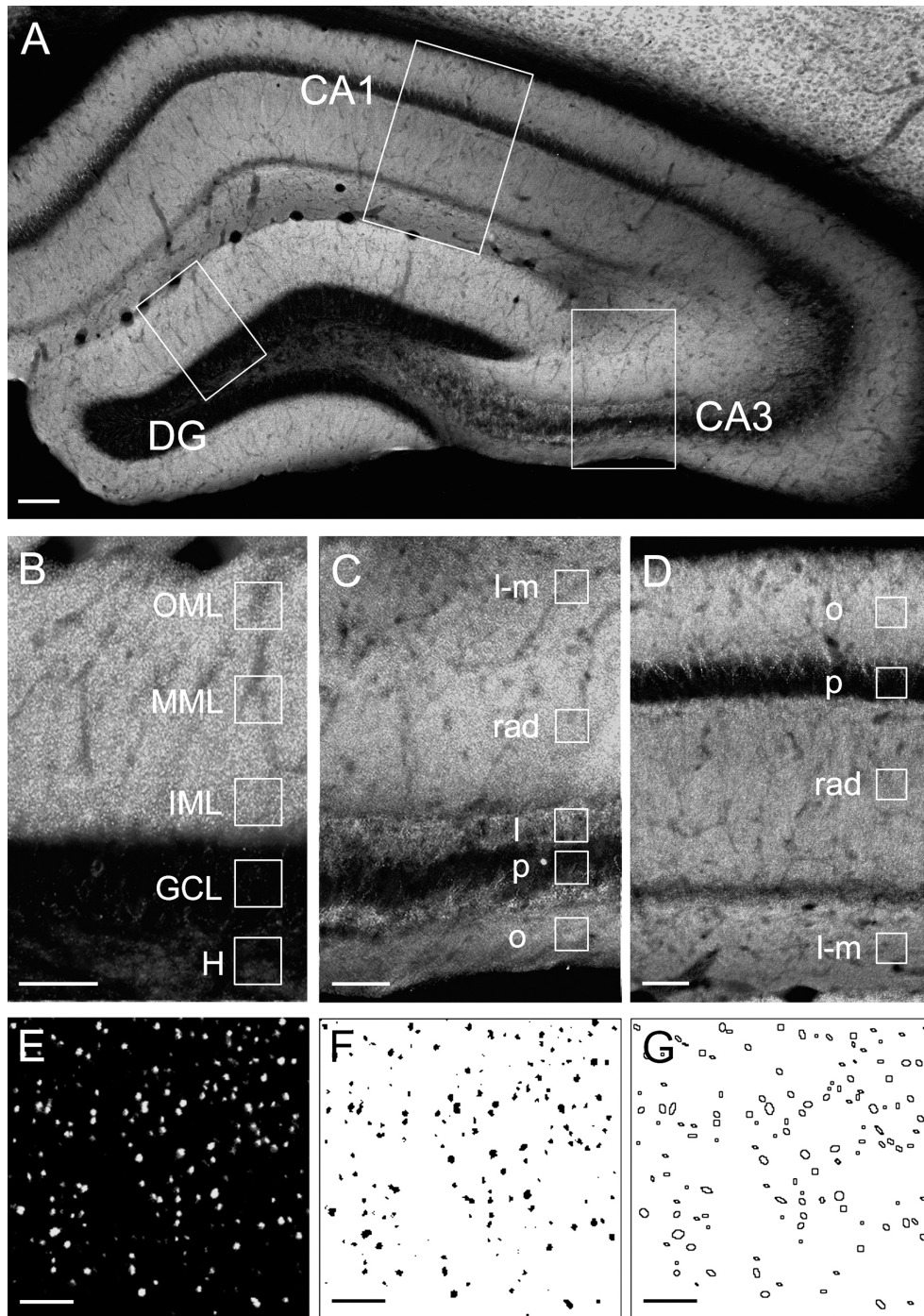
Figure 4. Heterogeneous synaptopodin puncta-densities in the mouse hippocampus.
A: Frontal section of mouse hippocampus stained for synaptopodin. Note layer- and region-specific differences in synaptopodin-immunoreactivity. **B-D:** Higher magnification photographs of the areas indicated in A, corresponding to dentate gyrus (B), area CA3 (C) and area CA1 (D). The densities of synaptopodin-positive puncta in different hippocampal layers were determined in representative areas (30 μm x 30 μm x 1 μm), indicated by frames in B,C,D. **E:** Higher magnification confocal image, showing single immunoreactive puncta, taken from the IML. **F:** Binary image of E, generated with the image analysis software by defining a lower threshold. Objects with lower intensity values than the threshold were set equal to background. **G:** Image showing the outlines of all particles, which were counted by the software. GCL, granule cell layer; H, hilus; IML, inner molecular layer; l, stratum lucidum; l-m, stratum lacunosum-moleculare; MML, middle molecular layer; o, stratum oriens; OML, outer molecular layer; p, stratum pyramidale; rad, stratum radiatum. Scale bars: A = 100 μm; B-D = 50 μm; E-G = 5 μm.
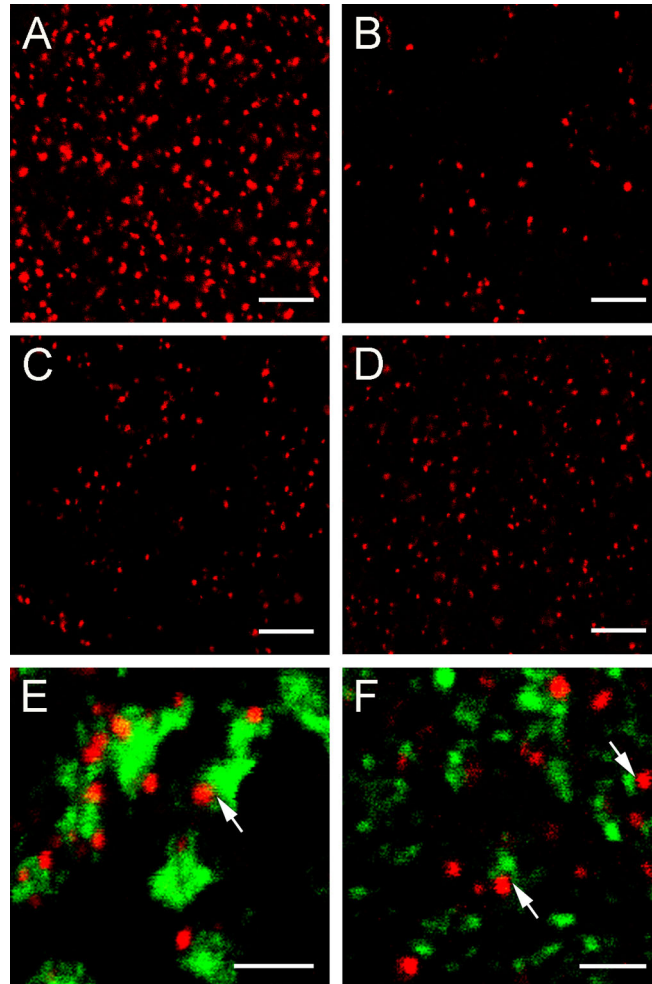
Figure 5. Laminar differences in synaptopodin puncta-densities in the mouse hippocampus.
A-D: High magnification confocal images, showing single synaptopodin-positive puncta, taken from the middle molecular layer (A), hilus (B), stratum lucidum of area CA3 (C), and stratum radiatum of area CA1 (D). Differences between layers are clearly visible. **E-F:** Double-immunolabeling for synaptopodin (red) and synaptophysin (green) in stratum lucidum of area CA3 (E) and stratum radiatum of area CA1 (F). Note close apposition of synaptopodin- and synaptophysin-positive structures (arrows). Synaptophysin-positive structures in E are large mossy fiber boutons in contact with complex spines of CA3 pyramidal cells.
Scale bars: A-D = 5 µm; E-F = 2 µm.

almost invariably contain a spine apparatus in one or more of their finger-like processes (Hamlyn, 1962; Deller et al., 2000a; Capani et al., 2001). Double-immunofluorescence for synaptopodin and synaptophysin nicely revealed the relationship between the mossy fiber boutons and the spine apparatus containing synaptopodin-positive thorny excrescences (Fig. 5 E). In none of these cases, however, a colocalization of the two markers was observed. Thus, synaptopodin-positive puncta are not located in presynaptic boutons but correspond to postsynaptic structures, most likely spine apparatus organelles.

4.1.3. Quantification of synaptopodin-immunoreactive puncta-densities - methodological aspects

Because synaptopodin-immunoreactive puncta were clearly distinct, a computer-based image analysis program (ImageJ) was employed to verify and quantify the layer-specific differences in synaptopodin puncta-densities (Fig. 4 F, G). Although computerized image analysis programs are highly convenient and widely used tools for quantitative analysis in many fields of science, they need to be carefully validated and standardized prior to analysis. Especially, the parameters chosen for analysis may influence the numerical value of the data set. Thus, the image analysis method was validated for synaptopodin-immunolabeling and a series of methodological experiments, in which threshold level (background suppression) and pixel size (automatic particle detection) were systematically altered, was performed (data not shown). These experiments revealed that the absolute values obtained for synaptopodin-puncta-densities noticeably depended on the parameters chosen by the investigator, i.e. the biological interpretation of the image. In contrast, relative differences between layers were robust within a very broad range of parameters (threshold level: 10-200; pixel size: 1-10) and remained statistically significant at comparable error levels. Therefore, absolute density values obtained with this method should be regarded with some caution. The relative differences between the layers, however, are fairly independent of these variables and, thus, reliable.

4.1.4. Quantitative analysis of synaptopodin-immunoreactive puncta-densities

Synaptopodin-densities were obtained for each layer and tested for significance against all other layers within a given subfield. In the following, the data are given as mean number of

puncta per 1000 µm³ ± 2 x SEM for each layer. All data were obtained in the dorsal hippocampus (see Methods).

In the dentate gyrus (Fig. 6 A), the number of synaptopodin-immunoreactive puncta was highest in the molecular layer, i.e. the zone of the granule cell dendrites. Interestingly, differences between the two major zones of the molecular layer could be detected: The number of synaptopodin-positive puncta was significantly higher in the middle and outer molecular layer, the "entorhinal zone" of the dentate gyrus (252.7 ± 11.8 and 238.4 ± 14 puncta per 1000 µm³ ± 2 x SEM, respectively), compared to the inner one third, the "hippocampal zone" of the dentate gyrus (163.5 ± 9.5). Only few immunoreactive puncta were counted in the hilus (32.2 ± 5.1) and even less were found in the granule cell layer (5.8 ± 1.4). No significant differences were found between the supra- and infrapyramidal blade of the dentate gyrus (data not shown).

In hippocampal subfield CA3 (Fig. 6 B), the numbers of synaptopodin-positive puncta in the dendritic fields were within the range of those found in the molecular layer of the dentate gyrus: stratum oriens (198.7 ± 28.9) and stratum radiatum (232.3 ± 22.1). Although numbers were not significantly different between these layers, the highest number of puncta was observed in the stratum radiatum. Stratum lucidum (122 ± 12.5) and stratum lacunosum-moleculare (183.5 ± 32.5) showed significantly less synaptopodin-positive puncta than stratum radiatum. The number of synaptopodin-positive puncta in stratum pyramidale (12.8 ± 4.1) was slightly, but significantly higher than the number of puncta found in the granule cell layer of the dentate gyrus.

In area CA1 (Fig. 6 C), only the number of synaptopodin-positive puncta in stratum lacunosum-moleculare (220 ± 38.9) was within the range of those found in the molecular layer of the dentate gyrus or in stratum radiatum and stratum oriens of CA3. In stratum oriens (102 ± 22.4) and stratum radiatum (152.3 ± 30) the number of synaptopodin-positive puncta was significantly lower compared to the same layers of area CA3. The number of synaptopodin-positive puncta in stratum pyramidale (6.5 ± 2.1) was similar to the number found in the granule cell layer of the dentate gyrus.
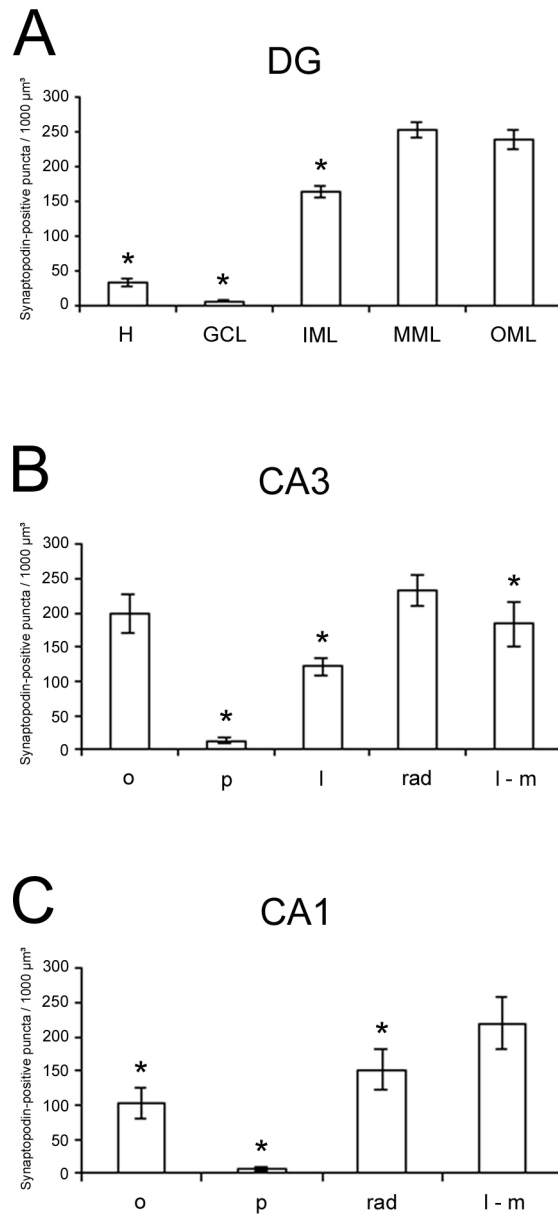
Fig. 6. Layer- and region-specific distribution of synaptopodin.
Mean densities of synaptopodin-positive puncta per 1000 μm^3 (± 2 SEM) are shown for the different layers of **A:** dentate gyrus (DG), **B:** hippocampal area CA3, and **C:** area CA1. In each subfield, the layer with the highest puncta-density was tested against the other layers of the same subfield. Asterisks indicate significant differences in puncta-densities between the subfield layers. GCL, granule cell layer; H = hilus; IML = inner molecular layer; l, stratum lucidum; l-m, stratum lacunosum-moleculare; MML, middle molecular layer; o, stratum oriens; OML, outer molecular layer; p, pyramidal cell layer; rad, stratum radiatum.

4.1.5. Cellular distribution of synaptopodin-positive structures in hippocampal principal cells

The cellular distribution of synaptopodin was determined using synaptopodin-immunostained hippocampal sections of Thy1GFP-M transgenic mice (Feng et al., 2000). These mice express enhanced green fluorescent protein (EGFP) in a subset of principal neurons of the hippocampal formation. EGFP-positive neurons are intensely fluorescent and their dendrites are stained in a Golgi-like manner.

This analysis was limited to hippocampal principal cell types that were EGFP-labeled in the transgenic mouse strain: dentate granule cells, CA3 pyramidal cells, and CA1 pyramidal cells. The morphology of these neurons is indistinguishable from the morphology of hippocampal neurons found in controls (M. Vuksic, D. Del Turco, T. Deller, unpublished observations). Dendritic segments of identified cells were analyzed in the various hippocampal laminae using three-dimensional reconstruction methods (Fig. 7 A-D; Fig. 8).

First, the location of synaptopodin-positive structures within single neurons was clarified. Although previous electron microscopic studies had primarily revealed synaptopodin in spines where it was associated with the spine apparatus, synaptopodin immunoreactivity was also observed in the dendritic shafts of some neurons (Deller et al., 2000a; Deller et al., 2002). Using three-dimensional confocal analysis (Fig. 7 C; Fig. 8 B, D) of synaptopodin-positive structures within EGFP-labeled dendrites, more than 95% of synaptopodin-positive puncta within a dendritic segment were found to be located in spines rather than the dendritic shaft (Table 1). This was the case for all laminae, with the notable exception of stratum lacunosum-moleculare of area CA1 where 18.5% of synaptopodin-positive puncta were found in dendritic shafts. Interestingly, synaptopodin-positive puncta were located at variable positions within spines (Fig. 7 C): Some were found exclusively in the spine head, others extended from the spine head into the neck, whereas again others were found in the spine neck or extended from the spine neck into the dendritic shaft.

Table 1: Percentage of synaptopodin-positive puncta in dendritic shafts and spines (mean ± SEM)

Area	DG		CA3			CA1		
Layer	IML	OML	o	rad	l-m	o	rad	l-m
n	333	477	161	198	170	108	114	118
Spine [%]	97.9 ± 0.4	97.9 ± 1.9	95.2 ± 0.9	96.9 ± 3.1	96.2 ± 2.6	97.7 ± 2.1	100 ± 0.0	81.5 ± 2.1
Shaft [%]	2.1 ± 0.4	2.1 ± 1.9	4.8 ± 0.9	3.1 ± 3.1	3.8 ± 2.6	2.3 ± 2.1	0 ± 0.0	18.5 ± 2.1
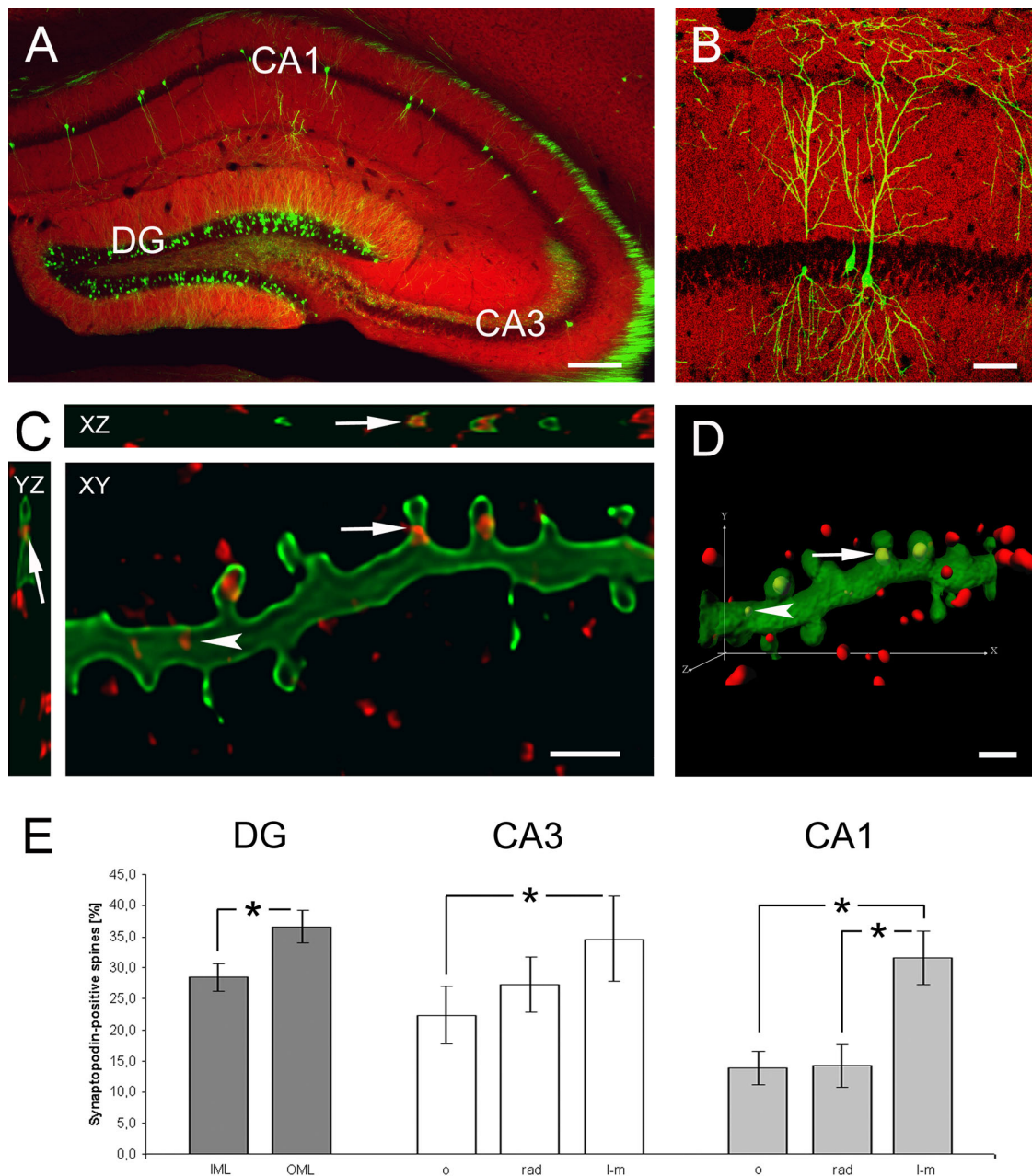
Figure 7. Laminar distribution of synaptopodin-positive puncta in dendritic segments of identified hippocampal principal cells.
A: Frontal section of the hippocampus (Thy1GFP-transgenic mouse) stained for synaptopodin (red). Several EGFP-labeled neurons (green) are visible in the dentate gyrus (DG), in subfield CA3, and in subfield CA1.
B: Higher magnification of EGFP-labeled neurons in area CA1. The entire dendritic arbor of EGFP-labeled neurons is stained in a Golgi-like fashion. **C:** Three-dimensional analysis of identified dendritic segments was performed using confocal imaging. The intracellular location of synaptopodin-puncta could be resolved by analyzing single sections from a confocal image stack in the XY-, XZ- and YZ-planes. In this pyramidal cell dendrite (CA1, stratum oriens), several synaptopodin-positive puncta are located in spines. The arrows indicate a synaptopodin-positive structure located within a spine neck. Occasionally, synaptopodin-positive puncta were found in dendrites (arrowhead). **D:** Three-dimensional reconstruction of the dendritic segment shown in C. Synaptopodin-positive structures located within the EGFP-labeled neuron are coded in yellow.
E: Percentage of synaptopodin-positive spines (± 2 SEM) in identified dendritic segments (IML, inner molecular layer; l-m, stratum lacunosum-moleculare; o, stratum oriens; OML, outer molecular layer; rad, stratum radiatum). Asterisks indicate significant differences between the layers. DG, dentate gyrus; area CA3, and area CA1.
Scale bars: A = 200 µm; B = 50 µm; C,D = 1 µm.
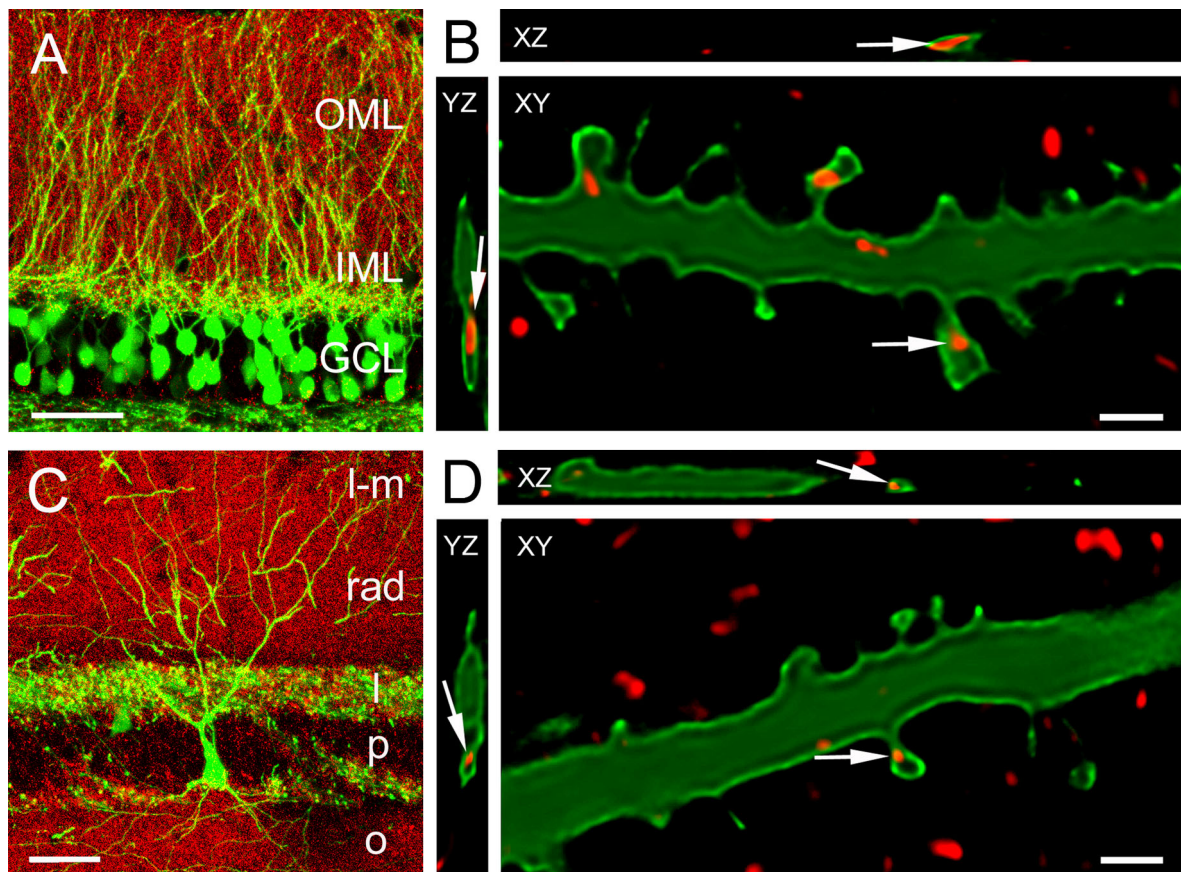
Figure 8. Distribution of synaptopodin-positive puncta in dendritic segments of EGFP-labeled granule cells and CA3 pyramidal cells.

A: Portion of the dentate gyrus of a Thy1GFP-transgenic mouse stained for synaptopodin (red). Numerous granule cells in the granule cell layer (GCL) are EGFP-labeled (green). A dendritic segment located in the outer two-thirds of the molecular layer (OML) is illustrated in B. **B:** Higher magnification of an EGFP-labeled granule cell dendrite in the OML. Single sections from a confocal image stack in XY-, XZ- and YZ-plane, respectively. Arrows point to a synaptopodin-positive dot located within a large spine. **C:** Portion of hippocampal subfield CA3 stained for synaptopodin. An EGFP-labeled pyramidal cell is illustrated. Note the EGFP-positive mossy fiber boutons in stratum lucidum (l). A dendritic segment located in stratum radiatum (rad) is illustrated at higher magnification in D. **D:** Higher magnification of an EGFP-labeled granule cell dendrite in stratum radiatum. Single sections from a confocal image stack in XY-, XZ- and YZ-plane, respectively. The arrows indicate a synaptopodin-positive structure located within a spine neck. IML, inner molecular layer; l-m, stratum lacunosum-moleculare; o, stratum oriens; p, stratum pyramidale.
Scale bars: A,C = 50 µm; B, D = 1 µm.

4.1.6. Laminar distribution of synaptopodin-positive spines along hippocampal principal cell dendrites

Next, the percentage of dendritic spines containing a synaptopodin-positive structure was determined. For this analysis, the same data set as outlined in the previous paragraph was used and the dendritic spine population was analyzed. Significant layer-specific differences in the percentage of synaptopodin-positive spines were revealed (Fig. 7 E). The highest percentage of synaptopodin-positive spines was found in the outer and middle molecular layer of the dentate gyrus, where 36.6% of all spines contained synaptopodin. The lowest percentage of synaptopodin-positive spines was found in stratum oriens of CA1, where only 13.9% of all spines contained a synaptopodin-positive structure. Thus, the percentage of synaptopodin-positive spines was 2.5 times higher in some dendritic segments compared to others. In CA1 a similar relationship was found even between different dendritic segments of the same cell type: The percentage of synaptopodin-positive spines was almost 2.3 times higher in stratum lacunosum-moleculare (31.7%) compared to stratum radiatum (14.3%) and stratum oriens (13.9%).

4.1.7. Presence of synaptopodin in dendritic spines of hilar mossy cells

Immunolabeling for synaptopodin revealed sparse immunoreactive-puncta in the hilus of the hippocampus (see above). In this area, the hilar mossy cell is the most common spine-bearing cell type (Amaral, 1978; Ribak et al., 1985; Frotscher et al., 1991; Soriano and Frotscher, 1994). Mossy cells are large glutamatergic neurons that innervate the inner molecular layer of the dentate gyrus (Soriano and Frotscher, 1994). They have been called "mossy" cells because their proximal dendrites are covered by numerous complex spines which give these dendrites the appearance of "tree branches covered with moss" (Ribak et al., 1985; Frotscher et al., 1991). These complex spines consist of multiple heads connected to the dendritic shaft by a single neck. Based on the distribution pattern of synaptopodin in the hilus, it was hypothesized that the synaptopodin-positive puncta observed in this hippocampal subfield are located within spines of mossy cells. To test this hypothesis, hippocampal sections of EGFP-mice were immunostained for synaptopodin and EGFP-expressing mossy cells were analyzed by confocal microscopy. Using this approach it could be shown that a substantial number of mossy cell dendritic spines contained synaptopodin-positive structures (Fig. 9). Often, two or more heads of a complex
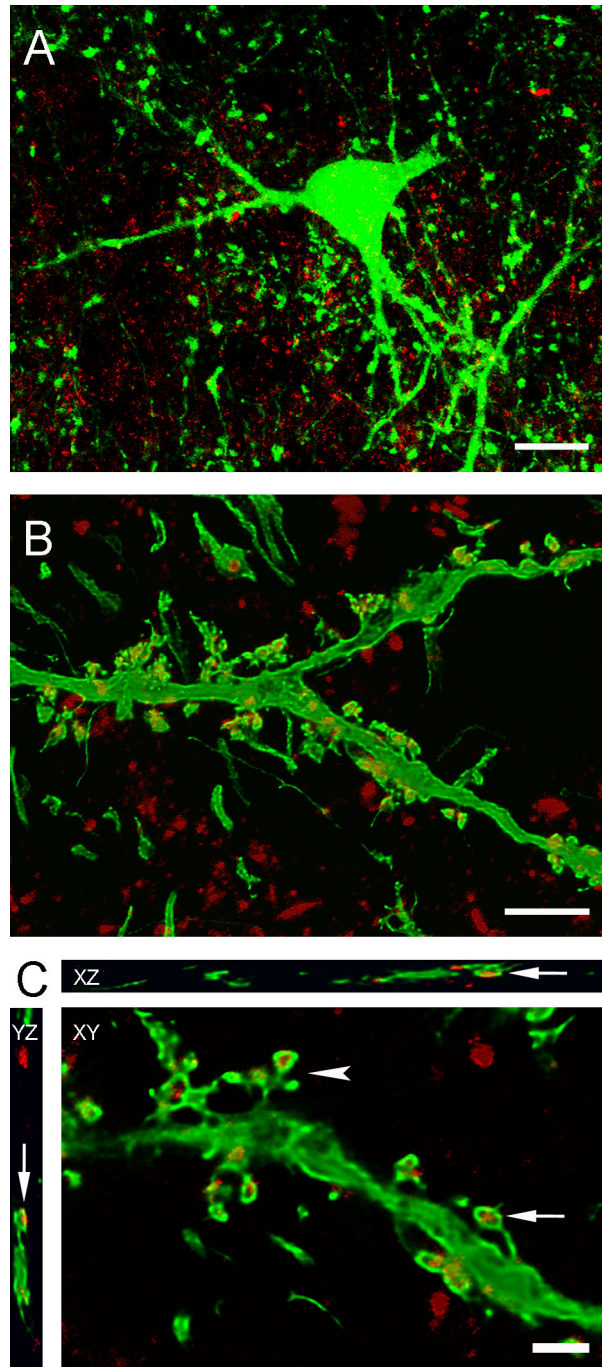
Figure 9. Synaptopodin-immunolabeling of EGFP-positive mossy cells.
A: Maximum intensity projection of a confocal image stack, showing an EGFP-positive mossy cell (green) in the hilus of a Thy1GFP-transgenic mouse. Note sparse synaptopodin-immunolabeling (red) in the vicinity of the cell. **B:** Maximum intensity projection of a mossy cell dentritic segment (green), showing numerous dendritic spines. Almost every spine is labeled with synaptopodin (red). **C:** Single optical sections of a part of the dendrite shown in B. A synaptopodin-positive spine is shown in the XY-, XZ- and YZ-plane (arrows). Note complex spine with a single neck and several heads (arrowhead). Two spine heads in this optical section contain synaptopodin.
Scale bars: A = 20 µm; B = 5 µm; C = 2 µm.

spine were positive for synaptopodin (Fig. 9 C). Because EGFP-positive mossy cells are rare in tissue from Thy1GFP mice, and because mossy cell dendrites are not oriented in a laminar fashion, this cell type was not included in the quantitative analysis described above.

4.1.8. Presence of synaptopodin in axon initial segments of principal neurons

In addition to the intense labeling of dendritic layers, synaptopodin-immunoreactivity could also be observed in cellular layers of the hippocampus (Deller et al., 2000a; this study). This staining could either be attributed to dendrites traversing the cellular layers or to an axonal localization of synaptopodin. To test whether synaptopodin is present in axons, immunofluorescence-labeling for synaptopodin and the membrane adaptor protein βIV-spectrin, a marker for the AIS (Berghs et al., 2000; Bennett and Baines, 2001) were combined. Confocal analysis of double-labeled brain sections revealed one or more synaptopodin-positive puncta within βIV-spectrin-positive profiles in the fascia dentata, in hippocampal subfields CA3 and CA1, and in the neocortex (Fig. 10). Synaptopodin-positive puncta located within βIV-spectrin-labeled AIS were significantly larger and more elongated than synaptopodin-puncta observed in dendritic layers (data not shown). To quantify synaptopodin-puncta in AIS, puncta were segmented on single confocal sections using the ImageJ software as described above (4.1.3.; see methods). Then, the number of puncta was determined in randomly selected βIV-spectrin-positive AIS-profiles (n=100). This analysis revealed 3.2 ± 0.9 (mean ± SD) synaptopodin-puncta per 10 μm of AIS. In the principal cell layers of the hippocampus the vast majority of synaptopodin-puncta was localized to βIV-spectrin-positive AIS, indicating that dendritic synaptopodin contributes little to the immunoreactivity observed in these layers.

To analyze whether synaptopodin is restricted to the AIS or whether it can also be found in more distal portions of the axon, brain sections from Thy1-GFP transgenic mice (Feng et al., 2000; Bas Orth et al., 2005) were employed and stained for βIV-spectrin as well as for synaptopodin. In these sections, individual hippocampal principal neurons and their axons are EGFP-positive, which makes it possible to localize synaptopodin in different portions of the axon. Again, the AIS was positive for βIV-spectrin and contained several synaptopodin-immunoreactive puncta (Fig. 11). In contrast, βIV-spectrin negative portions
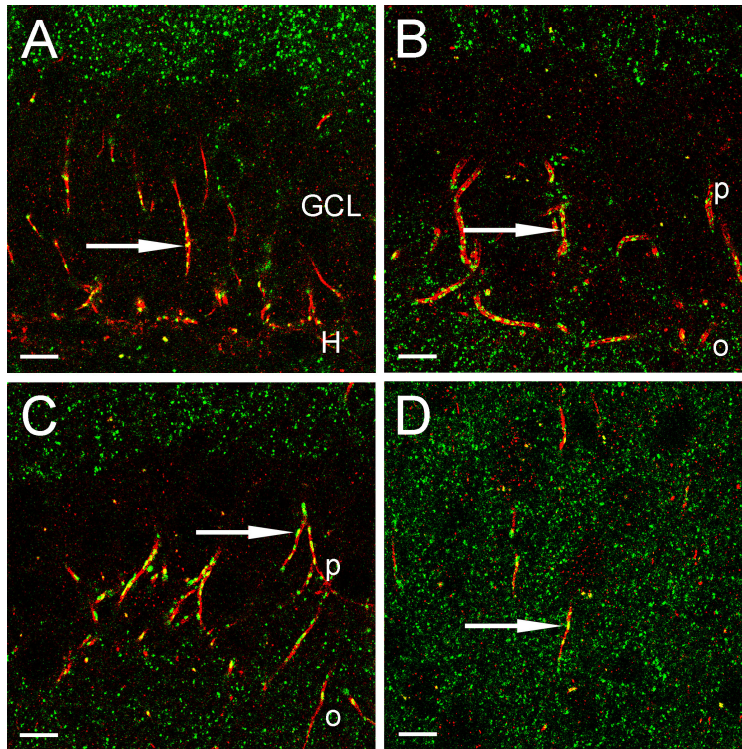
Fig. 10. Synaptopodin is present in axon initial segments.

Double immunofluorescence-labeling for synaptopodin (green) and βIV-spectrin (red) reveals numerous synaptopodin positive puncta within each axon initial segment in **A:** dentate gyrus, **B:** hippocampal area CA3, **C:** area CA1, and **D:** cerebral cortex. Images represent single confocal sections. GCL = granule cell layer, H = hilus, l = stratum lucidum, ML = molecular layer, o= stratum oriens, p = stratum pyramidale, rad = stratum radiatum. Scale bars: A-D = 10 μm.
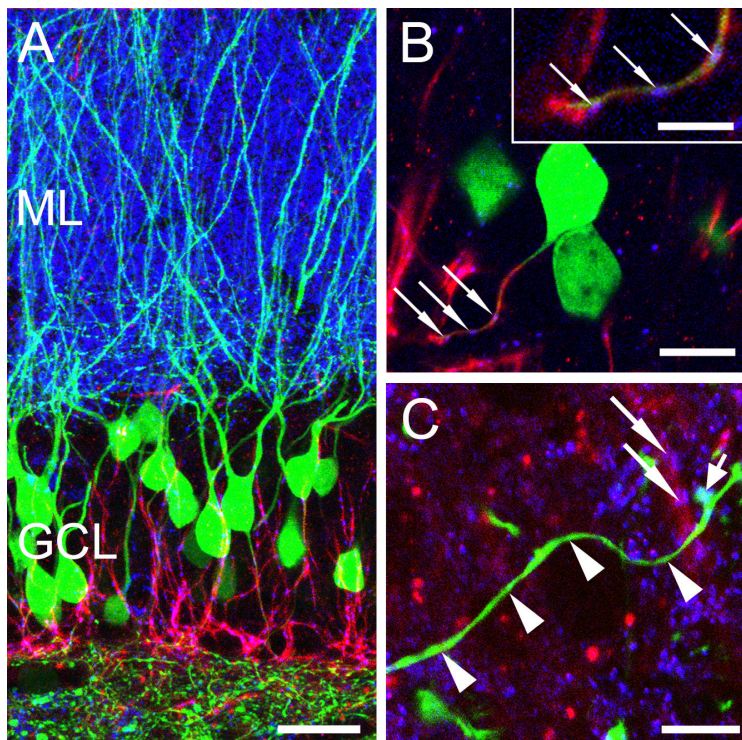
Figure 11. Axonal synaptopodin is restricted to the initial segment. Sections from Thy1-GFP transgenic mice were labeled for βIV-spectrin (red) and synaptopodin (blue). **A:** A portion of the fascia dentata is illustrated. Note abundant labeling for synaptopodin in the molecular layer (ML) and the string-like arrangement of synaptopodin-immunopositive puncta in the granule cell layer (GCL). **B:** A dentate granule cell (green) is illustrated at high magnification. The proximal portion of the axon is βIV-spectrin positive and contains three synaptopodin-puncta (arrows, see inset). **C:** A distal granule cell axon (green, arrowheads) in stratum lucidum of hippocampal area CA3 is illustrated. No synaptopodin-immunolabeling was observed in distal axons. Note presynaptic bouton making contact with synaptopodin-positive spines (small arrow) and βIV-spectrin-positive AIS of a CA3 pyramidal neuron, containing synaptopodin-puncta (large arrows).
Scale bars: A, inset in B = 25 μm; B,C = 10 μm.

51

of the axon, i.e. more distal portions of the axon, were devoid of synaptopodin (Fig. 11). Thus, axonal synaptopodin appears to be restricted to the AIS.

4.1.9. Ultrastructural localization of axonal synaptopodin

In dendritic spines, synaptopodin is tightly associated with a specific subcellular organelle, the spine apparatus. Therefore, it was hypothesized that synaptopodin could also be associated with a specific subcellular structure in the AIS. To test this hypothesis, preembedding immunogold-labeled sections of mouse hippocampus were analyzed using electron microscopy. In these sections, AIS could be distinguished based on the dense undercoating of their plasma membrane. Synaptopodin-immunoreactivity in AIS was closely associated with cisternal organelles (Fig. 12 A), where it predominantly labeled the dense plates that interdigitate the cisterns of endoplasmic reticulum. This ultrastructural localization very much resembled the situation in dendritic spines (Fig. 12 B), where synaptopodin is associated with the dense plates of the spine apparatus (Deller et al., 2000a).

4.1.10. Lack of cisternal organelles in synaptopodin deficient mice

The tight association of synaptopodin with the cisternal organelle raised the question whether synaptopodin is essential for its formation, as has been demonstrated for the spine apparatus (Deller et al., 2003). To address this issue, AIS of wildtype and synaptopodin-deficient mice were analyzed and the relative frequency of cisternal organelles within AIS profiles was quantified. To verify the detection of AIS in ultrathin sections, an antiserum against phosphorylated IκBα (Ser32), a robust marker for the AIS that can be used for electron microscopic studies (Schultz et al., 2006; Fig. 13) was employed.

The DAB-immunoprecipitate labeled the cytoplasm within the AIS in wildtype as well as synaptopodin-deficient mice (Fig. 13). Of note, cisternal organelles were not obscured by the DAB-immunoprecipitate and could readily be detected in wildtype specimens (Fig 13 B). In hippocampal area CA1 of wildtype mice, 4.6 ± 1.0 (mean $\pm$ SEM) cisternal organelles were found per 100 AIS profiles. Although single cisterns of smooth endoplasmic reticulum were occasionally observed in the AIS of synaptopodin-deficient mice, not a single cisternal organelle was detected.
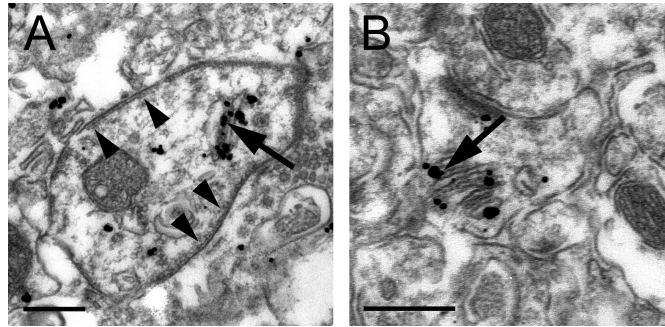
Fig. 12. Synaptopodin is localized to the cisternal organelle.
A: Preembedding immunogold labeling reveals a close association of synaptopodin with the dense plates of cisternal organelles (arrow). The axon initial segment can be identified based on the dense undercoating of its plasma membrane (arrowheads). **B:** Dendritic spines have no dense undercoating. In spines, synaptopodin is associated with the spine apparatus organelle (arrow).
Scale bars: A,B = 0.25 µm.
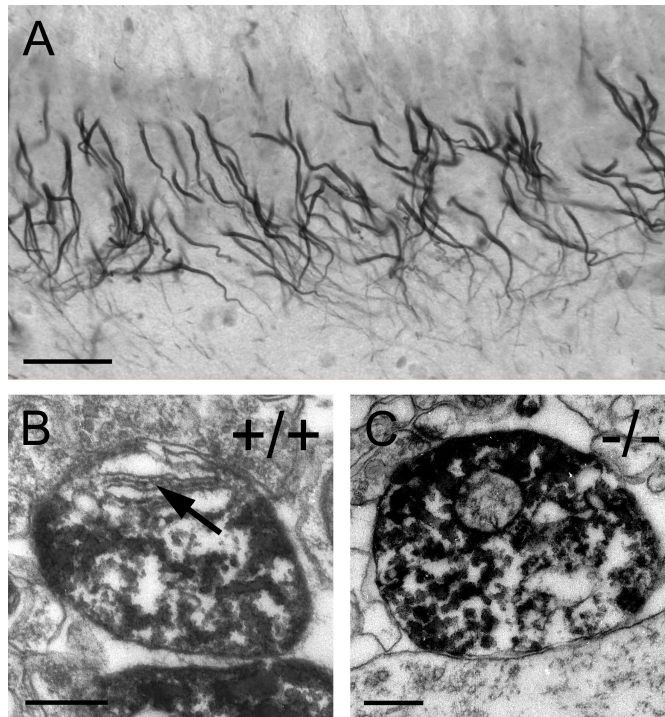
Fig. 13. Labeling of axon initial segments for the analysis of cisternal organelles.
A: Axon initial segments were selectively labeled by preembedding DAB immunohistochemistry for phosphorylated IκBα . **B-C:** The immunoprecipitate intensely stains the cytoplasm of initial segments in wildtype (B) and synaptopodin-deficient (C) mice. However, subcellular organelles like mitochondria (m) or cisternal organelles (co) remain free of reaction product and the dense plates of the latter can clearly be distinguished (arrow in B). No cisternal organelles were found in synaptopodin deficient mice.
Scale bars: A = 50 µm; B,C = 0.25 µm.

4.2. Denervation-induced changes in the distribution of synaptopodin

A further aim of this thesis was to investigate the role of synaptopodin in denervation-induced plasticity of dendritic spines. Before this question could be addressed, however, it had to be tested whether synaptopodin itself is influenced by denervation. This appeared to be necessary because the distribution of synaptopodin might be regulated by presynaptic signals, most likely synaptic activity (Yamazaki et al., 2001; Fukazawa et al., 2003; this thesis). Therefore, the distribution of synaptopodin in the molecular layer of the dentate gyrus was studied after entorhinal cortex lesion.

4.2.1. The distribution of synaptopodin is changed after entorhinal cortex lesion

The middle and outer molecular layer (MML and OML, respectively) of the dentate gyrus were denervated by entorhinal cortex lesion. In all animals lesion quality was tightly controlled (see Material and Methods). Lesions and quality controls were performed by Dr. Doris Dehn in our laboratory.

Immunostaining for synaptopodin revealed a loss of staining intensity in the denervated MML and OML after survival times of four days or more (Fig. 14). Also, the staining intensity in the non-denervated inner molecular layer (IML) was reduced at early time points post lesion, albeit these changes were not as pronounced as in the denervated zone. Synaptopodin-immunostaining in the different sublayers of the molecular layer recovered with long survival times (Fig. 14), likely associated with postlesional reorganization processes. In order to characterize these qualitative changes in synaptopodin-immunolabeling further, changes in synaptopodin-immunopositive puncta over time were quantified in the zone of denervation (MML and OML) and the non-denervated zone (IML).

4.2.2. Loss and reacquisition of synaptopodin-puncta in the denervated zone

Quantification of synaptopodin-immunoreactive puncta in the denervated zone (MML and OML) was performed using confocal microscopy in combination with computer based image analysis. In the denervated zone, synaptopodin puncta-density decreased to 13% of control values within the first days post lesion (Fig. 15). Over the course of the first month

post lesion synaptopodin-densities gradually recovered and reached 62 % of control values by 30 d and 78% of control values by 180 d post lesion (Fig. 15).

Changes in synaptopodin-densities were accompanied by shrinkage of the denervated zone (Fig. 14 A-C; Fig. 15 B). Significant shrinkage began around 7 days post lesion and progressed until 14 days post lesion. Thereafter, no further shrinkage was observed. Shrinkage of the denervated zone and the total ML reached 58 % (MML+OML) and 82 % (ML) of control width after 180 d post lesion (Fig. 15 B).

Since shrinkage increases the density of synaptopodin-puncta, values were shrinkage corrected (Fig. 15 C). This correction was especially important after day 7 post lesion because of the protracted time course of the shrinkage process. If shrinkage is considered, synaptopodin puncta-density in the denervated zone recovered to 35 % (30 d) and 46 % (180d) of pre-lesion density. Thus, synaptopodin-puncta appear to be permanently lost in the denervated zone following denervation.

4.2.3. Loss and reacquisition of synaptopodin-puncta in the non-denervated inner molecular layer

The IML of the dentate gyrus is not denervated by ECL. Nevertheless, considerable changes in synaptopodin puncta-densities were observed within this zone: Synaptopodin-densities decreased to 31 % of control levels within the first days post lesion (Fig. 14 A, B, J, K; Fig. 15 A, C). Thereafter, synaptopodin-densities rapidly recovered, reached control levels by 14 days post lesion, and 113 % of control levels by 180 d post lesion. These changes in synaptopodin-densities were accompanied by a significant expansion of the IML (Fig. 14 A-C; Fig. 15 B). By 180 days post lesion the IML had expanded by 37 µm (158 % of control width; Fig. 15 B) and covered 46 % of the total ML.

Similar to the situation in the denervated zone, puncta-densities in the non-denervated IML were corrected for the expansion of the IML (Fig. 15 C). Again, these changes in width were especially important during the late recovery phase. The expansion corrected data revealed that by 180 days post lesion synaptopodin-densities reached 178 % of control values. Thus, synaptopodin-puncta are only transiently lost in the non-denervated IML. Control densities are rapidly regained and - if the expansion of the IML is taken into account - additional synaptopodin-puncta are formed.
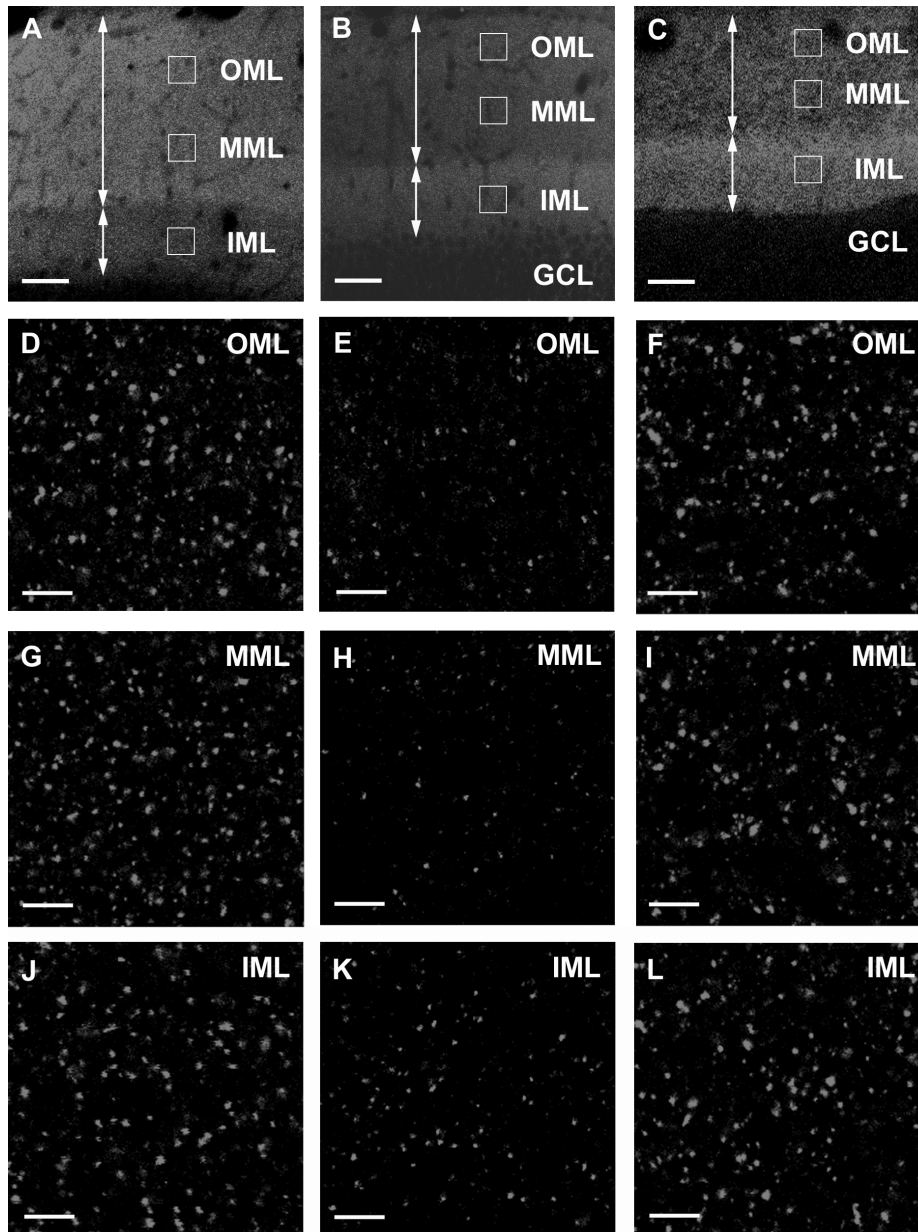
Figure 14. Loss and partial recovery of synaptopodin-positive puncta after entorhinal cortex lesion.

A-C: Low magnification confocal images of the molecular layer immunostained forsynaptopodin in a control rat (A), 4 days post lesion (B), and 180 days post lesion (C). Boxes indicate size (30 µm x 30 µm) and location of analyzed frames in the inner molecular layer(IML), middle molecular layer (MML), and outer molecular layer (OML). Arrows indicate width of the non-denervated zone (IML) and denervated zone (MML and OML). Note changes in the immunostaining pattern and the relative width of the IML. GCL, granule cell layer.

D-F: High magnification confocal images of the denervated OML in a control rat (d), 4 days post lesion (e), and 180 days post lesion (f). In the OML, the density of synaptopodin-positive puncta strongly decreases by 4 days post lesion and moderately recovers by 180 days post lesion.

G-I: High magnification confocal images of the denervated MML in a control rat (g), 4 days post lesion (h), and 180 days post lesion (i). In the MML, the density of synaptopodin-positive puncta strongly decreases by 4 days post lesion and moderately recovers by 180 days post lesion.

J-L: High magnification confocal images of the non-denervated IML stained for synaptopodin in a control rat (j), 4 days post lesion (k), and 180 days post lesion (l). In the IML, the density of synaptopodin-positive puncta decreases by 4 days post lesion. This decrease is moderate in comparison to the denervated zone (MML and OML). Control densities are reached again by 14 days post lesion (not shown) and puncta-density remains high until 180 days post lesion.

Scale bars: A-C = 50 µm; D-L = 5 µm.
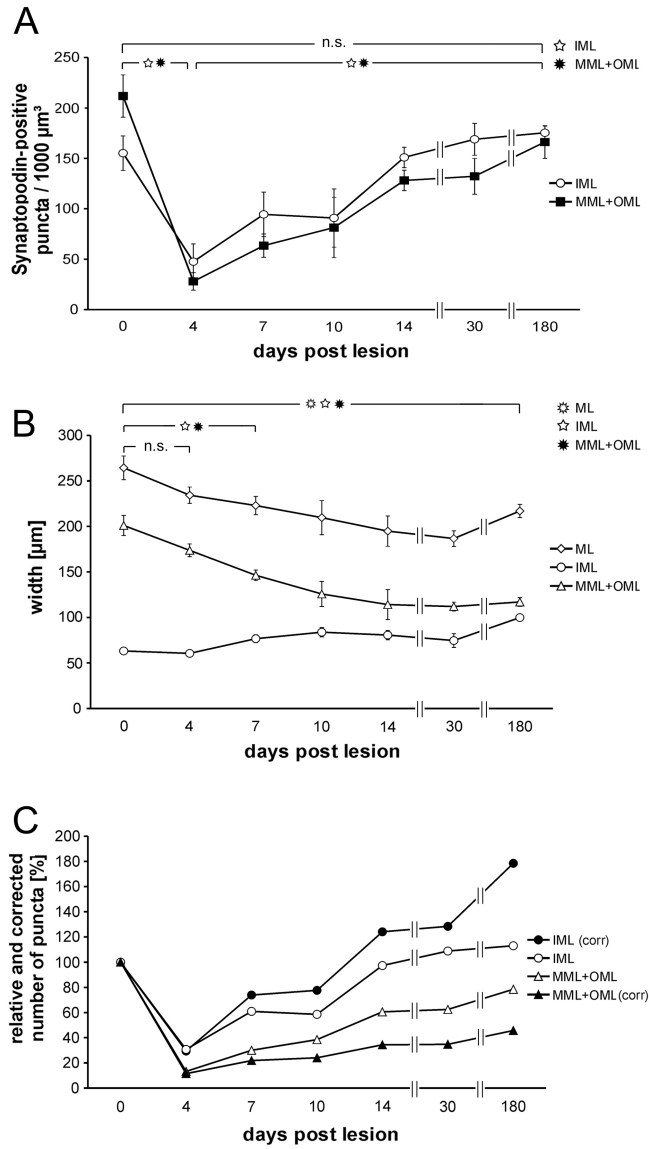
Figure 15. Changes in the density of synaptopodin-positive puncta following denervation.

A: Density of synaptopodin-positive puncta/1000 μm^3 in the non-denervated inner molecular layer (IML) and the denervated zone (middle and outer molecular layers; MML, OML) at different time points post lesion. By 4 days post lesion, synaptopodin-densities have dropped in all layers. In the non-denervated IML, the loss of synaptopodin-puncta is less severe and transient: Control levels are regained by two weeks post lesion. In contrast, synaptopodin densities only slowly recover in the denervated layers. Asterisks indicate significant differences for the two layers (p < 0.05). n.s., not significant. Error bars: ± SEM.

B: Width of the non-denervated IML, the denervated zone (MML + OML), and the total molecular layer (ML) at different time points post lesion. Following lesion, the denervated zone shrinks by 90 μm whereas the IML expands by 37 μm. Shrinkage of the OML stabilizes at 56% of control width. The expansion of the IML eventually reaches 158% of control values. Asterisks indicate significant differences (p < 0.05). n.s., not significant. Error bars: ± SEM.

C: Changes in the relative densities of synaptopodin-positive puncta in the IML and the denervated zone (MML + OML) compared to control densities. Relative changes of raw data and of data after shrinkage correction (corr) are shown.

4.3. Denervation-induced plasticity of dendritic spines

In this thesis, an in vitro entorhinal cortex lesion model (Prang et al., 2001; Prang et al., 2003; see Material and Methods) was used to (1) study the dynamics of denervation-induced spine plasticity in organotypic cultures and (2) test whether synaptopodin plays a role in denervation-induced spine changes. For these experiments, enhanced green fluorescent protein (EGFP)-expressing neurons were imaged by confocal time lapse microscopy.

4.3.1. Setting-up of the microscope and optimization of the imaging procedure

First, a setup for live imaging of organotypic cultures had to be established. Basically, two microscope configurations can be used for imaging of living organotypic cultures, namely an inverse microscope with a water immersion objective or an upright microscope with a dipping water immersion lens. Using an inverse microscope would make it possible to keep the cultures in a closed chamber during imaging, thereby preventing a contamination of the cultures via the air or the objective lens. On the other hand, using this configuration one has to image through the bottom of the chamber, the imaging buffer and the membrane of the culture insert, which decreases the optical resolution of the system. Indeed, when testing different inverse systems, it turned out that the resolution was too low to reliably resolve small structures like dendritic spines. Therefore, an upright microscope was chosen.

Next, two systems for three-dimensional fluorescence microscopy were tested, namely the apotome system from Zeiss and a confocal laser scanning microscope (LSM Pascal, Zeiss). The first system is based on a grid-like illumination of the sample combined with computer-aided deconvolution of the obtained images. It uses an arc lamp as a light source and a CCD camera as a detector. When comparing the two systems, the confocal microscope provided a better axial resolution. In addition, the light intensity of the laser could be set to extremely low levels, while the obtained images still had a sufficient signal to noise ratio. This low intensity illumination is very important to avoid phototoxic cell damage. Thus, a confocal laser scanning system was chosen.

After the microscope had been set up, a number of imaging experiments were performed to determine the optimal settings for the scanning parameters (scan speed, scan zoom, pixel size, light intensity). During these experiments a compromise between optimal image quality and lowest possible photodynamic stress of the cells had to be found. Finally,

settings were determined that allowed for repetitive high resolution imaging of individual dendritic segments for up to 42 days.

4.3.2. Stability of dendritic spines in organotypic slice cultures

First, the stability of dendritic spines in mature organotypic entorhino-hippocampal cultures was studied. Cultures were prepared at postnatal day 5 and allowed to mature for 18-20 days (d) before starting an imaging series. Three-dimensional image stacks of identified dendritic segments were recorded on day 0, 2, 4, 7, 10, 14, 21, 30 and 42. The number of dendritic spines was then counted for each day. Interestingly, the number of spines per dendritic segment remained constant throughout the entire observation period (n=6 cells for 21d and n=3 cells for 42d; Figs. 16; 17 A). However, this observation does not exclude the possibility of a substantial turnover of spines as long as gain and loss of spines are balanced. Therefore, to determine the amount of turnover, individual spines from the dataset were analyzed (n=72 spines from 3 cells). 66.8% of tracked spines were stable for more than 7 days, while 41.2% were stable for three weeks and still 27% were stable for the entire observation period of 6 weeks (Fig. 17 B). The average halflife of spines was 12.2 days. Thus, dendritic spines in mature organotypic cultures are stable for several days and in some cases up to several weeks.

4.3.3. Transient loss of dendritic spines following denervation

Upon denervation, a loss of spines was evident as early as two days post lesion (dpl). This loss continued until day 4, when $34.4 \pm 6.3\%$ (mean $\pm$ SD; n=10 cells) of dendritic spines were lost (Figs. 16; 17 A). Subsequently, the number of spines increased, most likely due to a reinnervation of the outer molecular layer by sprouting mossy cell axons (Prang et al., 2003). Although sprouting was not analyzed systematically in this study, an increased number of EGFP-positive axons was frequently observed in the outer molecular layer at 10 dpl and later (Fig. 18). Spine numbers reached $82.4 \pm 17.9\%$ and $92.9 \pm 22\%$ of control levels at 21 and 42 dpl, respectively (n=10 and 5 cells, respectively; Fig. 17 A). Interestingly, a subset of spines was still stable after denervation. While the average halflife of spines dropped to 3.6 days, 15.7% of the analyzed spine population (n=94 spines from 4 cells) remained stable for 6 weeks (Fig. 17 B).
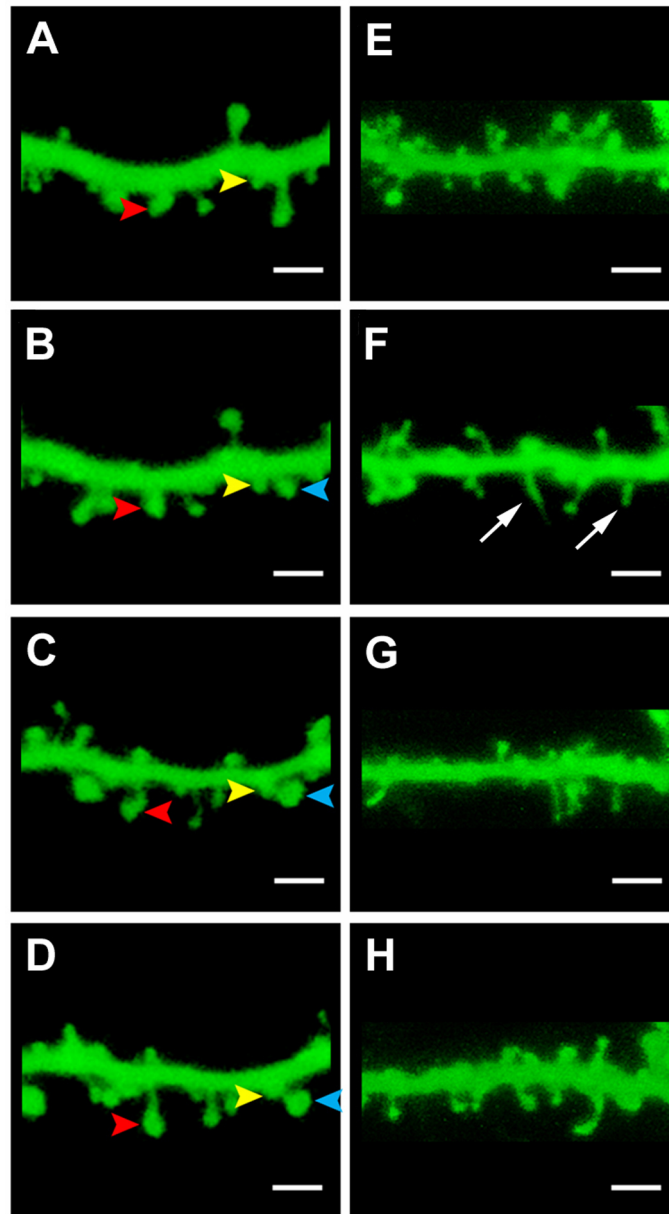
Figure 16. Denervation-induced loss and partial recovery of dendritic spines in vitro.
A-D: Non-denervated dendritic segment at days 0 (A), 2 (B), 7 (C), and 10 (D). Arrowheads indicate stable spines. **E-H:** Denervated dendritic segment at days 0 (E), 2 (F), 7 (G), and 10 (H) post lesion. Note appearance of filopodia-like processes at 2 days post lesion (F, arrows). Images are z-projections of confocal image-stacks.
Scale bars: A-H = 2 μm.
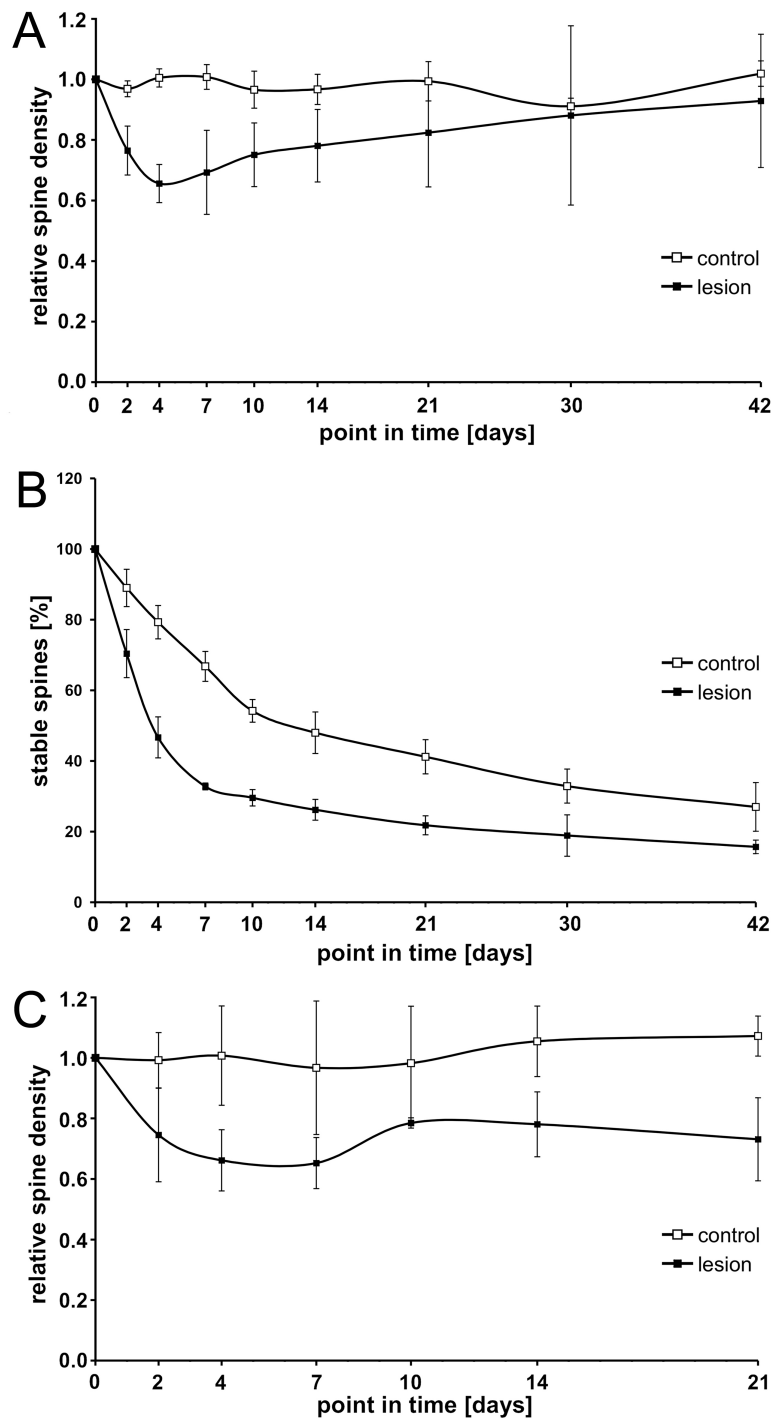
Figure 17. Long-term stability and denervation-induced changes of spines in vitro.
A: Individual dendritic segments in slice cultures from EGFP-transgenic mice were followed over time and the density of dendritic spines was calculated for each time point. In control cultures the density of spines remains constant throughout the entire observation period. In lesioned cultures 34% of spines are lost by day 4 post lesion. Spine density then recovers and reaches control levels by 30 days post lesion. **B:** To determine the amount of spine turnover in vitro, individual spines were followed over time. In control cultures spines have a mean halflife of 12.2 days and are stable for days or weeks. In lesioned cultures the mean halflife drops to 3.6 days but a subpopulation of spines still remains stable for 42 days. **C:** Dendritic segments in slice cultures from EGFP-transgenic synaptopodin-deficient mice were followed over time. In unlesioned cultures spine density remains constant during the entire observation period. Following lesion, spines are transiently lost and are partially recovered by 21 days post lesion. Extent and time course of spine changes did not differ significantly from lesioned synaptopodin wildtype cultures.
Error bars: ± SD.
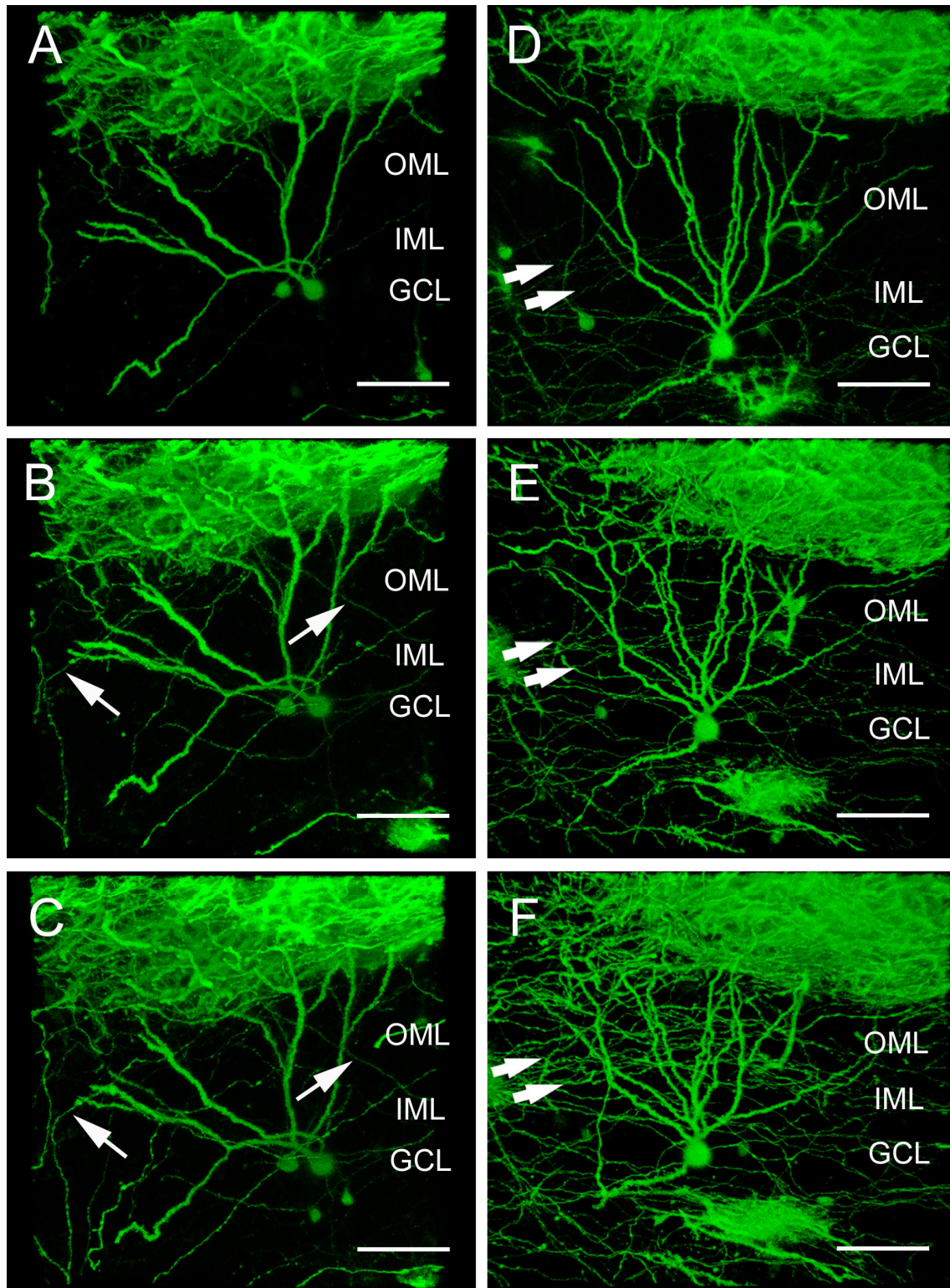
Figure 18. Denervation-induced sprouting of EGFP-labeled axons in vitro.

A-C: An EGFP-positive granule cell from an unlesioned slice culture imaged at days 0, 7, and 14 (A, B, and C, respectively) is illustrated. Only few EGFP-positive axons (arrows) are growing into the outer molecular layer (OML) during the observation period. **D-F:** A granule cell from a lesioned culture imaged at day 0 (D) and at days 7 (E) and 14 (F) post lesion is illustrated. Following denervation numerous axons (arrows) are growing into the OML. GCL = granule cell layer, IML = inner molecular layer.
Scale bars: A-F = 50 μm.

4.3.4. Denervation-induced spine changes in cultures of synaptopodin-deficient mice

To test whether the lack of synaptopodin and the spine apparatus organelle leads to changes in denervation-induced spine plasticity, organotypic cultures from EGFP-transgenic synaptopodin-deficient mice were analyzed. In unlesioned control cultures the density of dendritic spines was stable throughout the entire observation period (n=5 cells; Fig. 17 C). Following denervation, the dynamics of spine changes were similar to cultures from synaptopodin-wildtype mice. 33.8 ± 10.1% (mean ± SD; n=4 cells) of dendritic spines were lost by day 4 post lesion and numbers reached 73.1 ± 13.7% of control levels by 21 dpl (Fig. 17 C). Statistical analysis did not reveal a significant difference between cultures from synaptopodin-deficient and wildtype mice.

4.4. Generation of synaptopodin-transgenic mice

Results from the literature (Yamazaki et al., 2001; Fukazawa et al., 2003) and from this thesis suggest, that the distribution of synaptopodin is regulated under conditions of synaptic plasticity. To study the dynamic distribution of synaptopodin in more detail in future projects, transgenic mice expressing either an enhanced green fluorescent protein (EGFP)-synaptopodin fusion protein or an enhanced cyan fluorescent protein (ECFP)-synaptopodin fusion protein were generated. Using these mice, the redistribution of synaptopodin can be studied online in living tissues. In addition, synaptopodin-containing spines can be identified in living tissues and compared to synaptopodin-negative spines, enabling a direct comparison of anatomical (e.g. shape, motility) and physiological (e.g. calcium transients, electrical signals) parameters.

4.4.1. Determination of the correct cDNA sequence for the 100 kDa brain isoform

Synaptopodin has been shown to exist in at least two splice variants, namely a 110 kDa isoform in the kidney and a 100 kDa isoform in the brain (Mundel et al., 1997). The corresponding cDNA sequence for the brain isoform has been under debate, however. Whereas Mundel and colleagues suggest a 2070 bp coding sequence corresponding to 690 amino acids (Mundel et al., 1997; Asanuma et al., 2005), Kremerskothen and colleagues suggest a 2709 bp sequence coding for 903 amino acids (Kremerskothen et al., 2005).The sequence suggested by Kremerskothen and colleagues is largely identical to the sequence suggested by Mundel and colleagues, but contains additional carboxy-terminal amino

acids. Although only one protein isoform is present in brain, both the 2070 bp and the 2709 bp mRNA variant are detectable in brain lysates (Asanuma et al., 2005). Therefore, the correct coding sequence for the 100 kDa protein cannot be determined by RT-PCR analysis. Thus, to independently determine the correct sequence, a mass spectroscopic analysis of mouse brain synaptopodin was performed.

Total protein was extracted from the cerebral cortex of an adult C57BL/6 mouse and a heat-stable supernatant was obtained (see Material and Methods; Mundel et al., 1997). The integrity of synaptopodin protein was then checked by Western Blotting. The Western Blot showed a single synaptopodin-positive band at 100 kDa without any degradation products (Fig. 19 A). Next, a sample of the brain lysate was sent to a company (Proteome Factory, Berlin, Germany) for nano liquid-chromatography electron-spray-ionization mass spectroscopy (nanoLC-ESI-MS). There, the sample was fractionated by high pressure liquid chromatorgraphy (HPLC) and the single fractions were tested for the presence of synaptopodin by Dot Blotting. The fraction containing the highest amount of synaptopodin was then separated by SDS-PAGE and the 100 kDa band corresponding to synaptopodin was excised and subjected to nanoLC-ESI-MS (Fig. 19 B, C). A total of 13 peptides were identified in this analysis. Comparison of the identified peptides with the two different sequences revealed, that only peptides spanning the first 609 amino acids were detectable in the sample, covering 28 % of the shorter sequence (Fig. 19 D). Thus, the longer cDNA isoform appears not to correspond to the 100 kDa protein isoform found in brain.

4.4.2. Cloning of cDNA constructs

A plasmid containing the open reading frame of mouse brain synaptopodin fused to the 3' end of the open reading frame of EGFP (pEGFP-C1_SPfull) was generously provided by Dr. Peter Mundel (New York, USA). First, the synaptopodin sequence was cloned into the pECFP-C1 and pDsRed2-C1 vectors (Clontech) using the SacII and SalI restriction sites. Correct insertion of the synaptopodin sequence was verified by restriction digests using BamHI and XhoI (Fig. 20). The resulting plasmids (pECFP-C1_Synaptopodin and pDsRed2-C1_Synaptopodin) code for ECFP-synaptopodin and DsRed2-synaptopodin fusion proteins, respectively. They contain a CMV promoter and can be used for transient transfection of cells and tissues.
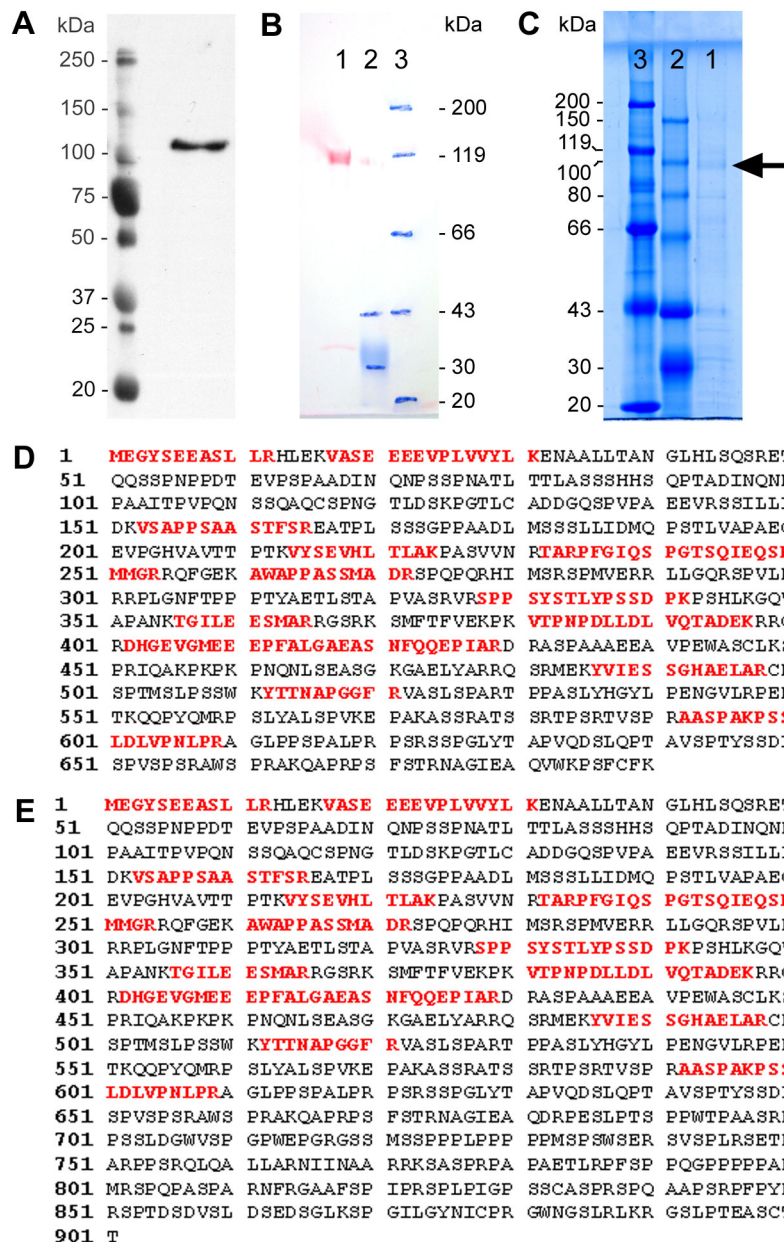
Figure 19. Protein-analysis of mouse brain synaptopodin.
A: Western Blot of mouse brain lysate labeled for synaptopodin. A single characteristic band at 100 kDa is visible, demonstrating the integrity of synaptopodin. **B-C:** Western Blot (B) and corresponding SDS-gel (C) containing the HPLC-fractionated lysate (1) and two size-markers (2,3). The gel was loaded in duplicate and one half was subjected to Western Blotting. From the remaining half of the gel, the 100 kDa band (arrow in C) corresponding to the synaptopodin-immunoreactive band on the blot (red band in B) was excised and processed for ESI-MS analysis. **D-E:** Comparison of the identified peptides from the ESI-MS analysis with the sequences for the short (B) and long (C) synaptopodin isoforms. Matched peptides (red) are distributed evenly across the short sequence, with a sequence coverage of 28%. No peptide matches were found for the additional C-terminus of the long isoform.
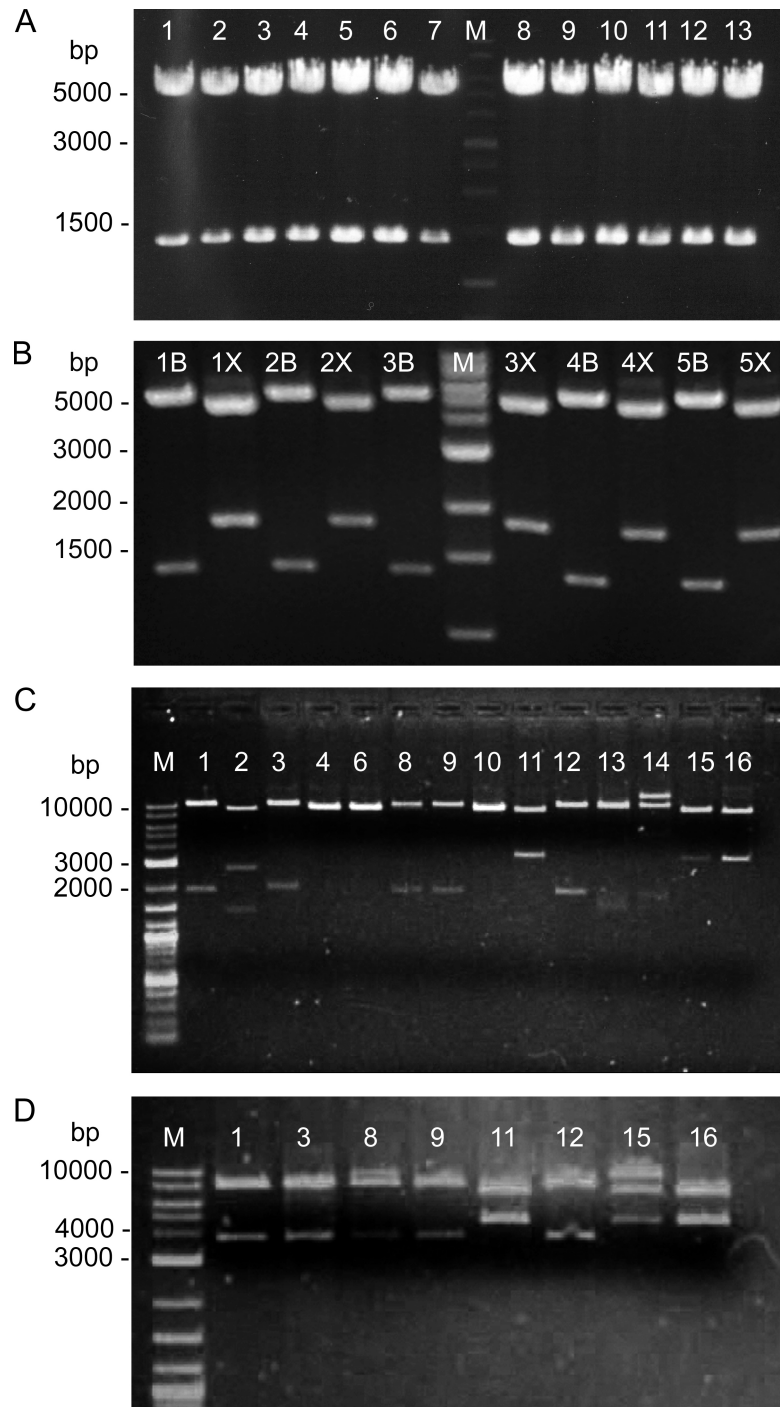
Fig. 20. Restriction-analysis of synaptopodin constructs.
A: Insertion of the synaptopodin open reading frame (ORF) into the pDsRed2-C1 vector was checked by restriction with BamHI. Clones 1-13 show a characteristic band at approx. 1400 bp, indicative for correct insertion. **B:** Correct insertion of the synaptopodin ORF into the pECFP-C1 vector was checked by restriction analysis. Clones 1-5 show characteristic bands at approx. 1400 bp and 1800 bp after digestion with BamHI (B) and XhoI (X), respectively. **C:** Insertion of the EGFP-synaptopodin (clones 1-8) and ECFP-synaptopodin (clones 9-16) ORFs into the pThy1.2 vector was checked by restriction with HindIII. Correct orientation of the insert results in a band at 1900 bp (clones 1, 3, 8, 9, 12), whereas wrong orientation leads to a band at 3200 bp. **D:** Potentially positive clones were further analyzed by restriction with BglII. Clones 1, 3, 8, 9, and 12 show the characteristic cleavage product with a size of 3300 bp, indicative for correct orientation.

Since DsRed and its derivatives tend to form aggregates when transgenically expressed (Dr. Frank Kirchhoff and Dr. Anna-Katerina Hadjantonakis, personal communication), only the EGFP- and ECFP-synaptopodin sequences were used for generation of the transgene constructs. This cloning step was performed in collaboration with PolyGene (Rümlang, Switzerland). For a neuronal expression of the transgene, the neuron-specific Thy1.2 promotor (generously provided by Dr. Pico Caroni, Basel, Switzerland; see also Vidal et al., 1990; Aigner et al., 1995) was chosen. The coding sequences for the fusion proteins were excised using Eco47III and SmaI restriction enzymes, resulting in blunt ended inserts. The vector harboring the promoter cassette was digested with XhoI and the resulting sticky ends were blunted. After blunt end ligation, clones were screened for correct insertion of the insert DNA by two restriction digests using HindIII and BglII, respectively (Fig. 20). For each construct, one positive clone was further verified by sequencing of the cloning sites.

4.4.3. Expression of transgene constructs in primary neurons

Before pronucleus injection, the constructs were tested for functionality by expression in primary neurons. 15 day old primary rat hippocampal neurons were transfected with pThy1-EGFP-Synaptopodin (Fig. 21) and pThy1-ECFP-Synaptopodin (data not shown). Both fusion proteins were strongly expressed after incubation for 24 h and were properly sorted to dendritic spines. Thus, the constructs were used for the generation of transgenic mice. After digestion of the DNA with NotI and PvuI to remove unneeded vector DNA, the fragments containing the promotor, coding sequence and polyA signal were purified and sent to Dr. Reifenberg (University of Mainz, Germany) for injection into pronuclei of fertilized C57BL/6J oocytes.

4.4.4. Identification of founder animals

A total offspring of 64 animals was obtained from the pronucleus injection experiments (35 animals from injection with the ECFP-Synaptopodin construct and 29 animals from injection with the EGFP-Synaptopodin construct). Among these animals, founders carrying the transgene were indentified by two separate PCR reactions using different primer pairs (Fig. 22). Primer pairs were designed to span the 5'- and 3'-cloning sites of the transgenic construct, respectively. In both cases, the same animals were identified as founders (Fig. 22). These included 7 animals carrying the ECFP- and 6 animals carrying the EGFP-Synaptopodin construct. Founders are currently being crossed with C57BL/6J mice and the resulting offspring will be used to characterize the individual transgenic lines.
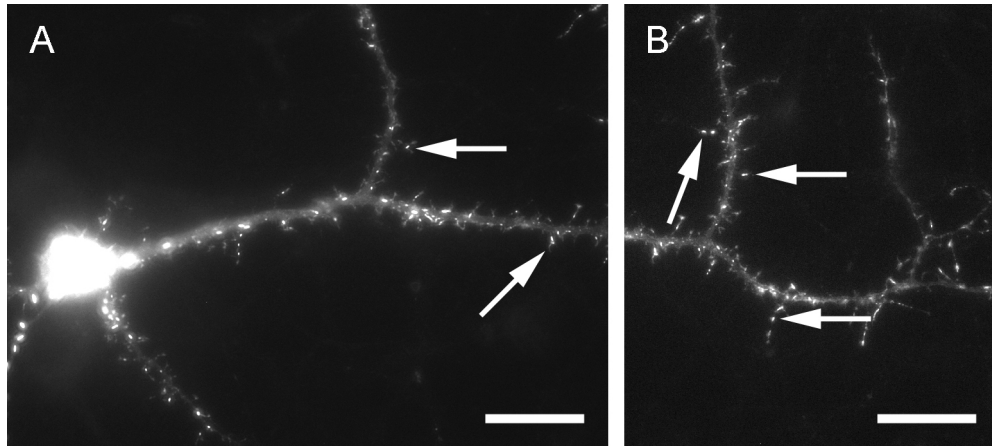
Fig. 21. Transfection of primary neurons with pThy1-EGFP-Synaptopodin.
A-B: 15 day old primary cultures of rat hippocampal neurons were transfected with pThy1-EGFP-Synaptopodin. The EGFP-synaptopodin fusionprotein is strongly expressed in the soma (A) and is distributed in a punctate pattern in proximal (A) and distal (B) dendrites. Individual puncta are predominantly sorted to dendritic spines (arrows).
Scale bars: A,B = 10 μm.
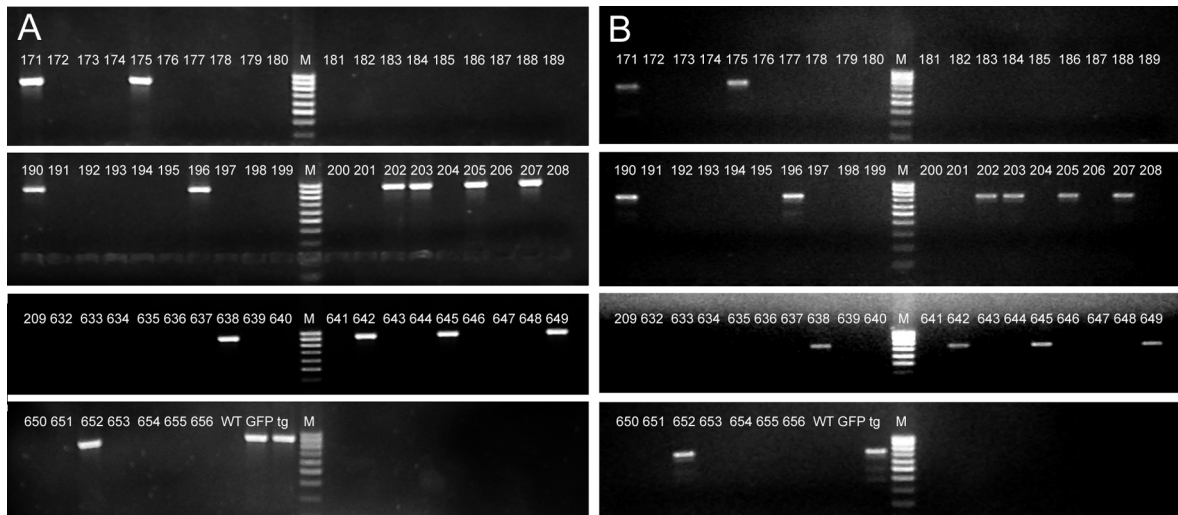
Fig. 22. Identification of transgenic founder animals by PCR.
A: PCR of tail tip DNA from putative founder animals was performed using a primer set that spans the 5'-cloning site of the transgenic construct (junction of Thy1.2- and ECFP/EGFP-sequences). Animals 171, 175, 190, 196, 202, 203, 205, 207, 638, 642, 645, 649 and 652 are positive for the transgene. Tail tip DNA from Thy1GFP-M mice (GFP) and pThy1-EGFP-Synaptopodin cDNA (tg) served as positive control. No signal was detected in tail tip DNA from wildtype C57BL/6 mice (WT). **B:** PCR using a second primer pair that spans the 3'-cloning site of the transgenic construct (junction of synaptopodin- and polyA-sequences) confirms the results of the first PCR. No signal was detected in wildtype (WT) or Thy1GFP-M (GFP) mice.

5. Discussion

This thesis project has focused on the role of synaptopodin in structural spine plasticity and has addressed three groups of questions: (1) What is the distribution of synaptopodin and the spine apparatus in identified hippocampal neurons? (2) Is the distribution of synaptopodin affected by denervation? (3) Is synaptopodin involved in the regulation of denervation-induced spine loss?

In the following, the data of the thesis will be interpreted and discussed in the context of the prevailing literature. First, the distribution of synaptopodin in hippocampal neurons will be summarized and its association with two cellular organelles, the spine apparatus and the cisternal organelle, will be discussed. Second, denervation-induced changes in the distribution of synaptopodin will be considered and it will be proposed that the distribution of synaptopodin in hippocampal neurons is regulated by presynaptic signals, most likely the activity of afferent fiber systems. Third, the dynamics of denervation-induced spine plasticity in control and lesioned cultures will be addressed and it will be discussed whether synaptopodin or the spine apparatus could play a regulatory role in this process. Finally, experiments leading to the identification of the brain isoform of synaptopodin will be critically reviewed and potential uses of synaptopodin-transgenic mice in future experiments will be pointed out.

5.1. The distribution of synaptopodin in hippocampal neurons

Synaptopodin is an actin-associated molecule essential for the spine apparatus organelle (Deller et al., 2003). Because synaptopodin and the spine apparatus are believed to play an important role in synaptic plasticity, it is of interest to know more about their normal distribution in the brain. Thus, a detailed immunohistochemical analysis was performed. The data can be summarized as follows: (1) Synaptopodin is distributed in a lamina-specific manner within dendritic segments of identified hippocampal principal neurons. (2) Synaptopodin-positive puncta in dendritic layers are primarily located in spines, where they are bona fide indicators of the spine apparatus organelle. (3) Synaptopodin is regularly present in dendritic spines of hilar mossy cells. (4) Synaptopodin is not only sorted to dendritic spines, but also to axon initial segments, where it is an essential component of the cisternal organelle.

5.1.1. Regional and laminar variations of synaptopodin are not caused by a presynaptic localization of synaptopodin protein

In previous analyses of synaptopodin in the rodent hippocampus a non-homogeneous immunostaining pattern was described (Deller et al., 2000a; Deller et al., 2002), which corresponded to the laminar organization of the hippocampus generated by the layer-specific termination of afferent fiber systems (Amaral and Witter, 1995). This pattern was intriguing, because synaptopodin, which is believed to be a postsynaptic molecule, follows a pattern generated by presynaptic structures. This suggested an intracellular sorting of synaptopodin into dendrites located within the various hippocampal laminae, most likely in response to presynaptic signals (Deller et al., 2002). Although such a hypothesis is plausible, proof for such a sorting process has yet to be provided and other explanations, such as a partial presynaptic localization of synaptopodin need to be firmly excluded.

In previous studies, the subcellular distribution of synaptopodin at the ultrastructural level was analyzed using pre- and postembedding immunogold techniques (Deller et al., 2000a; Deller et al., 2002). Although a presynaptic localization of synaptopodin was not observed in these analyses, a partial localization of synaptopodin on afferent terminals in some hippocampal layers may have escaped detection in these high-resolution studies. Thus, double-immunofluorescence for synaptophysin and synaptopodin was used, which made it possible to analyze a large number of pre- and postsynaptic structures in the various regions and layers of the hippocampus. Since not a single case of co-localization of synaptopodin with synaptophysin was observed, it can be concluded with confidence, that synaptopodin is not located on presynaptic afferent terminals in the hippocampus. Thus, the laminar immunostaining pattern of synaptopodin is not caused by a partial presynaptic localization of this molecule.

5.1.2. Regional and laminar variations of synaptopodin-immunostaining reflect the lamina-specific distribution of synaptopodin in hippocampal principal neurons

To provide positive proof for a lamina-specific distribution of synaptopodin at the cellular level, dendritic segments of EGFP-labeled hippocampal neurons were stained for synaptopodin and analyzed in the various hippocampal layers. In agreement with the intracellular sorting hypothesis, significant differences in the percentage of synaptopodin-positive spines were found between the layers (Fig. 7 E). In some regions, such as area

CA1, these differences were almost 2.3 fold between different dendritic segments of the same cell type. Thus, a lamina-specific distribution of synaptopodin is found at the cellular level.

5.1.3. Synaptopodin is present in dendritic spines of hilar mossy cells

Previous studies have reported the presence of synaptopodin mRNA expressing cells in the hilar region of the dentate gyrus (Deller et al., 2000a; Deller et al., 2002). On the basis of anatomical data, these cells were supposed to be mossy cells (Deller et al., 2000a). Mossy cells are large glutamatergic neurons that project to the ipsi- and contralateral hippocampus (Amaral, 1978; Ribak et al., 1985; Frotscher et al., 1991; Soriano and Frotscher, 1994; Wenzel et al., 1997; Zappone and Sloviter, 2001). They contain numerous spines on their basal and distal dendrites and are thus prime candidates for synaptopodin expressing cells in the hilus. The analysis of EGFP-expressing, synaptopodin-labeled mossy cells in the present study indeed revealed the presence of synaptopodin in mossy cell spines. Thus, in all subfields of the hippocampus synaptopodin is expressed by spine-bearing glutamatergic neurons.

5.1.4. Synaptopodin labels the spine apparatus organelle in spines of hippocampal principal neurons

Although synaptopodin has been previously recognized as a molecule which is essential for the formation of a spine apparatus (Deller et al., 2003), some doubts have remained whether or not synaptopodin is a reliable marker for this organelle. Especially, the detection of synaptopodin-positive material in dendrites (Deller et al., 2000a) raised the question whether synaptopodin could also be located to a large extent in dendritic shafts. This issue was addressed in the present thesis and the number of synaptopodin-positive puncta in spines and dendritic shafts was quantified in the different hippocampal layers. The resulting data show that the overwhelming majority (>95%; exception: stratum lacunosum-moleculare of CA1) of synaptopodin-positive puncta are located in spines. The size and location of these puncta correspond to the size and location of the spine apparatus organelle, as it has been documented and described in detail by others (Gray, 1959a; Spacek, 1985; Spacek and Harris, 1997). Moreover, the percentage of synaptopodin-positive puncta determined in stratum radiatum of CA1 nicely corresponds to the

percentage of spine apparatus-bearing spines determined by three-dimensional electron microscopic reconstruction in this layer in the rat (Spacek and Harris, 1997). Thus, synaptopodin appears to be a useful marker for labeling the spine apparatus organelle in the hippocampus.

5.1.5. The distribution of the spine apparatus in the mouse hippocampus is lamina-specific

Since the overwhelming majority of synaptopodin-puncta in dendritic layers represent spine apparatuses, one can conclude, that this intriguing organelle shows a lamina-specific distribution in the hippocampus. In mice, it appears to be most abundant in spines of dentate granule cells and relatively scarce in spines of CA1 pyramidal neurons. This differential distribution of the spine apparatus may be of functional importance, since this organelle has been assumed to be a calcium store (Fifkova et al., 1983; Lisman, 1989; Svoboda and Mainen, 1999), which is probably involved in calcium-dependent changes in synaptic plasticity (Miyata et al., 2000; Sabatini et al., 2002). In line with this interpretation, mice lacking the spine apparatus organelle showed deficits in long-term potentiation and impairment in learning and memory tests (Deller et al., 2003). It will now be of considerable interest to find out whether or not the presence of a spine apparatus influences Ca^{2+}-transients or synaptic plasticity of individual spines. The normal distribution of synaptopodin in identified hippocampal neurons is, however, an important baseline for this future work.

5.1.6. Synaptopodin is a molecular component of the cisternal organelle

In previous studies on the distribution of synaptopodin in the hippocampus a string-like labeling of synaptopodin-positive puncta was reported in hippocampal principal cell layers (Deller et al., 2000a). Although originally believed to represent synaptopodin-positive spine apparatuses in dendritic spines, an axonal localization of synaptopodin was also discussed on the basis of the morphological similarity between the spine apparatus and the cisternal organelle (Deller et al., 2000a; Deller et al., 2000b). In the present thesis, such an axonal localization of synaptopodin could be verified, using double-immunofluorescence-labeling of synaptopodin and βIV-spectrin, as well as synaptopodin-labeling of Thy1-GFP mouse hippocampus (Feng et al., 2000; Bas Orth et al., 2005). Using preembedding

immunogold-labeling, an association of the axonal synaptopodin-positive puncta with the cisternal organelle could also be shown. Thus, synaptopodin is a molecular component of the cisternal organelle and can be employed to label this organelle in the axon initial segment of neurons.

5.1.7. The cisternal organelle is a regular feature of the axon initial segment of telencephalic principal neurons

The association of synaptopodin with the cisternal organelle made it possible to estimate the number of cisternal organelles in axon initial segments (AIS) of hippocampal and cortical principal cells using light microscopy. In the analyzed material almost every AIS contained at least one synaptopodin-positive structure, indicating that synaptopodin-positive cisternal organelles are a regular feature of the AIS of telencephalic principal cells. Based on these light microscopic observations these neurons have on average 3.2 cisternal organelles per 10 μm AIS. Thus, this organelle appears to be a very regular and common feature of telencephalic principal axons, occurring more frequently than previously estimated on the basis of conventional electron microscopic analysis (Peters et al., 1968; Kosaka, 1980).

5.1.8. Synaptopodin is an essential component of the cisternal organelle

The tight association between synaptopodin and the cisternal organelle raised the question, whether synaptopodin is required for its formation. This question can be addressed by analyzing the AIS of synaptopodin-deficient mice (Deller et al., 2003). This approach is not trivial, however. Although AIS can be identified in the electron microscope based on their ultrastructural characteristics, they are rarely encountered in unstained brain sections. Furthermore, the cisternal organelle is a rather small structure compared to the entire initial segment (ca. 1-2 μm vs. ca. 20-40 μm) and, therefore, it is absent in the majority of AIS profiles (Peters et al., 1968). Thus, investigations were focused on the AIS of hippocampal CA1 pyramidal cells. These cells are densely packed in a single cell layer and have parallel axons, which are oriented towards the alveus. In addition, AIS were identified using an antibody against phosphorylated IκBα (Schultz et al., 2006), which allowed for a reliable identification of AIS located in and subjacent to the pyramidal cell layer of CA1. Using

this approach, it was revealed that synaptopodin-deficient mice lack a cisternal organelle, indicating that synaptopodin is required for its formation.

The finding that the cisternal organelle is absent in the AIS of synaptopodin-deficient mice is further corroborated by the fact that the distribution of the cisternal organelle correlates with the expression pattern of synaptopodin mRNA in rodent brain (Mundel et al., 1997; Deller et al., 2002): Cisternal organelles were described in small pyramidal neurons of the cerebral cortex (Peters et al., 1968), as well as in CA3 and CA1 pyramidal neurons of the hippocampus (Kosaka, 1980; Benedeczky et al., 1994), but not in cerebellar Purkinje cells (Somogyi and Hamori, 1976), motoneurons (Conradi, 1969), neurons of the medial accessory olive (de Zeeuw et al., 1990), or the trigeminal nucleus (Westrum, 1993). This distribution corresponds to the expression pattern of synaptopodin, which is restricted to telencephalic principal neurons (Mundel et al., 1997; Deller et al., 2000a). Thus, cisternal organelles have so far only been described in neurons that express synaptopodin. Conversely, neurons that do not express synaptopodin, either naturally or because of gene targeting, do not contain cisternal organelles.

5.1.9. The cisternal organelle of the axon initial segment and the spine apparatus of dendritic spines share morphological and molecular features

It has been pointed out on the basis of electron microscopic data that the cisternal organelle and the spine apparatus are morphologically very similar (Peters et al., 1968; Kosaka, 1980; Benedeczky et al., 1994). Both organelles contain stacks of smooth endoplasmic reticulum that are interconnected by dense plates (Gray, 1959a; Palay et al., 1968; Peters et al., 1968; Spacek, 1985). In addition, both the spine apparatus (Fifkova et al., 1983; Sharp et al., 1993; Korkotian and Segal, 1998) and the cisternal organelle (Benedeczky et al., 1994) have been implicated in local calcium trafficking. The present finding that synaptopodin is an essential component of both the cisternal organelle and the spine apparatus strengthens the hypothesis that these two organelles share many of their basic features. These morphological and functional similarities, however, do not preclude the involvement of the two organelles in very different and site-specific biological processes which are determined by the local molecular microenvironment of the spine and the axon initial segment, respectively.

5.2. Denervation-induced changes in the distribution of synaptopodin

In the present thesis, ECL was performed to analyze the effect of denervation on the distribution of synaptopodin in granule cell spines. The data can be summarized as follows: (1) In the denervated zone (MML and OML) of the dentate gyrus, where deafferentation-induced spine loss, synaptogenesis, and spinogenesis occurred, a rapid loss of synaptopodin was observed. In this zone, synaptopodin puncta-densities slowly recovered in parallel with spinogenesis. (2) In the non-denervated zone (IML), the layer without deafferentation-induced spine loss, a rapid loss of synaptopodin also occurred. In this layer, the recovery of synaptopodin puncta-densities was fast and correlated with plastic remodeling occurring at the synaptic level, as well as with postlesional recovery of spontaneous granule cell activity. Together, these data demonstrate layer-specific changes in the distribution of synaptopodin following partial denervation of granule cells.

5.2.1. In the denervated layers changes in synaptopodin parallel spine loss and spinogenesis

The outer two-thirds of the molecular layer are severely denervated following ECL. Plastic changes occurring within this zone have been thoroughly studied and the loss as well as the reacquisition of terminals, synapses, spines and dendrites have been documented (Parnavelas et al., 1974; Matthews et al., 1976a; Matthews et al., 1976b; Caceres and Steward, 1983; Steward and Vinsant, 1983; Steward et al., 1988; Steward, 1991; Nitsch and Frotscher, 1993; Diekmann et al., 1996; Rappert et al., 2004). As far as changes in spine-densities are concerned, Golgi studies indicate that up to 50% of spines are lost by 4 days post lesion (Parnavelas et al., 1974; Caceres and Steward, 1983; Steward, 1991). Concomitant with the reinnervation of the denervated zone, spine-densities recover and return to control values (Caceres and Steward, 1983). Interestingly, one of the earliest studies (Matthews et al., 1976a) noted an apparent reduction of spine apparatuses following ECL.

In the present study, changes in synaptopodin puncta-densities were observed in the denervated OML that followed a time course similar to the one reported for the entire spine population in this zone (Parnavelas et al., 1974; Caceres and Steward, 1983). This suggests that in the OML spine apparatuses are lost together with spines and, upon reinnervation and spine reconstruction, are formed anew.

5.2.2. In the non-denervated inner molecular layer changes in synaptopodin indicate a turnover of the spine apparatus

In contrast to the denervated zone, the IML of the fascia dentata is not directly denervated by ECL. Nevertheless, synaptic remodeling (e.g. turnover of synapses, reduction of convex and flat synapses with an concomitant increase of concave synapses, increase in the mean length of postsynaptic densities) also occurs within this zone (Hoff et al., 1981; Marrone et al., 2004a; Marrone et al., 2004b), indicating that adjacent afferents and proximal dendrites of granule cells also react to ECL. However, these changes occur primarily at the level of the synapse, are largely over by 10 to 14 days post lesion, and may represent structural correlates of functional changes (Marrone et al., 2004a; Marrone et al., 2004b). Importantly, these remodeling processes do not seem to affect the basic structural integrity of spines, since neither postlesional changes in the density nor in the shape of spines could be detected in the IML at the light microscopic level (Parnavelas et al., 1974; Caceres and Steward, 1983). Thus, granule cells maintain their spines in the non-denervated IML in spite of lesion-induced remodeling at the level of the synapse.

In the present study, changes in synaptopodin puncta-densities were also observed in the non-denervated IML. These changes cannot be attributed to an accidental denervation of this layer because (1) only animals with an undamaged hippocampus were used for analysis, and, (2) the time course of these changes corresponded to the time course reported for synaptic remodeling in the IML (Hoff et al., 1981; Marrone et al., 2004a; Marrone et al., 2004b) rather than to the time course reported for spine loss and spine reconstruction in the denervated zone (Parnavelas et al., 1974; Matthews et al., 1976a; Matthews et al., 1976b; Caceres and Steward, 1983). Therefore it is unlikely that these changes in synaptopodin-densities are caused by a lesion-induced loss of spines. Rather, the spine apparatus organelle is removed from intact spines and reconstructed within these spines in parallel with the synaptic remodeling of the IML. Conversely, these observations also imply that spines are structurally maintained following removal of a spine apparatus organelle, similar to the situation in synaptopodin-deficient mice (Deller et al., 2003). Thus, the structural integrity of spines alone is neither sufficient for a spine apparatus organelle nor is the presence of a spine apparatus organelle apparently required for spine maintenance.

5.2.3. The presence of synaptopodin and a spine apparatus organelle in spines may depend on neuronal activity

The turnover of spine apparatuses in the non-denervated IML following ECL raises the question, which signals regulate the loss and formation of spine apparatuses in these spines. An attractive hypothesis was proposed many years ago by Tarrant and Routtenberg (1979), who suggested that the presence of a spine apparatus organelle could be regulated by neuronal activity. In the light of recent data, which have demonstrated a considerable dynamics of several intraneuronal organelles, such as the endoplasmic reticulum and elements of the Golgi apparatus (Horton and Ehlers, 2003; Horton et al., 2005; Toresson and Grant, 2005), this implies that the spine apparatus organelle underlies a physiological turnover depending on the state of activation of individual spines.

Although this hypothesis has not yet been verified, the results from several studies suggest that sorting of synaptopodin occurs in response to signals provided by afferent fibers, most likely in response to their synaptic activity: First, the lamina-specific distribution of synaptopodin in normal mice and its loss in reeler mice indicate that the laminar fiber- and cytoarchitecture of the hippocampus underlies the distribution of synaptopodin-positive puncta (Deller et al., 2002). If the laminar organization of afferent fibers is disrupted, lamina-specific sorting does not occur. Next, following LTP synaptopodin mRNA and protein are upregulated by hippocampal neurons in vivo (Yamazaki et al., 2001; Fukazawa et al., 2003). Interestingly, synaptopodin protein was sorted to the stimulated fiber layers together with F-actin (Fukazawa et al., 2003), indicating that synaptopodin accumulates in stimulated spines under conditions of synaptic strengthening. Finally, changes in hippocampal synaptic activity following kainic acid injection (Roth et al., 2001) lead to lamina-specific alterations in the distribution of synaptopodin protein.

Taken together, these studies suggest that the changes observed in the non-denervated IML could be the result of changes in neuronal activity in this layer. In fact, the time course of the turnover of synaptopodin and the spine apparatus in the IML correlates well with previously described functional changes following ECL: Functional remodeling of afferents to the IML (West et al., 1975; Clusmann et al., 1994; Marrone et al., 2004a; Marrone et al., 2004b) as well as a depression of spontaneous granule cell activity (Reeves and Steward, 1988) occur within the same time window and are over by 10 to 14 days post lesion. Thus, changes of the density of synaptopodin and the spine apparatus organelle in

the IML correlate with changes in pre- as well as postsynaptic neuronal activity rather than with changes in spine size or number.

On the basis of these deliberations the following chain of events is proposed: After ECL, spines located on the distal dendritic segments of granule cells are denervated. Many of these spines degenerate and are removed together with their spine apparatus organelle. Upon reinnervation and spinogenesis, spine apparatuses are formed anew in this layer. In contrast, spines located on proximal dendritic segments are maintained after ECL. Nevertheless, many of these spines lose their spine apparatus because afferent and granule cell activity is depressed during the immediate postlesional time period. Upon the recovery of afferent and granule cell activity, spine apparatuses are formed anew in the IML.

Whether this proposed activity-dependent redistribution of the spine apparatus actually occurs can be tested in future experiments using fluorescently tagged synaptopodin (see section 5.4, below) to visualize spine apparatuses and using electrical stimulation or pharmacological substances (e.g. tetrodotoxin, glutamate) to experimentally alter synaptic activity.

5.3. Denervation-induced plasticity of dendritic spines

In the present thesis, denervation-induced plasticity of dendritic spines was investigated using organotypic entorhino-hippocampal slice cultures. The data can be summarized as follows: (1) Dendritic spines are stable for days and weeks in mature organotypic cultures. (2) Following partial denervation, dendritic spines are transiently lost. Time course and extent of these spine changes in vitro are similar to reported changes in vivo. (3) The dynamics of denervation-induced changes of dendritic spines in cultures from synaptopodin-deficient mice do not differ significantly from changes observed in lesioned wildtype cultures.

5.3.1. Stability of dendritic spines in organotypic cultures

Cultures were prepared from mouse brains at postnatal day 4-5 and cultured for 18-20 days before starting the experiments. During this cultivation period, organotypic slice cultures have been shown to mature morphologically (LaVail and Wolf, 1973; Heimrich and Frotscher, 1991; Caeser and Schuz, 1992; Buchs et al., 1993; Dailey and Smith, 1996) and

electrophysiologically (Muller et al., 1993) with a time course that is similar to the in vivo situation. After 12-14 days in vitro, neurons in slice culture show a mature appearance and contain many dendritic spines forming axospinous synapses. Also, axons in organotypic cultures differentiate and progressively lose their ability to grow. Accordingly, entorhinal neurons are unable to regenerate their axons following lesion after about two weeks in vitro (Woodhams et al., 1993; Prang et al., 2001). Thus, mature neurons were used for the present study.

The first result of the imaging experiments was the observation of a remarkable stability of dendritic spines in organotypic cultures. The density of spines on non-denervated granule cell dendrites remained constant throughout the entire observation period of 42 days. This stability could, however, either be due to a balanced loss and de novo formation of spines resulting in no net change, or the maintenance of individual spines. To distinguish between these two possibilities, the lifetimes of individual spines were determined. This analysis revealed that 67% of spines were stable for more than 7 days and that about 50% of spines were stable for more than two weeks, demonstrating that single spines are fairly stable under control conditions.

These findings are in line with recent studies using two-photon microscopy in the mouse neocortex in vivo, showing long-term stability of dendritic spines in adult animals (Grutzendler et al., 2002; Trachtenberg et al., 2002; Zuo et al., 2005). In one month old mice, which are comparable to the mature cultures used in the present study (P5+20DIV at start of imaging series), 60% of spines in the barrel cortex were stable for more than 8 days (Trachtenberg et al., 2002). In the visual cortex of adult mice (4 months), up to 96.5% of spines were stable for more than one month (Grutzendler et al., 2002), indicating that spine stability still increases during the first months of postnatal development. Alternatively, the different results might be due to the different neocortical areas studied.

The stability of dendritic spines has also been studied by others in vitro. In these reports it was shown that spines in developing hippocampal slice cultures (7DIV) are highly dynamic, forming and disappearing at a timescale of minutes to hours (Dailey and Smith, 1996). In contrast, in mature cultures (12DIV) and in acute slices prepared from 3 week old animals, spines were found to be stable for several hours (Hosokawa et al., 1992; Dailey and Smith, 1996). Unfortunately, the observation periods in these in vitro studies were limited and no statement on long-term stability of spines could be made. Thus, the

present thesis represents the first report on the long-term stability of dendritic spines in vitro.

5.3.2. Loss and recovery of dendritic spines following denervation in vitro

Following entorhinal denervation, a progressive loss of dendritic spines was observed on distal dendrites of granule cells. This loss continued until 4 dpl, when 34% of spines were lost. Interestingly, the time course and extent of spine loss observed in vitro were very similar to the situation in vivo, where about 30% of spines were lost at 5 days after ECL (Parnavelas et al., 1974). Subsequently, spine numbers recovered, again following the known time course from in vivo studies (82% of control value at 21 dpl in the present study vs. 80% of control value at 20 dpl in Parnavelas et al., 1974). This recovery was most likely due to a reinnervation of the outer molecular layer of the dentate gyrus by sprouting mossy cell axons. Denervation-induced sprouting of these fibers has been reported to start between 5 and 10 dpl (Prang et al., 2003) and the density of EGFP-positive axons in the outer molecular layer strongly increased during the period of spinogenesis.

While the dynamics of initial spine loss were very similar between individual cultures, clear differences in the recovery of spines were observed. Some cultures reached spine-densities undistinguishable from control values, while other cultures only slightly recovered. These differences might be due to different levels of reinnervation, which might in turn be due to different numbers of mossy cells between cultures. Alternatively, the observed differences might reflect discrepancies in the overall condition of individual cultures, since slice cultures become more heterogeneous the longer they are cultivated. Nevertheless, the potential for complete recovery of dendritic spines would not have been observed if cultures had only been studied for shorter time periods. Thus, the ability to repeatedly record individual dendrites and spines over a time period of up to six weeks is a clear advantage of the present model system.

5.3.3. Loss and recovery of dendritic spines in synaptopodin-deficient slice cultures

To investigate a potential role of synaptopodin and the spine apparatus in denervation-induced spine loss, slice cultures from synaptopodin-deficient Thy1GFP-transgenic mice were analyzed. Because this analysis focused on the dynamics of the initial spine loss

rather than on long term recovery, experiments were limited to an observation period of 3 weeks. First, unlesioned cultures were studied, revealing no change of spine density during the entire observation period. Thus, synaptopodin-deficient cultures had matured similar to cultures from wildtype animals, indicating that synaptopodin is not essential for the stability of dendritic spines under baseline conditions.

Following denervation, granule cells lost 34% of their spines on distal dendrites by 4 dpl. Thereafter, spine density increased, reaching 73% of control levels at 21 dpl. Thus, the dynamics as well as the extent of denervation-induced spine loss and recovery did not differ between cultures derived from synaptopodin-deficient or wildtype animals. At present, three possible explanations for this finding are being considered. (1) This result might suggest that internal calcium stores of dendritic spines are not critically involved in transneuronal spine changes. This would be in contrast to the original hypothesis and would imply a predominant role of extracellular calcium sources. This alternative hypothesis will be tested in future experiments by blocking calcium influx into spines. (2) Alternatively, dendritic spines in cultures from synaptopodin-deficient mice, although lacking a well organized spine apparatus organelle, might still contain other calcium stores. For example, in dendritic spines of synaptopodin-deficient mice in vivo, single cisterns of endoplasmice reticulum can occasionally be detected (Deller et al., 2003). Thus, the presence of any functional calcium stores needs to be excluded in future experiments by using pharmacological antagonists of internal calcium release channels, such as ryanodine and thapsigargin. (3) In the first part of the present thesis, it was shown that around 40% of dendritic spines in the outer molecular layer of the dentate gyrus contain synaptopodin. Therefore, this area appears to be a good model for studying the influence of synaptopodin on transneuronal spine changes. If, however, the percentage of synaptopodin-positive spines in the outer molecular layer is significantly lower in slice culture than in vivo, then a putative difference between synaptopodin-deficient and wildtype animals would be small in vitro and, thus, might not be detected. Therefore, the percentage of synaptopodin-positive spines in the outer molecular layer of the dentate gyrus in organotypic cultures needs to be determined in future experiments.

5.3.4. What could be the signals inducing transneuronal spine loss?

It is a well established fact that neurons depend on afferent input to develop and maintain dendritic spines. For example, granule cells in organotypic hippocampal cultures lacking entorhinal tissue develop shorter dendrites and less dendritic spines than granule cells in entorhino-hippocampal co-cultures (Zafirov et al., 1994; Drakew et al., 1999). Similarly, the removal of afferent input in adult animals induces a loss of dendritic spines (Parnavelas et al., 1974; Caceres and Steward, 1983; Frotscher, 1983). It is less clear, however, which are the signals that mediate denervation-induced spine loss. Available data from the literature support the following three possible mechanisms:

(1) The loss of afferent input could be signaled by an excess of extracellular glutamate, which is released from degenerating axon terminals. This could lead to excitotoxic effects mediated by a pathological influx of Ca^{2+} and the activation of proteases and phosphatases (Olney, 1969; Halpain et al., 1998; Ginsberg et al., 1999; Arundine and Tymianski, 2003; Wu et al., 2004). In line with this hypothesis, the application of MK-801, an antagonist of the NMDA subtype of glutamate receptors, has been shown to prevent the retraction and swelling of denervated dendrites following entorhinal cortex lesion (Nitsch and Frotscher, 1992). However, elevated levels of extracellular glutamate might not simply act as an unspecific toxic stimulus, but might rather activate specific signal transduction cascades. The effect of this signaling might then differ depending on the experimental conditions. For example, cholinergic deafferentation of the rat forebrain leads to an increase in spine density rather than degeneration and this effect is also sensitive to MK-801 (Garrett et al., 2006). This suggests that elevated levels of extracellular glutamate are not invariably associated with degenerative processes.

(2) The loss of afferent input could be signaled via a loss of synaptic activity. It has been shown, that a blockade of electrical activity by the sodium channel blocker tetrodotoxin (TTX) prevents the formation of dendritic spines in developing cell cultures (Collin et al., 1997; Kossel et al., 1997; Segal et al., 2003). Conversely, an increase in electrical activity after treatment of developing cultures with the GABA receptor antagonist picrotoxin leads to an increase in spine formation (Annis et al., 1994). This concept has been further refined by studies in mature slice cultures showing that miniature synaptic transmission via the AMPA subtype of glutamate receptors is essential for the maintenance of dendritic spines, while electrical activity and the activation of the NMDA subtype of glutamate receptors

are needed for spine maturation (Woolley and McEwen, 1994; McKinney et al., 1999; Frotscher et al., 2000).

(3) The loss of afferent input could be signaled via a loss of adhesion molecules or trophic factors. This would implicate that synaptic spines are normally stabilized via a direct interaction between pre- and postsynaptic adhesion molecules and/or a constant release of trophic factors from presynaptic cells. In line with this hypothesis, an overexpression of alpha N-catenin, which links the cell adhesion molecule cadherin to the actin-cytoskeleton, leads to an increase in spine density (Abe et al., 2004). This increase does not depend on electrical activity since it is not reduced by application of TTX. In addition, application of brain-derived neurotrophic factor to slice cultures also increases spine density independent of synaptic activity (Tyler and Pozzo-Miller, 2003).

Most likely, denervation-induced transneuronal plasticity is governed by a combination of the above mentioned mechanisms. In addition, glial cells may also play an important role in this context. For instance, an as yet unidentified astrocyte-secreted factor has been shown to increase spine density in cerebellar slice cultures (Seil et al., 1992; Seil, 1997). Furthermore, a lack of the chemokine receptor CXCR3 in microglial cells which renders these cells unresponsive to certain chemokines leads to reduced dendritic atrophy after entorhinal cortex lesion in vivo, indicating a function of microglia in denervation-induced remodeling (Rappert et al., 2004).

It will now be interesting to unravel the details and the interplay of the individual mechanisms of denervation-induced plasticity described above. The in vitro lesion model and the quantitative data reported in the present thesis provide an important baseline for these future experiments.

5.4. Generation of synaptopodin-transgenic mice

To perform experiments on the regulation of the dynamic distribution of synaptopodin in the future, transgenic animals expressing synaptopodin fused to either enhanced green or cyan fluorescent protein were generated. Before these animals could be generated, however, the correct cDNA sequence of the brain specific synaptopodin isoform had to be established. This was necessary because a study by Kremerskothen and colleagues claimed that the initially published 2070 bp sequence was incomplete (Kremerskothen et al., 2005). This statement was based on the discrepancy between the calculated molecular mass of

synaptopodin (74 kDa) and its apparent molecular weight in SDS-PAGE (100 kDa). Accordingly, these authors proposed a 2709 bp sequence with a calculated molecular mass of 96 kDa. In vitro translation of the latter sequence resulted in a protein with an apparent molecular weight of 100 kDa (Kremerskothen et al., 2005). In contrast, using an antibody that was specific for the carboxy terminus of the longer protein isoform, Asanuma and colleagues could not detect any synaptopdodin protein in the brain (Asanuma et al., 2005). Instead, they detected the well-known 110 kDa protein band in kidney, indicating that the 2709 bp sequence actually codes for the kidney isoform of synaptopodin.

Since the results from these two laboratories were clearly contradictory, the correct cDNA sequence of the brain-specific synaptopodin isoform needed to be determined independently. Because both mRNA variants are detectable in brain lysates, this analysis could not be performed by RT-PCR. Instead, a biochemical approach was chosen. Mass spectroscopic analysis of mouse brain synaptopodin protein revealed 13 peptides that could be aligned with the 2007 bp / 690 aa sequence. In contrast, no peptide corresponding to the additional carboxy terminus of the longer isoform was detected, indicating that the short cDNA sequence indeed codes for the complete brain specific protein. It has to be noted that it cannot be excluded with absolute certainty that carboxy terminal peptides were missed in this analysis. However, the present findings are also corroborated by data from the literature. For instance, it has been shown that proline- or glutamate-rich proteins can show discrepancies between calculated and apparent molecular mass of up to 50% (Gordon et al., 1988; Iakoucheva et al., 2001). More importantly, a re-screening of the Genebank database revealed two novel cDNA entries (accession numbers AK141564 and AK129267) that were identical to the short isoform proposed by Mundel and colleagues. Thus, the existence of the short isoform has been confirmed by three independent research groups.

5.5. Outlook

This thesis reports new data on the distribution of synaptopodin in identified hippocampal neurons. The findings provide further support for the hypothesis that synaptopodin and the spine apparatus organelle are regulated by presynaptic signals, most likely synaptic activity of afferent fibers. Using the transgenic mice generated in this thesis, this hypothesis can now be tested using modern electrophysiological and imaging techniques, such as glutamate uncaging and 2-photon microscopy. It is to be expected that these experiments will also contribute to the understanding of synaptic plasticity and will provide insight into the biological role of the spine apparatus and the cisternal organelle.

Furthermore, a time-lapse imaging system to study the dynamics of denervation-induced spine plasticity in vitro was established. Using this technology, quantitative data on the stability and the lesion-induced loss of dendritic spines in vitro have been obtained. These data will be the basis for further experiments aimed at unraveling the molecular and cellular mechanisms of denervation-induced spine loss.

6. Reference list

1. Abe K, Chisaka O, Van Roy F, Takeichi M (2004) Stability of dendritic spines and synaptic contacts is controlled by alpha N-catenin. Nat Neurosci 7: 357-363.

2. Aigner L, Arber S, Kapfhammer JP, Laux T, Schneider C, Botteri F, Brenner HR, Caroni P (1995) Overexpression of the neural growth-associated protein GAP-43 induces nerve sprouting in the adult nervous system of transgenic mice. Cell 83: 269-278.

3. Amaral DG (1978) A Golgi study of cell types in the hilar region of the hippocampus in the rat. J Comp Neurol 182: 851-914.

4. Amaral DG, Witter MP (1995) In: The Rat Nervous System (Paxinos G, ed), pp 443-494. San Diego: Academic Press.

5. Annis CM, O'Dowd DK, Robertson RT (1994) Activity-dependent regulation of dendritic spine density on cortical pyramidal neurons in organotypic slice cultures. J Neurobiol 25: 1483-1493.

6. Arundine M, Tymianski M (2003) Molecular mechanisms of calcium-dependent neurodegeneration in excitotoxicity. Cell Calcium 34: 325-337.

7. Asanuma K, Kim K, Oh J, Giardino L, Chabanis S, Faul C, Reiser J, Mundel P (2005) Synaptopodin regulates the actin-bundling activity of alpha-actinin in an isoform-specific manner. J Clin Invest 115: 1188-1198.

8. Asanuma K, Yanagida-Asanuma E, Faul C, Tomino Y, Kim K, Mundel P (2006) Synaptopodin orchestrates actin organization and cell motility via regulation of RhoA signalling. Nat Cell Biol 8: 485-491.

9. Bas Orth C, Vlachos A, Del Turco D, Burbach GJ, Haas CA, Mundel P, Feng G, Frotscher M, Deller T (2005) Lamina-specific distribution of Synaptopodin, an actin-associated molecule essential for the spine apparatus, in identified principal cell dendrites of the mouse hippocampus. J Comp Neurol 487: 227-239.

10. Beall B, Chalovich JM (2001) Fesselin, a synaptopodin-like protein, stimulates actin nucleation and polymerization. Biochemistry 40: 14252-14259.

11. Benedeczky I, Molnar E, Somogyi P (1994) The cisternal organelle as a Ca(2+)-storing compartment associated with GABAergic synapses in the axon initial segment of hippocampal pyramidal neurones. Exp Brain Res 101: 216-230.

12. Bennett V, Baines AJ (2001) Spectrin and ankyrin-based pathways: metazoan inventions for integrating cells into tissues. Physiol Rev 81: 1353-1392.

13. Berghs S, Aggujaro D, Dirkx R, Jr., Maksimova E, Stabach P, Hermel JM, Zhang JP, Philbrick W, Slepnev V, Ort T, Solimena M (2000) betaIV spectrin, a new spectrin localized at axon initial segments and nodes of ranvier in the central and peripheral nervous system. J Cell Biol 151: 985-1002.

14. Blanpied TA, Ehlers MD (2004) Microanatomy of dendritic spines: emerging principles of synaptic pathology in psychiatric and neurological disease. Biol Psychiatry 55: 1121-1127.

15. Bloodgood BL, Sabatini BL (2005) Neuronal activity regulates diffusion across the neck of dendritic spines. Science 310: 866-869.

16. Buchs PA, Stoppini L, Muller D (1993) Structural modifications associated with synaptic development in area CA1 of rat hippocampal organotypic cultures. Brain Res Dev Brain Res 71: 81-91.

17. Caceres A, Steward O (1983) Dendritic reorganization in the denervated dentate gyrus of the rat following entorhinal cortical lesions: a Golgi and electron microscopic analysis. J Comp Neurol 136: 287-295.

18. Caeser M, Schuz A (1992) Maturation of neurons in neocortical slice cultures: A light and electron microscopic study on in situ and in vitro material. J Hirnforsch 33: 429-443.

19. Capani F, Martone ME, Deerinck TJ, Ellisman MH (2001) Selective localization of high concentrations of F-actin in subpopulations of dendritic spines in rat central nervous system: a three-dimensional electron microscopic study. J Comp Neurol 435: 156-170.

20. Chan SL, Mattson MP (1999) Caspase and calpain substrates: roles in synaptic plasticity and cell death. J Neurosci Res 58: 167-190.

21. Clusmann H, Nitsch R, Heinemann U (1994) Long lasting functional alterations in the rat dentate gyrus following entorhinal cortex lesion: a current source density analysis. Neuroscience 61: 805-815.

22. Collin C, Miyaguchi K, Segal M (1997) Dendritic spine density and LTP induction in cultured hippocampal slices. J Neurophysiol 77: 1614-1623.

23. Conradi S (1969) Observations on the ultrastructure of the axon hillock and initial axon segment of lumbosacral motoneurons in the cat. Acta Physiol Scand Suppl 332: 65-84.

24. Cotman CW, Nadler JV (1978) Reactive synaptogenesis in the hippocampus. In: Neuronal Plasticity (Cotman CW, ed), pp 227-271. New York: Raven Press.

25. Czarnecki K, Haas CA, Bas Orth C, Deller T, Frotscher M (2005) Postnatal development of synaptopodin expression in the rodent hippocampus. J Comp Neurol 490: 133-144.

26. Dailey ME, Smith SJ (1996) The dynamics of dendritic structure in developing hippocampal slices. J Neurosci 16: 2983-2994.

27. de Zeeuw CI, Ruigrok TJ, Holstege JC, Schalekamp MP, Voogd J (1990) Intracellular labeling of neurons in the medial accessory olive of the cat: III. Ultrastructure of axon hillock and initial segment and their GABAergic innervation. J Comp Neurol 300: 495-510.

28. Dehn D, Burbach GJ, Schafer R, Deller T (2006) NG2 upregulation in the denervated rat fascia dentata following unilateral entorhinal cortex lesion. Glia 53: 491-500.

29. Del Turco D, Woods AG, Gebhardt C, Phinney AL, Jucker M, Frotscher M, Deller T (2003) Comparison of commissural sprouting in the mouse and rat fascia dentata after entorhinal cortex lesion. Hippocampus 13: 685-699.

30. Deller T, Frotscher M, Nitsch R (1996) Sprouting of crossed entorhinodentate fibers after a unilateral entorhinal lesion: anterograde tracing of fiber reorganization with Phaseolus vulgaris-leucoagglutinin (PHAL). J Comp Neurol 365: 42-55.

31. Deller T, Frotscher M (1997) Lesion-induced plasticity of central neurons: sprouting of single fibres in the rat hippocampus after unilateral entorhinal cortex lesion. Prog Neurobiol 53: 687-727.

32. Deller T (1998) The anatomical organization of the rat fascia dentata: new aspects of laminar organization as revealed by anterograde tracing with Phaseolus vulgaris-Luecoagglutinin (PHAL). Anat Embryol (Berl) 197: 89-103.

33. Deller T, Merten T, Roth SU, Mundel P, Frotscher M (2000a) Actin-associated protein synaptopodin in the rat hippocampal formation: localization in the spine neck and close association with the spine apparatus of principal neurons. J Comp Neurol 418: 164-181.

34. Deller T, Mundel P, Frotscher M (2000b) Potential role of synaptopodin in spine motility by coupling actin to the spine apparatus. Hippocampus 10: 569-581.

35. Deller T, Haas CA, Deissenrieder K, Del Turco D, Coulin C, Gebhardt C, Drakew A, Schwarz K, Mundel P, Frotscher M (2002) Laminar distribution of synaptopodin in normal and reeler mouse brain depends on the position of spine-bearing neurons. J Comp Neurol 453: 33-44.

36. Deller T, Korte M, Chabanis S, Drakew A, Schwegler H, Stefani GG, Zuniga A, Schwarz K, Bonhoeffer T, Zeller R, Frotscher M, Mundel P (2003) Synaptopodin-deficient mice lack a spine apparatus and show deficits in synaptic plasticity. Proc Natl Acad Sci U S A 100: 10494-10499.

37. Deller T, Bas Orth C, Vlachos A, Merten T, Del Turco D, Dehn D, Mundel P, Frotscher M (2006) Plasticity of synaptopodin and the spine apparatus organelle in the rat fascia dentata following entorhinal cortex lesion. J Comp Neurol 499: 471-484.

38. Desmond NL, Levy WB (1986) Changes in the postsynaptic density with long-term potentiation in the dentate gyrus. J Comp Neurol 253: 476-482.

39. Diekmann S, Ohm TG, Nitsch R (1996) Long-lasting transneuronal changes in rat dentate granule cell dendrites after entorhinal cortex lesion. A combined intracellular injection and electron microscopy study. Brain Pathol 6: 205-214.

40. Drakew A, Frotscher M, Heimrich B (1999) Blockade of neuronal activity alters spine maturation of dentate granule cells but not their dendritic arborization. Neuroscience 94: 767-774.

41. Eccles JC (1964) The Physiology of Synapses. Berlin: Springer.

42. Engert F, Bonhoeffer T (1999) Dendritic spine changes associated with hippocampal long-term synaptic plasticity. Nature 399: 66-70.

43. Fabian-Fine R, Skehel P, Errington ML, Davies HA, Sher E, Stewart MG, Fine A (2001) Ultrastructural distribution of the alpha7 nicotinic acetylcholine receptor subunit in rat hippocampus. J Neurosci 21: 7993-8003.

44. Feng G, Mellor RH, Bernstein M, Keller-Peck C, Nguyen QT, Wallace M, Nerbonne JM, Lichtman JW, Sanes JR (2000) Imaging neuronal subsets in transgenic mice expressing multiple spectral variants of GFP. Neuron 28: 41-51.

45. Fifkova E, Markham JA, Delay RJ (1983) Calcium in the spine apparatus of dendritic spines in the dentate molecular layer. Brain Res 266: 163-168.

46. Finch EA, Augustine GJ (1998) Local calcium signalling by inositol-1,4,5-trisphosphate in Purkinje cell dendrites. Nature 396: 753-756.

47. Frotscher M (1983) Dendritic plasticity in response to partial deafferentation. In: Neurobiology of the Hippocampus (Seifert W, ed), pp 65-80. New York: Academic Press.

48. Frotscher M (1988) Neuronal Elements in the Hippocampus and Their Synaptic Connections. Advances in Anatomy Embryology and Cell Biology 111: 2-19.

49. Frotscher M (1991) Target cell specificity of synaptic connections in the hippocampus. Hippocampus 1: 123-130.

50. Frotscher M, Seress L, Schwerdtfeger WK, Buhl E (1991) The mossy cells of the fascia dentata: a comparative study of their fine structure and synaptic connections in rodents and primates. J Comp Neurol 312: 145-163.

51. Frotscher M, Heimrich B (1993) Formation of layer-specific fiber projections to the hippocampus in vitro. Proc Natl Acad Sci U S A 90: 10400-10403.

52. Frotscher M, Drakew A, Heimrich B (2000) Role of afferent innervation and neuronal activity in dendritic development and spine maturation of fascia dentata granule cells. Cereb Cortex 10: 946-951.

53. Fukazawa Y, Saitoh Y, Ozawa F, Ohta Y, Mizuno K, Inokuchi K (2003) Hippocampal LTP is accompanied by enhanced F-actin content within the dendritic spine that is essential for late LTP maintenance in vivo. Neuron 38: 447-460.

54. Garrett JE, Kim I, Wilson RE, Wellman CL (2006) Effect of N-methyl-d-aspartate receptor blockade on plasticity of frontal cortex after cholinergic deafferentation in rat. Neuroscience 140: 57-66.

55. Ginsberg SD, Portera-Cailliau C, Martin LJ (1999) Fimbria-fornix transection and excitotoxicity produce similar neurodegeneration in the septum. Neuroscience 88: 1059-1071.

56. Globus A, Scheibel AB (1966) Loss of dendrite spines as an index of pre-synaptic terminal patterns. Nature 212: 463-465.

57. Goetze B, Grunewald B, Kiebler MA, Macchi P (2003) Coupling the iron-responsive element to GFP--an inducible system to study translation in a single living cell. Sci STKE 2003: L12.

58. Gordon J, Kovala T, Dales S (1988) Molecular characterization of a prominent antigen of the vaccinia virus envelope. Virology 167: 361-369.

59. Gray EG (1959a) Axo-somatic and axo-dendritic synapses of the cerebral cortex: an electron microscopic study. J Anat 83: 420-433.

60. Gray EG (1959b) Electron microscopy of synaptic contacts on dendrite spines of the cerebral cortex. Nature 183: 1592-1593.

61. Grutzendler J, Kasthuri N, Gan WB (2002) Long-term dendritic spine stability in the adult cortex. Nature 420: 812-816.

62. Guthrie PB, Segal M, Kater SB (1991) Independent regulation of calcium revealed by imaging dendritic spines. Nature 354: 76-80.

63. Halpain S, Hipolito A, Saffer L (1998) Regulation of F-actin stability in dendritic spines by glutamate receptors and calcineurin. J Neurosci 18: 9835-9844.

64. Hamlyn LH (1962) The fine structure of the mossy fibre endings in the hippocampus of the rabbit. J Anat 97: 112-120.

65. Harris KM, Stevens JK (1989) Dendritic spines of CA 1 pyramidal cells in the rat hippocampus: serial electron microscopy with reference to their biophysical characteristics. J Neurosci 9: 2982-2997.

66. Harris KM, Kater SB (1994) Dendritic spines: cellular specializations imparting both stability and flexibility to synaptic function. Annu Rev Neurosci 17: 341-371.

67. Harris KM (1999) Structure, development, and plasticity of dendritic spines. Curr Opin Neurobiol 9: 343-348.

68. Heimrich B, Frotscher M (1991) Differentiation of dentate granule cells in slice cultures of rat hippocampus: a Golgi/electron microscopic study. Brain Res 538: 263-268.

69. Hoff SF, Scheff SW, Kwan AY, Cotman CW (1981) A new type of lesion-induced synaptogenesis: I. Synaptic turnover in non-denervated zones of the dentate gyrus in young adult rats. Brain Res 222: 1-13.

70. Horton AC, Ehlers MD (2003) Dual modes of endoplasmic reticulum-to-Golgi transport in dendrites revealed by live-cell imaging. J Neurosci 23: 6188-6199.

71. Horton AC, Racz B, Monson EE, Lin AL, Weinberg RJ, Ehlers MD (2005) Polarized secretory trafficking directs cargo for asymmetric dendrite growth and morphogenesis. Neuron 48: 757-771.

72. Hosokawa T, Bliss TV, Fine A (1992) Persistence of individual dendritic spines in living brain slices. Neuroreport 3: 477-480.

73. Hsu SM, Raine L, Fanger H (1981) The use of antiavidin antibody and avidin-biotin-peroxidase complex in immunoperoxidase technics. Am J Clin Pathol 75: 816-821.

74. Iakoucheva LM, Kimzey AL, Masselon CD, Smith RD, Dunker AK, Ackerman EJ (2001) Aberrant mobility phenomena of the DNA repair protein XPA. Protein Sci 10: 1353-1362.

75. Irwin SA, Patel B, Idupulapati M, Harris JB, Crisostomo RA, Larsen BP, Kooy F, Willems PJ, Cras P, Kozlowski PB, Swain RA, Weiler IJ, Greenough WT (2001) Abnormal dendritic spine characteristics in the temporal and visual cortices of patients with fragile-X syndrome: a quantitative examination. Am J Med Genet 98: 161-167.

76. Kiss J, Buzsaki G, Morrow JS, Glantz SB, Leranth C (1996) Entorhinal cortical innervation of parvalbumin-containing neurons (Basket and Chandelier cells) in the rat Ammon's horn. Hippocampus 6: 239-246.

77. Knott GW, Holtmaat A, Wilbrecht L, Welker E, Svoboda K (2006) Spine growth precedes synapse formation in the adult neocortex in vivo. Nat Neurosci 9: 1117-1124.

78. Korkotian E, Segal M (1998) Fast confocal imaging of calcium released from stores in dendritic spines. Eur J Neurosci 10: 2076-2084.

79. Korkotian E, Holcman D, Segal M (2004) Dynamic regulation of spine-dendrite coupling in cultured hippocampal neurons. Eur J Neurosci 20: 2649-2663.

80. Kosaka T (1980) The axon initial segment as a synaptic site: ultrastructure and synaptology of the initial segment of the pyramidal cell in the rat hippocampus (CA3 region). J Neurocytol 9: 861-882.

81. Kossel AH, Williams CV, Schweizer M, Kater SB (1997) Afferent innervation influences the development of dendritic branches and spines via both activity-dependent and non-activity-dependent mechanisms. J Neurosci 17: 6314-6324.

82. Kremerskothen J, Plaas C, Kindler S, Frotscher M, Barnekow A (2005) Synaptopodin, a molecule involved in the formation of the dendritic spine apparatus, is a dual actin/alpha-actinin binding protein. J Neurochem 92: 597-606.

83. Laemmli UK (1970) Cleavage of structural proteins during the assembly of the head of bacteriophage T4. Nature 227: 680-685.

84. LaVail JH, Wolf MK (1973) Postnatal development of the mouse dentate gyrus in organotypic cultures of the hippocampal formation. Am J Anat 137: 47-65.

85. Li D, Field PM, Starega U, Li Y, Raisman G (1993) Entorhinal axons project to dentate gyrus in organotypic slice co-culture. Neuroscience 52: 799-813.

86. Li D, Field PM, Raisman G (1995) Failure of axon regeneration in postnatal rat entorhinohippocampal slice coculture is due to maturation of the axon, not that of the pathway or target. Eur J Neurosci 7: 1164-1171.

87. Lin F, Yu YP, Woods J, Cieply K, Gooding B, Finkelstein P, Dhir R, Krill D, Becich MJ, Michalopoulos G, Finkelstein S, Luo JH (2001) Myopodin, a synaptopodin homologue, is frequently deleted in invasive prostate cancers. Am J Pathol 159: 1603-1612.

88. Lisman J (1989) A mechanism for the Hebb and anti-Hebb processes underlying learning and memory. Proc Natl Acad Sci U S A 86: 9574-9578.

89. Lynch G, Matthews DA, Mosko S, Parks T, Cotman C (1972) Induced acetylcholinesterase-rich layer in rat dentate gyrus following entorhinal lesions. Brain Res 42: 311-318.

90. Malenka RC, Bear MF (2004) LTP and LTD: an embarrassment of riches. Neuron 44: 5-21.

91. Maletic-Savatic M, Malinow R, Svoboda K (1999) Rapid dendritic morphogenesis in CA1 hippocampal dendrites induced by synaptic activity. Science 283: 1923-1927.

92. Marrone DF, LeBoutillier JC, Petit TL (2004a) Changes in synaptic ultrastructure during reactive synaptogenesis in the rat dentate gyrus. Brain Res 1005: 124-136.

93. Marrone DF, LeBoutillier JC, Petit TL (2004b) Comparative analyses of synaptic densities during reactive synaptogenesis in the rat dentate gyrus. Brain Res 996: 19-30.

94. Matsuzaki M, Honkura N, Ellis-Davies GC, Kasai H (2004) Structural basis of long-term potentiation in single dendritic spines. Nature 429: 761-766.

95. Matthews DA, Cotman C, Lynch G (1976a) An electron microscopic study of lesion-induced synaptogenesis in the dentate gyrus of the adult rat. I. Magnitude and time course of degeneration. Brain Res 115: 1-21.

96. Matthews DA, Cotman C, Lynch G (1976b) An electron microscopic study of lesion-induced synaptogenesis in the dentate gyrus of the adult rat. II. Reappearance of morphologically normal synaptic contacts. Brain Res 115: 23-41.

97. Matthews, MR, Cowan, WM, and Powell, TPS. (1960) Transneuronal cell degeneration in the lateral geniculate nucleus of the macaque monkey. Journal of Anatomy 94: 145-169.

98. McKinney RA, Capogna M, Durr R, Gahwiler BH, Thompson SM (1999) Miniature synaptic events maintain dendritic spines via AMPA receptor activation. Nat Neurosci 2: 44-49.

99. Miyata M, Finch EA, Khiroug L, Hashimoto K, Hayasaka S, Oda SI, Inouye M, Takagishi Y, Augustine GJ, Kano M (2000) Local calcium release in dendritic spines required for long-term synaptic depression. Neuron 28: 233-244.

100. Muller D, Buchs PA, Stoppini L (1993) Time course of synaptic development in hippocampal organotypic cultures. Brain Res Dev Brain Res 71: 93-100.

101. Muller W, Connor JA (1991) Dendritic spines as individual neuronal compartments for synaptic Ca2+ responses. Nature 354: 73-76.

102. Mullis K, Faloona F, Scharf S, Saiki R, Horn G, Erlich H (1986) Specific enzymatic amplification of DNA in vitro: the polymerase chain reaction. Cold Spring Harb Symp Quant Biol 51 Pt 1: 263-273.

103. Mundel P, Heid HW, Mundel TM, Kruger M, Reiser J, Kriz W (1997) Synaptopodin: an actin-associated protein in telencephalic dendrites and renal podocytes. J Cell Biol 139: 193-204.

104. Nadler JV, Cotman CW, Lynch GS (1977) Histochemical evidence of altered development of cholinergic fibers in the rat dentate gyrus following lesions. I. Time course after complete unilateral entorhinal lesion at various ages. J Comp Neurol 171: 561-587.

105. Nakada C, Ritchie K, Oba Y, Nakamura M, Hotta Y, Iino R, Kasai RS, Yamaguchi K, Fujiwara T, Kusumi A (2003) Accumulation of anchored proteins forms membrane diffusion barriers during neuronal polarization. Nat Cell Biol 5: 626-632.

106. Nimchinsky EA, Sabatini BL, Svoboda K (2002) Structure and function of dendritic spines. Annu Rev Physiol 64: 313-353.

107. Nitsch R, Frotscher M (1992) Reduction of posttraumatic transneuronal "early gene" activation and dendritic atrophy by the N-methyl-D-aspartate receptor antagonist MK-801. Proc Natl Acad Sci U S A 89: 5197-5200.

108. Nitsch R, Frotscher M (1993) Transneuronal changes in dendrites of GABAergic parvalbumin-containing neurons of the rat fascia dentata following entorhinal lesion. Hippocampus 3: 481-490.

109. O'Brien RJ, Kamboj S, Ehlers MD, Rosen KR, Fischbach GD, Huganir RL (1998) Activity-dependent modulation of synaptic AMPA receptor accumulation. Neuron 21: 1067-1078.

110. Olney JW (1969) Brain lesions, obesity, and other disturbances in mice treated with monosodium glutamate. Science 164: 719-721.

111. Palay SL, Sotelo C, Peters A, Orkand PM (1968) The axon hillock and the initial segment. J Cell Biol 38: 193-201.

112. Parnavelas JG, Lynch G, Brecha N, Cotman CW, Globus A (1974) Spine loss and regrowth in hippocampus following deafferentation. Nature 248: 71-73.

113. Paxinos G, Watson C (1982) Atlas of the rat brain in stereotaxic coordinates. Academic Press, San Diego.

114. Peters A, Proskauer CC, Kaiserman-Abramof IR (1968) The small pyramidal neuron of the rat cerebral cortex. The axon hillock and initial segment. J Cell Biol 39: 604-619.

115. Peters A, Kaiserman-Abramof IR (1970) The small pyramidal neuron of the rat cerebral cortex. The perikaryon, dendrites and spines. Am J Anat 127: 321-355.

116. Pierce JP, van Leyen K, McCarthy JB (2000) Translocation machinery for synthesis of integral membrane and secretory proteins in dendritic spines. Nat Neurosci 3: 311-313.

117. Pierce JP, Mayer T, McCarthy JB (2001) Evidence for a satellite secretory pathway in neuronal dendritic spines. Curr Biol 11: 351-355.

118. Prang P, Del Turco D, Kapfhammer JP (2001) Regeneration of entorhinal fibers in mouse slice cultures is age dependent and can be stimulated by NT-4, GDNF, and modulators of G-proteins and protein kinase C. Exp Neurol 169: 135-147.

119. Prang P, Del Turco D, Deller T (2003) Associational sprouting in the mouse fascia dentata after entorhinal lesion in vitro. Brain Res 978: 205-212.

120. Racca C, Stephenson FA, Streit P, Roberts JD, Somogyi P (2000) NMDA receptor content of synapses in stratum radiatum of the hippocampal CA1 area. J Neurosci 20: 2512-2522.

121. Ramon y Cajal S (1888) Estructura de los centros nerviosos de las aves. Rev Trim Histol Norm Pat 1: 1-10.

122. Ramon y Cajal S (1891) Significación fisiológica de las expansiones protoplásmicas y nerviosas de la sustancia gris. Revista de ciencias médicas de Barcelona 17: 23-37.

123. Ramon y Cajal S (1896) Las espinas colaterales de las células del cerebro teñidas por el azul de metileno. Revista Trimestral Micrográfica 1: 123-136.

124. Rao A, Craig AM (1997) Activity regulates the synaptic localization of the NMDA receptor in hippocampal neurons. Neuron 19: 801-812.

125. Rappert A, Bechmann I, Pivneva T, Mahlo J, Biber K, Nolte C, Kovac AD, Gerard C, Boddeke HW, Nitsch R, Kettenmann H (2004) CXCR3-dependent microglial recruitment is essential for dendrite loss after brain lesion. J Neurosci 24: 8500-8509.

126. Reeves TM, Steward O (1988) Changes in the firing properties of neurons in the dentate gyrus with denervation and reinnervation: implications for behavioral recovery. Exp Neurol 102: 37-49.

127. Ribak CE, Seress L, Amaral DG (1985) The development, ultrastructure and synaptic connections of the mossy cells of the dentate gyrus. J Neurocytol 14: 835-857.

128. Roth SU, Sommer C, Mundel P, Kiessling M (2001) Expression of synaptopodin, an actin-associated protein, in the rat hippocampus after limbic epilepsy. Brain Pathol 11: 169-181.

129. Rudelli RD, Brown WT, Wisniewski K, Jenkins EC, Laure-Kamionowska M, Connell F, Wisniewski HM (1985) Adult fragile X syndrome. Clinico-neuropathologic findings. Acta Neuropathol (Berl) 67: 289-295.

130. Sabatini BL, Oertner TG, Svoboda K (2002) The life cycle of Ca(2+) ions in dendritic spines. Neuron 33: 439-452.

131. Schikorski T, Stevens CF (1997) Quantitative ultrastructural analysis of hippocampal excitatory synapses. J Neurosci 17: 5858-5867.

132. Schultz C, Konig HG, Del Turco D, Politi C, Eckert GP, Ghebremedhin E, Prehn JH, Kogel D, Deller T (2006) Coincident enrichment of phosphorylated IkappaBalpha, activated IKK, and phosphorylated p65 in the axon initial segment of neurons. Mol Cell Neurosci 33: 68-80.

133. Segal M, Greenberger V, Korkotian E (2003) Formation of dendritic spines in cultured striatal neurons depends on excitatory afferent activity. Eur J Neurosci 17: 2573-2585.

134. Segal M (2005) Dendritic spines and long-term plasticity. Nat Rev Neurosci 6: 277-284.

135. Seil FJ, Eckenstein FP, Reier PJ (1992) Induction of dendritic spine proliferation by an astrocyte secreted factor. Exp Neurol 117: 85-89.

136. Seil FJ (1997) Cerebellar culture models of dendritic spine proliferation after transplantation of glia. J Neural Transplant Plast 6: 1-10.

137. Sharp AH, McPherson PS, Dawson TM, Aoki C, Campbell KP, Snyder SH (1993) Differential immunohistochemical localization of inositol 1,4,5-trisphosphate- and ryanodine-sensitive Ca2+ release channels in rat brain. J Neurosci 13: 3051-3063.

138. Shi S, Hayashi Y, Esteban JA, Malinow R (2001) Subunit-specific rules governing AMPA receptor trafficking to synapses in hippocampal pyramidal neurons. Cell 105: 331-343.

139. Somogyi P, Hamori J (1976) A quantitative electron microscopic study of the Purkinje cell axon initial segment. Neuroscience 1: 361-365.

140. Somogyi P, Smith AD, Nunzi MG, Gorio A, Takagi H, Wu JY (1983) Glutamate decarboxylase immunoreactivity in the hippocampus of the cat: distribution of immunoreactive synaptic terminals with special reference to the axon initial segment of pyramidal neurons. J Neurosci 3: 1450-1468.

141. Soriano E, Frotscher M (1994) Mossy cells of the rat fascia dentata are glutamate-immunoreactive. Hippocampus 4: 65-69.

142. Spacek J (1985) Three-dimensional analysis of dendritic spines. II. Spine apparatus and other cytoplasmic components. Anat Embryol (Berl) 171: 235-243.

143. Spacek J, Harris KM (1997) Three-dimensional organization of smooth endoplasmic reticulum in hippocampal CA1 dendrites and dendritic spines of the immature and mature rat. J Neurosci 17: 190-203.

144. Steward O (1991) Synapse replacement on cortical neurons following denervation. Cereb Cortex 9: 81-132.

145. Steward O (1994) Reorganization of Neuronal Circuitry Following Central Nervous System Trauma: Naturally Occurring Processes and Opportunities for Therapeutic

Intervention. In: The Neurobiology of Central Nervous System Trauma (Salzman SK, Faden AI, eds), pp 266-287. New York: Oxford University Press.

146. Steward O, Vinsant SL (1983) The process of reinnervation in the dentate gyrus of the adult rat: a quantitative electron microscopic analysis of terminal proliferation and reactive synaptogenesis. J Comp Neurol 214: 317-386.

147. Steward O, Vinsant SL, Davis L (1988) The process of reinnervation in the dentate gyrus of adult rats: an ultrastructural study of changes in presynaptic terminals as a result of sprouting. J Comp Neurol 267: 203-210.

148. Stoppini L, Buchs PA, Muller D (1991) A simple method for organotypic cultures of nervous tissue. J Neurosci Methods 37: 173-182.

149. Stuart G, Schiller J, Sakmann B (1997) Action potential initiation and propagation in rat neocortical pyramidal neurons. J Physiol 505 (Pt 3): 617-632.

150. Suetsugu M, Mehraein P (1980) Spine distribution along the apical dendrites of the pyramidal neurons in Down's syndrome. A quantitative Golgi study. Acta Neuropathol (Berl) 50: 207-210.

151. Svoboda K, Tank DW, Denk W (1996) Direct measurement of coupling between dendritic spines and shafts. Science 272: 716-719.

152. Svoboda K, Mainen ZF (1999) Synaptic [Ca^{2+}]: intracellular stores spill their guts. Neuron 22: 427-430.

153. Takashima S, Ieshima A, Nakamura H, Becker LE (1989) Dendrites, dementia and the Down syndrome. Brain Dev 11: 131-133.

154. Takumi Y, Ramirez-Leon V, Laake P, Rinvik E, Ottersen OP (1999) Different modes of expression of AMPA and NMDA receptors in hippocampal synapses. Nat Neurosci 2: 618-624.

155. Tarrant SB, Routtenberg A (1979) Postsynaptic membrane and spine apparatus: proximity in dendritic spines. Neurosci Lett 11: 289-294.

156. Toni N, Buchs PA, Nikonenko I, Bron CR, Muller D (1999) LTP promotes formation of multiple spine synapses between a single axon terminal and a dendrite. Nature 402: 421-425.

157. Toresson H, Grant SG (2005) Dynamic distribution of endoplasmic reticulum in hippocampal neuron dendritic spines. Eur J Neurosci 22: 1793-1798.

158. Trachtenberg JT, Chen BE, Knott GW, Feng G, Sanes JR, Welker E, Svoboda K (2002) Long-term in vivo imaging of experience-dependent synaptic plasticity in adult cortex. Nature 420: 788-794.

159. Trommald M, Hulleberg G (1997) Dimensions and density of dendritic spines from rat dentate granule cells based on reconstructions from serial electron micrographs. J Comp Neurol 377: 15-28.

160. Tyler WJ, Pozzo-Miller L (2003) Miniature synaptic transmission and BDNF modulate dendritic spine growth and form in rat CA1 neurones. J Physiol 553: 497-509.

161. Van Harreveld A, Fifkova E (1975) Swelling of dendritic spines in the fascia dentata after stimulation of the perforant fibers as a mechanism of post-tetanic potentiation. Exp Neurol 49: 736-749.

162. Vidal M, Morris R, Grosveld F, Spanopoulou E (1990) Tissue-specific control elements of the Thy-1 gene. EMBO J 9: 833-840.

163. Volfovsky N, Parnas H, Segal M, Korkotian E (1999) Geometry of dendritic spines affects calcium dynamics in hippocampal neurons: theory and experiments. J Neurophysiol 82: 450-462.

164. Wenzel HJ, Buckmaster PS, Anderson NL, Wenzel ME, Schwartzkroin PA (1997) Ultrastructural localization of neurotransmitter immunoreactivity in mossy cell axons and their synaptic targets in the rat dentate gyrus. Hippocampus 7: 559-570.

165. West JR, Deadwyler S, Cotman CW, Lynch G (1975) Time-dependent changes in commissural field potentials in the dentate gyrus following lesions of the entorhinal cortex in adult rats. Brain Res 97: 215-233.

166. Westrum LE (1993) Axon hillocks and initial segments in spinal trigeminal nucleus with emphasis on synapses including axo-axo-axonic contacts. J Neurocytol 22: 793-803.

167. Westrum LE, Blackstad TW (1962) An electron microscopic study of the stratum radiatum of the rat hippocampus (regio superior, CA 1) with particular emphasis on synaptology. J Comp Neurol 119: 281-309.

168. Winckler B, Forscher P, Mellman I (1999) A diffusion barrier maintains distribution of membrane proteins in polarized neurons. Nature 397: 698-701.

169. Woodhams PL, Atkinson DJ, Raisman G (1993) Rapid decline in the ability of entorhinal axons to innervate the dentate gyrus with increasing time in organotypic co-culture. Eur J Neurosci 5: 1596-1609.

170. Woolley CS, McEwen BS (1994) Estradiol regulates hippocampal dendritic spine density via an N-methyl-D-aspartate receptor-dependent mechanism. J Neurosci 14: 7680-7687.

171. Wu HY, Tomizawa K, Oda Y, Wei FY, Lu YF, Matsushita M, Li ST, Moriwaki A, Matsui H (2004) Critical role of calpain-mediated cleavage of calcineurin in excitotoxic neurodegeneration. J Biol Chem 279: 4929-4940.

172. Wyszynski M, Kharazia V, Shanghvi R, Rao A, Beggs AH, Craig AM, Weinberg R, Sheng M (1998) Differential regional expression and ultrastructural localization of alpha-actinin-2, a putative NMDA receptor-anchoring protein, in rat brain. J Neurosci 18: 1383-1392.

173. Yamazaki M, Matsuo R, Fukazawa Y, Ozawa F, Inokuchi K (2001) Regulated expression of an actin-associated protein, synaptopodin, during long-term potentiation. J Neurochem 79: 192-199.

174. Yuste R, Bonhoeffer T (2001) Morphological changes in dendritic spines associated with long-term synaptic plasticity. Annu Rev Neurosci 24: 1071-1089.

175. Zafirov S, Heimrich B, Frotscher M (1994) Dendritic development of dentate granule cells in the absence of their specific extrinsic afferents. J Comp Neurol 345: 472-480.

176. Zappone CA, Sloviter RS (2001) Commissurally projecting inhibitory interneurons of the rat hippocampal dentate gyrus: a colocalization study of neuronal markers and the retrograde tracer Fluoro-gold. J Comp Neurol 441: 324-344.

177. Zimmer J, Laurberg S, Sunde N (1986) Non-cholinergic afferents determine the distribution of the cholinergic septohippocampal projection: a study of the AChE staining pattern in the rat fascia dentata and hippocampus after lesions, X-irradiation, and intracerebral grafting. Exp Brain Res 64: 158-168.

178. Zuo Y, Lin A, Chang P, Gan WB (2005) Development of long-term dendritic spine stability in diverse regions of cerebral cortex. Neuron 46: 181-189.

7. Curriculum Vitae

Given-, and last name: Carlos Bas Orth

Date of birth: 25.02.1978

Place of birth: Ludwigshafen am Rhein, Germany

Parents: José Antonio Bas García and

Eva Maria Bas García (neé Orth)
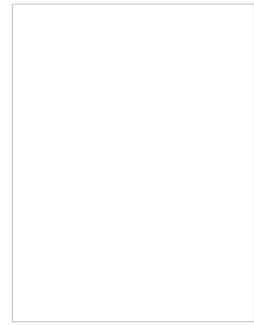
Education

Jun 1997   School leaving examination ("Abitur") at Moll-Gymnasium, Mannheim

Oct 1997 – Oct 2002   Studies of biology at University of Heidelberg, Germany

Main subjects: molecular cell biology, animal physiology and biochemistry

Graduation as "Diplombiologe"

Feb 2000 - Jul 2000   Courses of biology at Flinders University and Flinders Medical Center, Adelaide, Australia

Practical work in the laboratory of Prof. Dr. Robert Rush, Dept. of Human Physiology, Flinders Medical Center

Jan 2002 - Sep 2002   Diploma thesis in the laboratory of Prof. Dr. Roland Brandt, Institute of Neurobiology, University of Heidelberg, Germany

Analysis of the function of the A-kinase anchoring protein gravin in neurons

Nov 2002 - present   PhD-student in the laboratory of Prof. Dr. T. Deller, Institute of Clinical Neuroanatomy, J.W. Goethe-University, Frankfurt/Main, Germany

Feb 2003 – Feb 2006   Member of graduate program "neuronal plasticity" at University of Frankfurt

8. Publications

Papers

Bas Orth, C., Vlachos, A., Del Turco, D., Burbach, G.J., Haas, C.A., Mundel, P., Feng, G., Frotscher, M., and Deller, T. (2005) Lamina-Specific Distribution of Synaptopodin, an Actin-Associated Molecule Essential for the Spine Apparatus, in Identified Principal Cell Dendrites of the Mouse Hippocampus. J Comp Neurol 487:227-239.

Czarnecki, K., Haas, C.A., Bas Orth, C., Deller, T., and Frotscher, M. (2005) Postnatal Development of Synaptopodin Expression in the Rodent Hippocampus. J Comp Neurol 490:133-144.

Deller, T., Bas Orth, C., Vlachos, A., Merten, T., Del Turco, D., Dehn. D., Mundel, P., and Frotscher, M. (2006) Plasticity of Synaptopodin and the Spine Apparatus Organelle in the Rat Fascia Dentata Following Entorhinal Cortex Lesion. J Comp Neurol 499:471-484.

Deller, T., Bas Orth, C., Del Turco, D., Vlachos, A., Burbach, G.J., Drakew, A., Chabanis, S., Korte, M., Schwegler, H., Haas, C.A., and Frotscher, M. (2007) A Role for Synaptopodin and the Spine Apparatus in Hippocampal Synaptic Plasticity. Review, Ann Anat 189:5-16.

Submitted papers

Bas Orth, C.[*], Schultz, C.[*], Müller, C.M., Frotscher, M., and Deller, T. (2007) Loss of the cisternal organelle in the axon initial segment of cortical neurons in synaptopodin-deficient mice. [*]Authors contributed equally.

Abstracts

Bas Orth, C., Del Turco, D., Burbach, G.J., Haas, C.A., Mundel, P., Frotscher, M., and Deller, T. Layer- and Region-Specific Expression of Synaptopodin, an Actin-Associated Molecule Essential for the Spine Apparatus, in the Mouse Hippocampus. Poster, Neurochemistry Winter Conference, 03/27/04 – 04/01/04, Sölden, Austria.

Vuksic, M., Del Turco, D., Bas Orth, C., Burbach, G.J., Schwarzacher, S.W., Feng, G., and Deller, T. MorphologicalAnalysis of Hippocampal Neurons in Green Fluorescent Protein Expressing Transgenic Mice. Poster, Neurochemistry Winter Conference, 03/27/04 – 04/01/04, Sölden, Austria.

Bas Orth, C., Vlachos, A., Del Turco, D., Burbach, G.J., Feng, G., Haas, C.A., Mundel, P., Frotscher, M., and Deller, T. Layer and region-specific distribution of the spine apparatus in the mouse hippocampus. Poster, Program No. 614.9. 34th annual meeting of the American Society for Neuroscience, 10/23/04 – 10/27/04, San Diego, USA.

Schultz C., Bas Orth C., Mundel P., Frotscher M., and Deller T. Synaptopodin is associated with the cisternal organelle of the axon initial segment. Talk, 22nd annual workshop of the Anatomische Gesellschaft, 09/28/05 – 09/30/05, Würzburg, Germany.

Deller, T., Del Turco, D., Bas Orth, C., Burbach, G.J., Dehn, D., Vlachos, A., Merten, T., Haas, C.A., Mundel, P., and Frotscher, M. Plasticity of synaptopodin and the spine apparatus organelle in rat hippocampal granule cells following entorhinal cortex lesion. Poster, Program No. 848.3. 35th annual meeting of the American Society for Neuroscience, 11/12/05 – 11/16/05, Washington, USA.

Bas Orth, C., Vlachos, A., and Deller, T. Imaging of denervation-induced dendritic spine loss in organotypic slice cultures. Poster, Neurochemistry Winter Conference, 03/25/06 – 03/30/06, Sölden, Austria.

Jedlicka, P., Schwarzacher, S.W., Bas Orth, C., Frotscher, M., and Deller, T. In vivo electrophysiological characterization of the dentate gyrus in adult synaptopodin-deficient mice. Poster, Neurochemistry Winter Conference, 03/25/06 – 03/30/06, Sölden, Austria.

Bas Orth, C., Schultz, C., Müller, C.M., Frotscher, M., and Deller, T. The actin-associated molecule synaptopodin is essential for the cisternal organelle in the axon initial segment. Poster, Program No. A193.2. 5th Forum of European Neuroscience, 07/08/06 – 07/12/06, Vienna, Austria.

Jedlicka, P., Schwarzacher, S.W., Bas Orth, C., Frotscher, M., and Deller, T. Synaptopodin-deficient mice show deficits in neuronal plasticity following perforant pathway stimulation in vivo. Poster, Program No. A085.11. 5th Forum of European Neuroscience, 07/08/06 – 07/12/06, Vienna, Austria.

Schultz C., Bas Orth C., Lacas-Gervais S., Solimena M., Frotscher M., and Deller T. Partial loss of the cisternal organelle in βIV-spectrin-deficient mice. Talk, 23rd annual workshop of the Anatomische Gesellschaft, 09/27/06 – 09/29/06, Würzburg, Germany.

9. Acknowledgement

First, I thank my thesis supervisor Prof. Dr. Thomas Deller for initiating this interesting project, for his continuous support and mentoring, and for stimulating discussions.

I am also grateful to Prof. Dr. Herbert Zimmermann and Dr. Gabi Lahner for their dedication as chair and coordinator, respectively, of the graduate program "Neural Plasticity." I profited enormously from this program, both scientifically and on a human level.

Next, I cordially thank my colleagues at the Anatomical Institute I of the J.W. Goethe-University. Working on this project would have been much more troublesome and much less enjoyable without their support, their helpful discussions, the excellent working atmosphere, and the constant supply of first-class culinary delicacies.

Above all, my warmest thanks go to my friends and my family, especially Daniela and Emily, for their understanding and their constant encouragement during times that were sometimes fascinating, sometimes frustrating, but always exciting.

10.Zusammenfassung (Deutsch)

Das Aktin-assoziierte Protein Synaptopodin – Verteilung in Neuronen des Hippokampus und Rolle bei Plastizität dendritischer Dornen

Dissertation zur Erlangung des Doktorgrades der Naturwissenschaften

vorgelegt beim Fachbereich Biowissenschaften
der Johann Wolfgang Goethe-Universität
Frankfurt am Main

von
Carlos Bas Orth
aus Ludwigshafen am Rhein

Frankfurt am Main 2007

Das Aktin-assoziierte Protein Synaptopodin kommt in einer Subpopulation von dendritischen Dornen telenzephaler Prinzipalneurone vor. Dort ist es eng mit dem Dornapparat, einem putativen Kalziumspeicher, assoziiert. Synaptopodin-defiziente Mäuse bilden keine Dornapparate aus und weisen Defizite in Langzeitpotenzierung und räumlichem Lernen auf. Diese Befunde deuten darauf hin, dass Synaptopodin eine Rolle bei synaptischer Plastizität spielt.

In dieser Arbeit wurden drei Fragestellungen bearbeitet: (1) Wie sind Synaptopodin und der Dornapparat in einzelnen Neuronen des Hippokampus verteilt? (2) Wird die Verteilung von Synaptopodin durch eine partielle Deafferenzierung beeinflusst? (3) Ist Synaptopodin an der Regulation des läsionsinduzierten Verlusts von dendritischen Dornen beteiligt?

Die Ergebnisse dieser Arbeit sind: (1) Immunhistochemische Untersuchungen im Hippokampus der Maus zeigten schichtenspezifische Unterschiede in der Häufigkeit Synpaptopodin-positiver Dornen in identifizierten Neuronen. (2) Licht- und elektronenmikroskopische Untersuchungen ergaben, dass Synaptopodin auch im Axoninitialsegment von Prinzipalneuronen vorkommt; dort ist es essentieller Bestandteil der zisternalen Organelle. (3) Immunhistochemische Färbungen der Fascia dentata zu verschiedenen Zeitpunkten nach entorhinaler Läsion wiesen signifikante Änderungen in der Dichte von Synaptopodin-Punkten nach. Diese Veränderungen lassen darauf schließen, dass Synaptopodin durch präsynaptische Signale reguliert wird. (4) Mittels konfokaler Langzeitbeobachtung von Neuronen in organotypischen Hippokampuskulturen wurde die Dynamik von Dornen nach Deafferenzierung untersucht. Während Dornen unter Kontrollbedingungen eine bemerkenswerte Stabilität aufwiesen, führte die Deafferenzierung zunächst zum Verlust und schließlich zur Neubildung dendritischer Dornen. Die Untersuchung von Kulturen aus Synaptopodin-defizienten Mäusen zeigte keine signifikanten Unterschiede im Vergleich zu Kulturen aus Kontrollmäusen. (5) Um zukünftige Experimente zur Dynamik und Funktion von Synaptopodin zu ermöglichen, wurden transgene Mäuse erzeugt, die neuronal fluoreszenzmarkiertes Synaptopodin exprimieren.

Zusammengefasst liefert diese Arbeit neue Erkenntnisse zu (1) der subzellulären Verteilung von Synaptopodin in Dornen und im Axoninitialsegment, (2) zur molekularen Zusammensetzung der zisternalen Organelle und (3) zur Dynamik dendritischer Dornen und des Dornapparates nach Deafferenzierung in vivo und in vitro.

Einleitung

Nervenzellen sind stark polarisierte Zellen welche eine Vielzahl langer Zellausläufer bilden. Einer dieser Ausläufer entwickelt sich zum Axon und dient der Weiterleitung von elektrischen Signalen an andere Nervenzellen. Die übrigen Ausläufer entwickeln sich zu Dendriten, welche dem Empfang von elektrischen Signalen dienen. Zellkörper und Dendriten bilden dabei das basolaterale Zellkompartiment, während das Axon das apikale Kompartiment darstellt. Entsprechend unterscheiden sich Axone und Dendriten hinsichtlich ihrer Morphologie und ihrer molekularen Ausstattung. Ein typisches Merkmal von Dendriten einer Vielzahl von Nervenzelltypen ist die Ausbildung von kleinen Fortsätzen, den Dornen, welche die Hauptkontaktstellen für erregende Synapsen darstellen. Vermutlich dienen dendritische Dornen dazu, einzelne Synapsen biochemisch voneinander zu isolieren und damit synapsenspezifische Modifikationen zu ermöglichen. Dendritische Dornen sind keine statischen Strukturen sondern weisen eine beachtliche Plastizität auf. So führt eine geeignete elektrische Stimulation zur Vergrößerung vorhandener Dornen und zur Bildung neuer Dornen. Im Gegenzug führt die Blockade der synaptischen Transmission oder der Verlust afferenter Fasern zu einem Verlust von dendritischen Dornen. Auch bei einer Reihe von Erbkrankheiten mit geistiger Retardierung (z.B. Down-Syndrom, Fragiles X-Syndrom) wurden Störungen in der Bildung bzw. Reifung von dendritischen Dornen nachgewiesen. Dendritische Dornen scheinen also von grundlegender Bedeutung für synaptische Plastizität, Lernen und Gedächtnis zu sein. Ein an synaptischer Plastizität beteiligtes Molekül, welches in dendritischen Dornen vorkommt, ist das Aktin-assoziierte Protein Synaptopodin. Dieses kommt in einer Subpopulation von dendritischen Dornen telenzephaler Prinzipalneurone vor. Es ist ein Bestandteil des Dornapparates, eines putativen Kalziumspeichers. Synaptopodin-defiziente Mäuse bilden keine Dornapparate aus und weisen Defizite in Langzeitpotenzierung und räumlichem Lernen auf. Umgekehrt wurde gezeigt, dass eine elektrische Stimulation des Hippokampus zu einer Hochregulation von Synaptopodin führt. Dies bedeutet, dass Synaptopodin Einfluss auf die Ausprägung synaptischer Plastizität hat und gleichzeitig vermutlich selbst durch synaptische Aktivität reguliert wird.

Ziel dieser Arbeit war, mehr über die Rolle von Synaptopodin bei synaptischer Plastizität zu lernen. Dazu wurden folgende Aufgabenstellungen bearbeitet:

(1) Zunächst wurde eine detaillierte, quantitative Analyse der Verteilung von Synaptopodin im Hippokampus der Maus durchgeführt.

(2) Danach wurde der Einfluss einer partiellen Denervierung auf diese Verteilung in vivo untersucht.

(3) Als nächstes wurden die Dynamik und das Ausmaß des läsionsinduzierten Dornenverlustes in vitro untersucht.

(4) Des Weiteren wurde ein möglicher Einfluss von Synaptopodin auf diesen Dornverlust überprüft.

(5) Schließlich wurden Synaptopodin-transgene Mäuse erzeugt, um zukünftige Untersuchungen zur Dynamik von Synaptopodin nach Deafferenzierung zu erleichtern.

Material, Methoden und Ergebnisse

Um die Verteilung von Synaptopodin im Hippokampus zu untersuchen, wurden immunhistochemische Färbungen von Schnitten perfusionsfixierter Mausgehirne angefertigt. Dazu wurden C57BL6/J Mäuse sowie EGFP-transgene Mäuse verwendet. In den transgenen Mäusen exprimieren einzelne Prinzipalneurone das grün fluoreszierende Protein (EGFP), wodurch sich die Morphologie dieser Zellen im konfokalen Mikroskop dreidimensional darstellen lässt. Die Analyse EGFP-positiver Dendriten ergab, dass über 95% der Synaptopodin-positiven Punkte in dendritischen Dornen lokalisiert waren. Dies zeigte, dass Synaptopodin in der Tat als guter lichtmikroskopischer Marker für den Dornapparat betrachtet werden kann. Eine computergestützte automatisierte Segmentierung und Quantifizierung der konfokalen Bilddaten belegte darüber hinaus, dass die Dichte von Synaptopodin signifikante Unterschiede zwischen einzelnen Schichten des Hippokampus aufweist. Eine dreidimensionale Analyse einzelner EGFP-positiver Dendriten bestätigte diese schichtenspezifischen Unterschiede auf der Ebene individueller Neurone. So zeigten beispielsweise Pyramidenzellen in Feld CA1 deutliche Unterschiede zwischen proximalen und distalen Dendriten. Während ca. 32% der Dornen im distalen *Stratum lacunosum-molekulare* Synaptopodin enthielten, betrug dieser Wert für das proximale *Stratum radiatum* nur ca. 14%.

Als weiteres Ergebnis dieser immunhistochemischen Arbeiten konnte die Anwesenheit von Synaptopodin auch im Axoninitialsegment (AIS) von kortikalen und hippokampalen Prinzipalneuronen nachgewiesen werden. Dabei stellte sich heraus, dass nahezu jedes AIS mehrere Synaptopodin-immunreaktive Punkte aufweist. Elektronenmikroskopische Untersuchungen ergaben, dass Synaptopodin im AIS eng mit der zisternalen Organelle, einem putativen axonalen Homolog des dendritischen Dornapparates, assoziiert ist. Bei der Analyse von Synaptopodin-defizienten Mäusen wurden keine zisternalen Organellen gefunden, was darauf hinweist, dass Synaptopodin ein essentieller Bestandteil dieser axonalen Organelle ist.

Um den Einfluss einer partiellen Denervation auf die Verteilung von Synaptopodin zu untersuchen, wurden immunhistochemische Färbungen von Hirnschnitten der Ratte vor und zu verschiedenen Zeitpunkten (4, 7, 10, 14, 30, 180 Tage) nach einer entorhinalen Läsion angefertigt. Diese Läsion führt zu einer Degeneration der durchtrennten Fasern des *Tractus perforans* und damit zu einer Deafferenzierung der distalen Dendriten der Körnerzellen der Fascia dentata. Veränderungen der Synaptopodin-Dichte wurden mittels automatisierter computergestützter Analyse von konfokalen Bildern quantifiziert. In der denervierten äußeren Molekularschicht wurde vier Tage nach Läsion ein Absinken der Synaptopodin-Dichte auf 13% des Kontrollwertes beobachtet. Anschließend stieg die Dichte langsam an und erreichte 62% am Tag 30 und 78% am Tag 180 nach Läsion. Interessanterweise wurde auch eine Veränderung der Synaptopodin-Dichte in der nicht-denervierten inneren Molekularschicht der Fascia dentata beobachtet. Hier fiel der Wert auf 31% am Tag vier nach Läsion ab. Im Gegensatz zur äußeren Molekularschicht wurde dieser Verlust nach 14 Tagen vollständig ausgeglichen.

Für die Untersuchung der läsionsinduzierten Plastizität dendritischer Dornen wurde das in der Arbeitsgruppe etablierte Modell der in vitro Läsion von entorhino-hippokampalen Schnittkulturen verwendet. Um die Dynamik der Dornveränderungen beobachten zu können, wurde zunächst eine Methode zur Langzeitbeobachtung lebender EGFP-positiver Neurone in Schnittkulturen etabliert. Nach einer Reihe von Vorversuchen wurde ein aufrechtes konfokales Laserscanningmikroskop gewählt und beschafft. Anschließend wurden die Aufnahmeparameter optimiert, um eine wiederholte dreidimensionale Beobachtung identifizierter Neurone und Dendriten über einen Zeitraum von bis zu 6 Wochen zu ermöglichen. Die Beobachtung von reifen Kontrollkulturen zeigte, dass die Dichte von dendritischen Dornen in Kultur über einen Zeitraum von 6 Wochen konstant

bleibt. Die Analyse individueller Dornen ergab dabei eine mittlere Lebenszeit von 12,2 Tagen. 27% der Dornen blieben über den gesamten Beobachtungszeitraum erhalten. Nach einer entorhinalen Läsion wurde ein deutlicher Verlust von dendritischen Dornen an distalen Körnerzelldendriten beobachtet. Vier Tage nach Läsion waren nur noch 66% der Dornen erhalten. Danach stieg die Dichte der Dornen langsam an und erreichte 82% an Tag 21 und 93% an Tag 42 nach Läsion. Es gibt Hinweise in der Literatur, dass ein pathologischer Anstieg der intrazellulären Kalziumkonzentration maßgeblich an läsionsinduzierten Veränderungen von Dendriten und dendritischen Dornen beteiligt ist. Daher wurde in dieser Arbeit auch untersucht, ob sich das Fehlen des dendritischen Dornapparates als intrazellulärer Kalziumspeicher auf diese Form der Plastizität auswirkt. Die Untersuchung von Kulturen aus EGFP-transgenen, Synaptopodin-defizienten Mäusen ergab jedoch keinen signifikanten Unterschied im Vergleich zu Kulturen aus Kontrollmäusen.

Daten in der Literatur sowie Befunde dieser Arbeit deuten darauf hin, dass die Verteilung von Synaptopodin dynamisch reguliert wird. Um die Verteilung von Synaptopodin in lebenden Zellen in vitro und in vivo mittels moderner Verfahren (2-Photonen-Mikroskopie) zu ermöglichen, wurden Synaptopodin-transgene Mäuse erzeugt. Diese Tiere exprimieren ein Fusionsprotein aus Synaptopodin und dem grün-fluoreszierenden Protein bzw. aus Synaptopodin und dem cyan-fluoreszierenden Protein unter der Kontrolle des neuronalen Thy1.2 Promotors. Die Tiere wurden mittels Pronukleus-Injektion des transgenen Konstrukts hergestellt und es konnten insgesamt 13 Founder-Tiere identifiziert werden. Mit diesen Tieren werden zurzeit transgene Zuchtlinien aufgebaut, die in weiterführenden Untersuchungen zum Thema eingesetzt werden sollen. Sobald die ersten transgenen Nachkommen vorhanden sind, können die einzelnen Linien charakterisiert werden.

Diskussion

Daten aus dieser Arbeit zeigen, dass Synaptopodin innerhalb des Hippokampus schichtenspezifisch verteilt ist. Da Synaptopodin als geeigneter Marker für den Dornapparat angesehen werden kann, legen diese Beobachtungen nahe, dass auch die Organelle schichtenspezifisch im Hippokampus vorkommt. Interessanterweise korreliert das Verteilungsmuster von Synaptopodin mit dem bekannten Terminationsmuster

hippokampaler Afferenzen. Die Verteilung von Synaptopodin und dem Dornapparat könnte also durch präsynaptische Signale reguliert werden.

Weiterhin wurde in dieser Arbeit gezeigt, dass Synaptopodin ein essentieller Bestandteil der zisternalen Organelle im Axoninitialsegment von kortikalen und hippokampalen Prinzipalneuronen ist. Die Verwendung von Synaptopodin als Marker ermöglichte dabei erstmals eine lichtmikroskopische Abschätzung der Häufigkeit dieser Organelle. In der Tat kommt die zisternale Organelle regelmäßig im AIS vor. Jedes untersuchte AIS besaß mindestens einen Synaptopodin-immunreaktiven Punkt, wobei im Durchschnitt 3,2 Punkte pro 10 µm AIS beobachtet wurden. Die zisternale Organelle kommt damit deutlich häufiger vor, als es frühere elektronenmikroskopische Arbeiten vermuten lassen. Die Assoziation von Synaptopodin mit dem Dornapparat und der zisternalen Organelle ist ein Beleg für die molekulare Ähnlichkeit dieser beiden Strukturen.

Die Analyse der Verteilung von Synaptopodin in der denervierten Fascia dentata zeigte Veränderungen sowohl in der deafferenzierten als auch in der nicht-deafferenzierten Schicht. In der denervierten äußeren Molekularschicht wurde ein deutlicher Verlust an Synaptopodin-Punkten am Tag vier nach Läsion, gefolgt von einer langsamen und unvollständigen Erholung der Synaptopodin-Dichte beobachtet. Dieser Verlauf entspricht dem in diesem Modell bekannten Verlust dendritischer Dornen. Daraus lässt sich schließen, dass in dieser Schicht nach einer entorhinalen Läsion zunächst Dornen zusammen mit ihrem Dornapparat abgebaut werden. Dornen welche während der Erholungsphase neu gebildet werden, bilden dabei auch wieder einen Dornapparat aus. In der nicht-denervierten inneren Molekularschicht wurde ebenfalls ein Verlust von Synaptopodin-Punkten am Tag vier nach der Läsion beobachtet. Allerdings erreichte die Synaptopodin-Dichte hier bereits an Tag 14 nach Läsion wieder Kontrollwerte. Interessanterweise ist diese Schicht nicht von einem Verlust dendritischer Dornen betroffen. Vielmehr wurden in dieser Schicht ein transienter Rückgang synaptischer Aktivität sowie eine Remodellierung synaptischer Kontakte beschrieben. Der Zeitverlauf dieser Prozesse passt gut mit den beobachteten Veränderungen der Synaptopodin-Dichte in dieser Schicht zusammen und weist daher auf eine präsynaptische, möglicherweise aktivitätsabhängige Regulation der Verteilung von Synaptopodin hin.

In dieser Arbeit wurde des Weiteren eine Methode für die Langzeitbeobachtung lebender Neurone in organotypischen Schnittkulturen etabliert. Mit Hilfe dieser Methode konnte gezeigt werden, dass dendritische Dornen auch in Kultur über Tage bis Wochen stabil sind.

Diese Beobachtungen stehen im Einklang mit aktuellen in vivo Untersuchungen und liefern den ersten Beleg für die Stabilität dendritischer Dornen in vitro. Infolge einer partiellen Denervierung der distalen Körnerzelldendriten durch eine Läsion des entorhinalen Kortex wurde ein transienter Verlust von dendritischen Dornen beobachtet. Auch in diesem Fall waren Ausmaß und Zeitverlauf der Veränderungen vergleichbar mit der bekannten in vivo Situation. Dies bedeutet, dass das vorliegende System ein experimentell gut zugängliches in vitro Modell zur Untersuchung läsionsinduzierter Dornplastizität darstellt. Die Untersuchung von Kulturen aus Synaptopodin-defizienten Mäusen zeigte keine signifikanten Unterschiede im Vergleich zu Kulturen aus Kontrollmäusen. Dies könnte darauf hindeuten, dass der Dornapparat keine essentielle Rolle bei läsionsinduzierter Dornplastizität spielt. Ob dies tatsächlich der Fall ist und welche anderen Kalziumquellen an den beobachteten Prozessen beteiligt sein könnten, wird in zukünftigen Experimenten untersucht werden. Das in dieser Arbeit etablierte Modellsystem und die erhobenen Daten bilden für diese weiterführenden Untersuchungen eine wichtige Ausgangsbasis.

Ausblick

Die vorliegende Arbeit liefert neue und detaillierte Informationen zur Verteilung von Synaptopodin im Hippokampus. Interessanterweise ergaben sich darüber hinaus Hinweise für eine präsynaptische Regulation des postsynaptischen Proteins Synaptopodin und des Dornapparates. Diese Daten und die in dieser Arbeit generierten transgenen Mäuse bilden eine wichtige Grundlage für zukünftige Experimente zur Regulation und Funktion von Synaptopodin in vitro und in vivo. Des Weiteren wurde in dieser Arbeit ein Modellsystem zur Untersuchung der läsionsinduzierten Plastizität dendritischer Dornen etabliert und es wurden quantitative Daten zur Stabilität und zur läsionsinduzierten Plastizität dendritischer Dornen erhoben. Aufbauend auf diesen Befunden und diesem Modellsystem sind weitere Experimente geplant, um die Funktion von Synaptopodin und die molekularen Mechanismen des läsionsinduzierten Dornverlusts aufzuklären.

11. Lebenslauf

Vor- und Zuname:	Carlos Bas Orth
Geburtsdatum und -ort:	25.02.1978, Ludwigshafen am Rhein, Deutschland
Eltern:	José Antonio Bas García und
	Eva Maria Bas García (geborene Orth)

Ausbildung

Jun 1997	Abitur am Moll-Gymnasium in Mannheim
Okt 1997 – Okt 2002	Studium der Biologie an der Ruprecht-Karls Universität Heidelberg Schwerpunkte: Zellbiologie, Tierphysiologie und Biochemie Abschluss als „Diplombiologe"
Feb 2000 - Jul 2000	Studium der Biologie an der Flinders University und am Flinders Medical Center, Adelaide, Australien Praktikum in der Arbeitsgruppe von Prof. Dr. Robert Rush, Dept. of Human Physiology, Flinders Medical Center
Jan 2002 - Sep 2002	Diplomarbeit in der Arbeitsgruppe von Prof. Dr. Roland Brandt, Institut für Neurobiologie, Universität Heidelberg Titel der Arbeit: „Analyse der Funktion des A-Kinase verankernden Proteins Gravin in Nervenzellen"
seit Nov 2002	Doktorand in der Arbeitsgruppe von Prof. Dr. T. Deller, Institut für klinische Neuroanatomie, J.W. Goethe-Universität, Frankfurt/Main
Feb 2003 – Feb 2006	Kollegiat im Graduiertenkolleg „Neuronale Plastizität: Moleküle, Strukturen, Funktionen"